Investigation of the importance of wind field modelling for loads on a bottom fixed and a spar floater wind turbine

Master in Energy
Renewable Energy

Maylinn Haaskjold Myrtvedt

University of Bergen
Faculty of Mathematics and Natural Sciences

A thesis submitted for the degree of
Master of Science

Supervised by Professor Finn Gunner Nielsen
and
Ph.d. candidate Astrid Nybø

AUGUST 2019

Table of Contents

Acknowledgement *16*

Abstract *17*

Nomenclature *18*

1 Introduction *21*

2 Background theories and methods *24*

2.1 Wind field analysis **24**

2.1.1 Point statistics 24

2.1.2 Atmospheric stability 25

2.1.3 Wind profiles 27

2.1.4 Spectral analysis 30

2.2 Standard turbulence models **32**

2.2.1 The kaimal spectrum and exponential coherence model 33

2.2.2 The Mann uniform shear model 35

2.3 Data selection **36**

2.3.1 Measurements 37

2.3.2 Selection process 39

2.4 Wind field simulation **43**

2.4.1 TurbSim 43

2.4.2 DTU Mann generator 44

2.4.3 Simulation cases 45

2.4.4 Wind field simulation: TIMESR 47

2.4.5 Wind field simulation: Kaimal 49

2.4.6 Wind field simulation: Mann 50

3 Offshore wind turbine characteristics 53

3.1 DTU 10 MW RWT 53

3.2 Support structures 54

3.2.1 Monopile 54

3.2.2 Spar 55

3.3 Modification of the spar floater 58

3.3.1 Tower adjustment 58

3.3.2 Controller adjustment 59

3.3.3 Decay tests 62

3.4 Dynamic analysis 64

3.4.1 Simulation tool 65

3.4.2 Input parameters for load analysis 65

3.4.3 Turbine control systems 65

3.4.4 Natural frequency assessment 67

3.4.5 Tower bottom bending moment 70

3.4.6 Flapwise bending moment 70

4 Simulation results & discussion 72

4.1 Wind field simulation results 73

4.1.1 The wind profiles 73

4.1.2 The generated wind turbulence 74

4.2 Results of simulated loads 81

4.2.1 Tower bottom fore-aft bending moment – Bottom fixed turbine 83

4.2.2 Flapwise bending moment in the blade root – Bottom fixed 89

4.2.3 Tower bottom fore-aft bending moment – Spar floater 95

4.2.4 Flapwise bending moment in the blade root – Spar floater 100

5 Summary & conclusion 105

6 Further work 107

References 108

7 Appendix A 113

7.1 Selection process 113

7.1.1 Below rated (7.5 m/s) 113

7.1.2 Close to rated (12.5 m/s) 114

7.1.3 Above rated (17.5 m/s) 116

8 Appendix B 118

8.1 Input files and descriptions 118

8.1.1 Description 118

8.1.2 Simulation input files 125

8.1.3 Environmental input in SIMA 137

9 Appendix C 139

9.1 Wind turbine tests 139

9.1.1 Controller modification test 139

9.1.2 The floating turbine becomes unstable 141

9.1.3 The approach to find the damping values to the spar 145

Appendix E ***153***

9.2 Overview of dynamical load response **153**

9.2.1 Below rated 153

9.2.2 Rated 153

9.2.3 Above rated 153

10 Appendix F ***154***

10.1 MATLAB codes **154**

List of figures

Figure 2-iii - Mean and fluctuating wind speed 27

Figure 2-iv - Environmental components affecting the wind profile [27] 29

Figure 2-v Spectra estimated by Welch's algorithm in six segments by hamming window using 50 % overlap 31

Figure 2-vi Wind shear motion affecting the turbulent eddy [14] 35

Figure 2-vii - Processing procedure to obtain quality of sampled data followed by a stationarity assessment 38

Figure 2-viii - Available turbulence intensity as a function of wind speed at 119 m with associated atmospheric stability (30-minutes periods) 40

Figure 2-ix 90th percentile for selecting time series 41

Figure 2-x By combining spectral and coherence models, TurbSim creates a full wind field for load simulation for offshore wind turbines [44] 43

Figure 2-xi Flow chart of the simulation by TurbSim [10] 44

Figure 2-xii Three-dimensional turbulent wind box simulated by DTU Mann generator. Where $d_{x,y,z}$ is the distance between simulated points and $L_{x,y,z}$ is the length scale of the turbulent eddies [14] 45

Figure 3-i HAWT wind turbine 53

Figure 3-ii Offshore wind turbines with different substructures (https://www.windpowerengineering.com/projects/offshore-wind/foundations-that-float/) 54

Figure 3-iii The degrees of freedoms of a floating sub-structure [51]. 55

Figure 3-iv Example of at mooring system with crowfoot configuration for a spar sub-structure [52]..... 57

Figure 3-v The pitch motion response to uniform 12 m/s wind test (0.02 Hz)..... 60

Figure 3-vi The pitch motion response to uniform 12 m/s wind test (0.01Hz)..... 61

Figure 3-vii Performed decay test to investigate the damping ratio of the surge motion. 63

Figure 3-viii Performed decay test to investigate the damping ratio of the pitch motion. 63

Figure 3-ix Performed decay test to investigate the damping ratio of the heave motion. 64

Figure 3-x Performed decay test to investigate the damping ratio of the yaw motion. 64

Figure 3-xi Diagram of captured wind power. 66

Figure 3-xii Wind turbine thrust force at different wind speeds 66

Figure 3-xiii Power spectrum as function of frequency [60]..... 68

Figure 3-xiv Undisturbed wind forces on the tower to the left and 3P load on the right due to blade shadowing effects [56] 69

Figure 3-xv Contribution of the wind forces to flapwise bending moment in the blade root (Mb) and tower bottom bending moment (Mt) [63]. 71

Figure 4-i The wind profiles of the simulated wind fields for the below, close to and above rated selected scenarios. Blue: unstable situations, red: stable situations and green: neutral situations. 73

Figure 4-ii The PSD at hub centre provides the energy spectrum for the below rated simulated wind fields in neutral (left), stable (centre) and unstable (right) atmosphere. 74

Figure 4-iii The PSD at hub centre provides the energy spectrum for the close to rated simulated wind fields in neutral (left), stable (centre) and unstable (right) atmosphere. 75

Figure 4-iv The PSD at hub centre provides the energy spectrum for the above rated simulated wind fields in neutral (left), stable (centre) and unstable (right) atmosphere. 75

Figure 4-v Vertical co-coherence of uu-component of measurements between 40 and 80 m with the velocities of 12.5 m/s in neutral condition [6] 77

Figure 4-vi The lateral and vertical coherence of the turbulent wind field [14]. 77

Figure 4-vii Co-coherence of the longitudinal wind component (u) at points with vertical separation distance of ½ D (89.15 m) to the left and 1 D (178.3 m) to the right. The co-coherence is illustrated for the wind speeds a) below rated, b) close to rated and c) above rated. 78

Figure 4-viii Co-coherence of the longitudinal wind component (u) at points with lateral separation distance of ½ D (89.15 m) to the left and 1D (178.3 m) to the right. The co-coherence is illustrated for the wind speeds a) below rated, b) close to rated and c) above rated. 80

Figure 4-ix Standard deviation of tower bottom fore-aft bending moment. Results from below rated, close to rated and above rated inflow fields for the bottom fixed wind turbine. Various atmospheric stabilities and wind field simulation techniques are considered. 84

Figure 4-x Comparison of the bottom fixed wind turbine response in terms of load spectra for the three flow-simulation methods [Kaimal (blue), TIMESR (red) and Mann (yellow)] and various atmospheric conditions: neutral (left), stable (middle) and unstable (right). Given for the tower bottom fore-aft bending moment in the below rated wind-speed scenario. 86

Figure 4-xi Comparison of the bottom fixed wind turbine response in terms of load spectra for the three flow-simulation methods [Kaimal (blue), TIMESR (red) and Mann (yellow)] and various atmospheric conditions: neutral (left), stable (middle) and unstable (right). Given for the tower bottom fore-aft bending moment in the close to rated wind-speed scenario. 87

Figure 4-xii The load spectra of tower bottom fore-aft bending moment, with a logarithmic x-axis (0 – 3 Hz) and a linear y-axis. Given for the bottom fixed wind turbine in the close to rated wind speed scenario. 87

Figure 4-xiii Comparison of the bottom fixed wind turbine response in terms of load spectra for the three flow-simulation methods [Kaimal (blue), TIMESR (red) and Mann (yellow)] and various atmospheric conditions: neutral (left), stable (middle) and unstable (right). Given for the tower bottom fore-aft bending moment in the above rated wind-speed scenario. 88

Figure 4-xiv Standard deviation of the flapwise bending moment in the blade root. Results from below rated, close to rated and above rated inflow fields for the bottom fixed wind turbine. Various atmospheric stabilities [(neutral, stable and unstable)] and wind field simulation techniques are considered. 90

Figure 4-xv Comparison of the bottom fixed wind turbine response in terms of load spectra for the three flow-simulation methods [Kaimal (blue), TIMESR (red) and Mann (yellow)] and various atmospheric conditions: neutral (left), stable (middle) and unstable (right). Given for the flapwise bending moment in the blade root for the below rated wind-speed scenario. . 92

Figure 4-xvi Comparison of the bottom fixed wind turbine response in terms of load spectra for the three flow-simulation methods [Kaimal (blue), TIMESR (red) and Mann (yellow)] and various atmospheric conditions: neutral (left), stable (middle) and unstable (right). Given for the flapwise bending moment in the blade root for the close to rated wind-speed scenario. 92

Figure 4-xvii The load spectra of flapwise bending moment, with a logarithmic x-axis (0 – 3 Hz) and a linear y-axis. Given for the close to rated wind speed scenario. 93

Figure 4-xviii Comparison of the bottom fixed wind turbine response in terms of load spectra for the three flow-simulation methods [Kaimal (blue), TIMESR (red) and Mann (yellow)] and various atmospheric conditions: neutral (left), stable (middle) and unstable (right). Given for the flapwise bending moment in the blade root for the above rated wind-speed scenario..... 94

Figure 4-xx Standard deviation of tower bottom fore-aft bending moment. Results from below rated, close to rated and above rated inflow fields for the spar floating wind turbine. Various atmospheric stabilities and wind field simulation techniques are considered. 96

Figure 4-xxi Load spectrum of tower bottom fore-aft bending moment given for the spar floater – BR 97

Figure 4-xxii Load spectrum of tower bottom fore-aft bending moment given for the spar floater – R 98

Figure 4-xxiii Load spectrum of tower bottom fore-aft bending moment, with a logarithmic x-axis (0 – 0.2 Hz) and a linear y-axis..... 98

Figure 4-xxiv TBBM AR 99

Figure 4-xxv Standard deviation of tower bottom fore-aft bending moment. Results from below rated, close to rated and above rated inflow fields for the spar floating wind turbine. Various atmospheric stabilities and wind field simulation techniques are considered. 101

Figure 4-xxvi Comparison of the spar floating wind turbine response in terms of load spectra for the three flow-simulation methods [Kaimal (blue), TIMESR (red) and Mann (yellow)] and various atmospheric conditions: neutral (left), stable (middle) and unstable (right). Given for the flapwise bending moment in the blade root for the below rated wind-speed scenario. 102

Figure 4-xxvii Comparison of the spar floating wind turbine response in terms of load spectra for the three flow-simulation methods [Kaimal (blue), TIMESR (red) and Mann (yellow)] and various atmospheric conditions: neutral (left), stable (middle) and unstable (right). Given for the flapwise bending moment in the blade root for the close to rated wind-speed scenario. 103

Figure 4-xxviii Load spectrum of flapwise bending moment, with a logarithmic x-axis (0 – 3 Hz) and a linear y-axis..... 103

Figure 4-xxix Comparison of the spar floating wind turbine response in terms of load spectra for the three flow-simulation methods [Kaimal (blue), TIMESR (red) and Mann (yellow)] and

various atmospheric conditions: neutral (left), stable (middle) and unstable (right). Given for the flapwise bending moment in the blade root for the above rated wind-speed scenario. 104

Figure 8-i Simulation by DTU Mann generator 137

List of tables

Classification of stability 26

The correction factor for all atmospheric stability conditions 30

Kaimal spectrum parameters 34

Required parameters in the Mann model 36

Selected time series for generating turbulence wind fields 42

Below rated wind speed generated wind fields 46

Rated wind speed generated wind fields 46

Above rated wind speed generated wind fields 46

The decay coefficient obtained from measurements and used as input in TIMESR 49

Power law exponent (αp) derived for neutral, stable and unstable atmosphere. 50

Input parameters for simulating Mann turbulent wind field. 51

Key parameters of the 10 MW reference turbine [12] 53

The modes of motion for a floating sub-structure 56

Structural properties of the spar floater [54]. 56

Properties of the mooring system [54]. 58

Adjustment on the spar sub-structure 59

Modification of the PI gain constants of the DTU blade pitch controller. 60

Natural periods of the spar floater obtained by decay tests 62

Natural frequency of the whole bottom fixed wind turbine obtain with SIMA by Sørum et al.[11] 69

Simulation input in SIMA..... 83

Statistics of the mean (MNm) for the load of the tower bottom fore-aft bending moment. Results from below rated, close to rated and above rated inflow fields for the bottom fixed wind turbine. Various atmospheric stabilities and wind field simulation techniques are considered. 83

Statistics of the standard deviation (MNm) for the load of the tower bottom fore-aft bending moment. Results from below rated, close to rated and above rated inflow fields for the bottom fixed wind turbine. Various atmospheric stabilities and wind field simulation techniques are considered. Green indicates an underestimated load and blue indicates an overestimated load. 85

Simulation input in SIMA..... 89

Statistics of computed mean (MNm) load of the flapwise bending moment in the blade root. Results from below rated, close to rated and above rated inflow fields for the bottom fixed wind turbine. Various atmospheric stabilities and wind field simulation techniques are considered. 89

Statistics of the standard deviation (MNm) for the load of the flapwise bending moment in the blade root. Results from below rated, close to rated and above rated inflow fields for the bottom fixed wind turbine. Various atmospheric stabilities and wind field simulation techniques are considered. Green indicates an underestimated load and blue indicates an overestimated load. 91

Simulation table 95

Statistics of the mean (MNm) for the load of the tower bottom fore-aft bending moment. Results from below rated, close to rated and above rated inflow fields for the bottom fixed

wind turbine. Various atmospheric stabilities and wind field simulation techniques are considered. 95

Statistics of the computed standard deviation (MNm) load for the tower bottom fore-aft bending moment. Results from below rated, close to rated and above rated inflow fields for the bottom fixed wind turbine. Various atmospheric stabilities and wind field simulation techniques are considered. Green indicates an underestimated load and blue indicates an overestimated load. 96

Simulation input in SIMA 100

Statistics of the mean (MNm) load of the flapwise bending moment. Results from below rated, close to rated and above rated inflow fields for the bottom fixed wind turbine. Various atmospheric stabilities and wind field simulation techniques are considered. 100

Statistics of the computed standard deviation load (MNm) for the flapwise bending moment in the blade root. Results from below rated, close to rated and above rated inflow fields for the bottom fixed wind turbine. Various atmospheric stabilities and wind field simulation techniques are considered. Green indicates an underestimated load and blue indicates an overestimated load. 102

Inputs TurbSim simulation [10]. Yellow indicates values for TIMESR, green indicates values for Kaimal, black if they use the same value and black for the parameters that is not used. 118

Inputs in DTU Mann generator 124

Acknowledgement

There is no such thing as a self-made man. You will reach your goals only with the help of others

- *George Shinn*

This 60 ECTS thesis is written as a part of the Master's program in Energy with specialisation in renewable energy. The program is run by the University of Bergen Geophysical institute.

It is a great pleasure to acknowledge my gratitude and thank the people who helped and supported me during this work:

A special thanks to my main supervisor, Professor Finn Gunner Nielsen. I am grateful for his guidance, advise and support throughout the entire process. Thank you for introducing me to the field of offshore wind and to made me develop an understand of dynamic load response of the turbines.

To Astrid Nybø for all helps and advices. Thank you for always quick and good feedback. I am grateful for the encouragement and making me believe that I can complete this master thesis on time.

To my fellow students Ida Isabell Hartveit and Phani Kumar Manne for discussions, advises and encouragement.

Finally, a special thanks to my family and friends for their continuous, positive and moral support. I could not have done this without you.

Maylinn Haaskjold Myrtvedt

Bergen, August 2019

Abstract

The international standard for wind turbine design recommends two turbulence-generation models, which is the Kaimal spectral and exponential coherence model and the Mann spectral tensor model. These wind models are currently used in the simulation of dynamic loads on wind turbines. These models are developed for small onshore wind turbines and designed for neutral atmospheric conditions. Nowadays, these standard inflow formulations are challenged as the size of the turbine's rotor increases and the turbines are placed offshore. The turbine will no longer be fully immersed in the surface layer, which increase the need to account for unstable and stable atmospheric conditions. The turbulence models from the standards have a spectrum formulation with standardized parameters that do not represent the spatial and the temporal distribution of the turbulence in a consistent way. In this study, flow fields are generated using the recommended standard turbulence models and compared to wind fields constructed from offshore measurements. Various atmospheric stabilities are considered. When comparing the generated turbulent wind fields, it was showed largest variation in the low-frequency part of the wind energy spectrum across the three mentioned wind field generation methods. The temporal distribution of co-coherence is investigated in the vertical and the lateral direction and compared across the various generated wind fields. This is found to have significant differences depending on which simulation methods used, especially in the low-frequency range. This frequency range that is especially important for the floating wind turbine. Further, these flow fields are used as input in the wind turbine simulations of a wind turbine mounted on a monopile foundation and on a spar sub-structure. The impact of various turbulence formulations on loads and responses of large offshore wind turbine is uncertain. The response is therefore investigated for various formulations. The load analysis showed that the various formulations yields different loads and that the loads response are sensitive to atmospheric stability.

Nomenclature

Latin characters

C	Coherence decay constant
D	Rotor diameter
d_x	Grid spacing in x-direction
d_y	Grid spacing in y-direction
d_z	Grid spacing in z-direction
f	Frequency
g	Acceleration of gravity
k	Von Kármán constant
K	Wave number
L	Obukhov length
L_M	Turbulent length scale
L_c	The coherence scale parameter
N_x	Number of grid points in x-direction
N_y	Number of grid points in y-direction
N_z	Number of grid points in z-direction
u	Velocity
u_*	Friction velocity
Z	Height
z_0	Surface roughness length

Greek characters

α_p	Empirical power law exponent
α_C	Charnock constant
A	Three-dimensional Kolmogorov constant
θ	Heat
ζ	Stability parameter

ψ	Stability function
Λ	Turbulence scale parameter
σ	Standard deviation
γ	Coherence parameter
Γ	Anisotropy parameter
ϵ	Turbulent kinetic energy dissipation
δ	Separation distance
Φ_{ij}	Spectral velocity tensor, (i and j are to be replaced by u, v or w)

Symbols

u	Component u
$\bar{u}$	Mean component of u
u'	fluctuating component of u

Subscripts

ref	Reference
k	Turbulent velocity direction
T	Analysis time for wind field simulation

Abbreviation

DNV-GL	Det Norske Veritas-Germanischer Lloyd
DOF	Degrees of freedom
DTU	Danmarks Tekniske Universitet
FBM	Flapwise bending moment
FINO	Forschungsplattformen in Nord-und Ostsee
HAWC2	Horizontal axis wind turbine simulation Code 2nd generation
HAWT	Horizontal axis wind turbine
IEC	International Electrotechnical Commission
LLJs	Low-level jets
MATLAB	Matrix Laboratory

PSD	Power spectral density
RIFLEX	Riser system analysis program
SIMA	Simulation of Marine Operations
SIMO	Simulation of Marie Operations
SWL	Sea water level
TI	Turbulence intensity
TP	Transition piece
TBBM	Tower bottom bending moment

1 Introduction

In the process of designing wind turbines, information about the wind is needed to analyse the turbines functionality under the influence of the wind environment and to estimate loads on the turbine structure. Offshore wind is an up and coming research topic, there are therefore few site measurements available, which is also related to the high cost of the offshore measurement platform, both for establishment and maintenance. The wind industry today make use of simple stochastic models to generate wind fields, which are based upon standards described in the IEC standards [1][2] and in the DNVGL standards [3][4]. The two recommended turbulence-generation models in the standards are either the Kaimal spectral and exponential coherence model or Mann spectral model, these are hereafter denoted as Kaimal and Mann. The models are defined differently. Kaimal define turbulence by a one-point spectra and a coherence function, while Mann takes advantage of spectral velocity tensor. Kaimal only consider coherence between points for the longitudinal velocity component. While, the turbulence generation by spectral tensors, will provide coherence in all three wind directions. Both simulated wind fields, from the use of these turbulence models, can provide similar information about turbulent wind spectra, but the coherence between points in the fields, may differ. The latter is a measure of the degree of relationship between two time series [5]. Coherent structures is referred to as spatial correlation and temporally coherence can be illustrated at a certain separation distance over various frequencies [6]. Several studies have used these models to evaluate their differences and to investigate how they affect the dynamic response of large offshore wind turbines [6][7][5]. All the studies agree that the models differ in the representation of turbulent structures, which will impact the offshore wind turbines.

The turbulent wind models, which represents wind characteristics based on statistical and spectral methods are both included with standardized parameters. These models are developed for small onshore wind turbines. The different representation of spatial distribution of turbulence were not crucial for small turbine rotors, but as the size of the wind turbines rotor increases as well as the structure is placed offshore, the need for accurate wind models will increase. Eliassen et al. [8] found that the spatial distribution of wind turbulence will influence the wind turbine response. Beside the wind speed and the turbulence intensity, which impact the wind turbine response, it highlights the importance of being able to represent the spatially wind variation over the whole rotor swept area. The lowest relevant frequency for load analysis of a large bottom fixed wind turbine, is the nominal rotor frequency of about 10 RPM (revolutions per minute), 0.16 Hz. The energy in the lower frequency range however, is more important for a floating turbine, here it must account for natural periods of six rigid body modes of motions. The natural periods of these motions might range from a few seconds to about 140 seconds (0.007 Hz).

To have accuracy in wind load presentation, one must also be able to model all classes of stability. Nybø et al. [6] found that the spatial distribution and temporal distribution of coherence differ scientifically across methods of generated wind fields and atmospheric stability conditions. Doubrawa et al. [7] found that the turbine loading is sensitive to atmospheric stability, even when the turbulence intensity remains fairly constant. The standard models are developed for neutral atmospheric conditions. Nowadays offshore turbines may no longer be fully immersed in the atmospheric surface layer, which makes the neutral assumption to be a limitation. Therefore it is possible to assume that the standard turbulence models fail to simulate turbulence characteristics which are relevant for the large offshore wind turbines [7]. The offshore mast, FINO-1, located in the North Sea, has provided this study with time series of measured wind at different heights at sea. The wind data, together with an processing procedure for offshore wind turbine applications by Nybø et al. [9], made it possible to create wind fields directly from point measurements and to establish alternative parameter values for the standard wind fields. This study has included the site-specific parameters in the generation of standard wind field, which opens the possibility to represent these fields by other atmospheric stability than neutral. One can say that Mann and Kaimal are fitted to measurements. A third wind field generation function is used to represent the offshore wind field. This was performed by using point measurements together with the TIMESR function in the turbulence simulator, TurbSim [10]. The standard wind fields are compared with the offshore measurements through this third method. TIMESR contains assumptions and simplifications due to the processing procedure, together with the simple Davenport coherence model, to represent the coherence in the measurements. It is thus not possible to consider this as a true offshore wind field, but it gives the ability to a closer representation to the offshore conditions.

The significance of various formulations for loads and response to large offshore wind turbines is still uncertain. It has therefore been an aim for this study to investigate different responses with the different formulations. However, to perform this task, it required an available modelled offshore wind turbine. This study received two turbines, one bottom fixed 10 MW, modelled by Sørum et al. [11], which is based on the DTU 10 MW reference turbine [12]. The other one was modelled on a spar sub-structure [9]. It was a desire that the two turbines were identical, in order to compare the different responses from the various wind field formulations projected on these turbines. Thus, the floating wind turbine was modified by mounting the bottom fixed wind turbine on the spar sub-structure. Both turbines have a hub height at 119 m, the blades sweep with a diameter of 178.3 m and the turbine rated wind speed is referred as 11.4 m/s. The generated wind fields are used as the environmental loading to find the structural loads on the wind turbine. The goal was to project loads with different atmospheric stabilities and wind speed to investigate the response of both turbines. The focused response in this study is the tower bottom bending moment, along the wind direction, and the flapwise bending moment in the blade root. The various generated wind fields are used in the dynamic response analysis, which have been the main loading projected on the turbines. Nine wind

fields were simulated for each simulation method (Kaimal, Mann and TIMESR) for the situations of below rated, close to rated and above rated wind speeds in neutral, stable and unstable atmosphere. The simulations are performed for 1 hour and 200 s, where the latter are a transient time to account for the ramp up of the loads under turbine simulations. The main aim in this thesis is to investigate the turbine response under simulation of the various inflow load, including an evaluation of the effect of atmospheric stability and the effect of turbulence characteristics within the different simulated flows. This is performed by comparing the standard generated wind fields with each other and with TIMESR.

2 Background theories and methods

In order to investigate the structural analysis by simulating loads on the two wind turbines, the present study has been performed in four steps.

1. Wind data selection. The aim is to select favourable time series (stationary, homogeneous), which shall be used when generating various wind fields, this is explained further in the sub-chapter 2.3.

2. Wind field simulation. The aim is to create wind fields based on standard turbulence models and to compare it with wind fields obtained from offshore measurements as described in the sub-chapter 2.4.

3. Modification of a floating wind turbine. To compare the structural loads on the two turbines assessed in the present study, the spar floater has been modified to be the same turbine as the bottom fixed, except for the substructures which separates them for being identical. The intention is to have the same starting point for both turbines when they are affected by the wind fields. The modifications are discussed in sub-chapter 3.3.

4. Simulation of the dynamic response of the wind turbines in the various wind fields. Dynamic analysis is described in sub-chapter 3.4.

2.1 Wind field analysis

2.1.1 Point statistics

The most frequently way to characterize the turbulence of the wind field is by point statistics [6]. By decomposing an instantaneous wind speed u, into the mean wind speed, $\bar{u}$ and fluctuation wind speed, u', one can write the decomposition like this:

$$u = \bar{u} + u'. \tag{2-1}$$

The mean wind speed is determined by averaging 10 minutes blocks of sampled data from point measurements. The fluctuations are related to this mean value. This gives important knowledge of the frequency distribution of the wind speed. According to Nybø et al. [6], the 10 minutes averaged intervals will resolve all relevant frequencies, meaning that this is an important range for the wind turbine response. (Increasing the averaging length will in most cases also increase the computed standard deviation). When a floating wind turbine is introduced, the low frequency region becomes highly important when consider the dynamic

response. The study also states that it is normal to calculate turbulence intensity (TI) from 1 Hz measurements. Hence, the measurements are resampled from 10 Hz and 20 Hz measurements to 1 Hz sampling frequency. TI can be characterized as the strength of the occurring turbulence and is defined as standard deviation of the mean wind speed, σ_u, divided by the mean wind speed, $\bar{u}$, giving:

$$TI = \frac{\sigma_u}{\bar{u}}. \tag{2-2}$$

The IEC guideline 61400-1 [1], describes that wind speed and its fluctuation is addressed does not have the same values of every sites. This means that it must be handled as a site-specific parameter. Turbulent motions are named eddies and a turbulent flow is a gathering of several eddies. Different sizes of eddies are distributed with unequal amount of energy, which will depend on stability of the atmosphere. Thus, it is important to consider different stability conditions in the atmosphere, to understand the energy content that hits the turbine. Turbulence is often characterized as stationary, homogeneous and isotropic, meaning that, it is uniform in space, constant in time and the eddies have equal size in all directions [13]. Generation of turbulent wind in the marine atmospheric boundary layer creates random and stochastic processes within a wind field. The main contributor of load on a structure is the velocity, u, in the longitudinal direction, due to higher energy content than in the lateral and vertical direction. Lateral, v, and vertical, w, velocity components can contribute to wind turbine resonance by loads and the components can change the angle of attack on the blades, which is highly relevant when studying wind turbines [14].

2.1.2 Atmospheric stability

Wind shear represent the variation of mean wind speed over the rotor height and will, together with turbulence conditions, affect the wind turbine with dynamic loads. They are however, depending on atmospheric stability [6]. By having the correct understanding of the stability that stratifies the atmosphere, it is possible to obtain accurate estimates of the vertical wind profile [15]. This is due to the three stability situations in the atmosphere, defined as neutral, stable or unstable conditions. Stable and unstable can also be classified as very stable and very unstable. These stability conditions affect the wind profile, resulting in various representation of the wind speed for each situation.

The stability of a flow is how the air respond to small disturbances and may be explained by the displaced air from its initial position. The stability of a flow is how the air respond to small disturbances and may be explained by the displaced air from its initial position. With unstable atmospheric condition, the air parcel that is disturb from its location will continue to move away. The generated turbulence is high in the unstable atmosphere. In a stable atmospheric condition, the air parcel will return to its initial position. This generates lower turbulence. The

neutral stratified atmosphere has air parcels that moves from its location and will then stay at the new location. This creates moderate turbulence.

In this study, the atmospheric stability is described by the parameter Obukhov length, L. The length scale, first introduced by Obukhov in 1946 [16], is used to classify the stability present in the atmosphere, captured by offshore measurements. The Obukhov length is defined as the height above the surface where buoyancy produced turbulence, dominates over mechanical produced turbulence. A negative value implies unstable atmosphere and buoyancy developed turbulence, while a stable atmosphere with mechanical generated turbulence, shear, is classified by a positive value. It is formulated by a combination of momentum surface flux, also called a surface vertical kinematic eddy heat flux, $(\overline{w'\theta_v})_s$, via friction velocity, $u_* = \sqrt{\overline{u'w'} + \overline{v'w'}}$ and heat, $\bar{\theta}_v$. It also includes the von Karman constant, $\mathrm{k} = 0.4$, and gravitational acceleration, g [17]. This is only valid when the wind is not calm and friction velocity is greater than zero. The Obukhov length (L) is limited to the surface layer and is given by [17]:

$$L = \frac{-\bar{\theta}_v u_*^3}{\mathrm{kg}(\overline{w'\theta_v})_s}. \tag{2-3}$$

Table 2-a below illustrates the stability classification based on the calculated Obukhov lengths. The range is given by Van Wijk et al [18] which provide a wide range of unstable and stable Obukhov lengths:

Table 2-a Classification of stability

Stability	Obukhov length range (m)
Very stable	0<L<200m
Stable	200<L<1000m
Near-neutral	|L|>1000m
Unstable	-1000<L<-200m
Very unstable	-200<L<0m

2.1.3 Wind profiles

In wind energy, information about the mean wind speed and turbulence as a function of height is important knowledge in order to understand how a wind turbine will perform and to estimate the loads on these turbines [19]. The vertical velocity of air flow near the surface is zero and will increase upwards with the height, z. This is caused by a gradient in the wind speed. The differences in the velocities from the surface and upwards may cause atmospheric turbulence, which mixes the air. Generated turbulence causes the wind profile to deviate from the mean wind by its fluctuations as Figure 2-i illustrates [20].

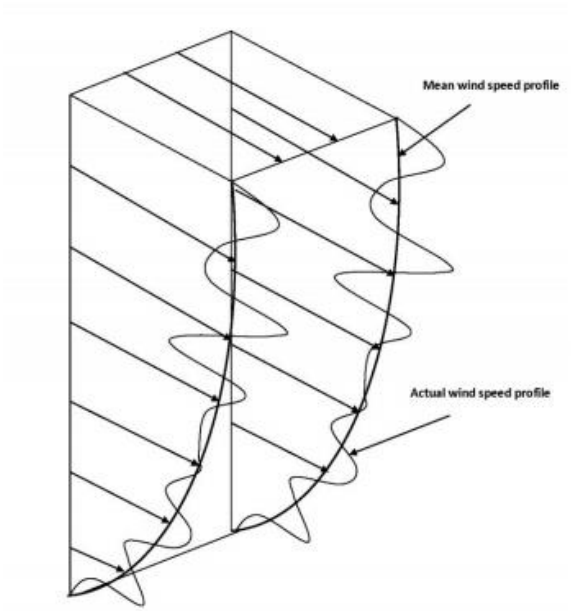

Figure 2-i - Mean and fluctuating wind speed

In wind energy, the wind speed as a function of height is commonly formulated by either the power law or the logarithmic law [1]. Common for both is that the wind speed is near zero towards the surface due to frictional drag and they are only valid in the surface layer, but commonly used above. Surface layer forms about 10 % of the total atmospheric boundary layer height. Yet, the surface layer height will vary according to atmospheric stability [21] and will be even lower over the sea in contrast to boundary layer over land. The remaining 90 % is called the Ekman layer [19]. Larsen et al. [22] discuss that the wind above the surface layer has a tendency to increase more than logarithmically as a result of either the boundary length scale or the influence of stability. In the Ekman layer, a third force, the Coriolis force (due to the earth's rotation), is added to the balance of pressure gradient and frictional gradients, which is the major elements in the surface layer. The Coriolis force affects the wind behaviour by bending the wind direction with the height [19]. Most offshore wind turbines are large structures and will therefore operate in the surface layer as well as in the lower Ekman layer.

With the increase in modern offshore wind turbines, it is desirable to gain new and better knowledge of an extended wind profile beyond the surface layer. The wind profile which is based on the surface layer theory and the Obukhov scaling, is only valid to a height of 50 to 80 m for neutral conditions, thus several studies has aimed to extend the wind profile to cover the entire boundary layer height, such as discussed in reference [23]. However, this study is performed for onshore sites. Even though the wind profiles are created for onshore sites, it is generally used offshore. There are two wind profiles assessed in this thesis; the power law wind profile and the logarithmic wind profile.

- *Power law wind profile*

The power law is recommended by the IEC standard, to define the normal wind speed profile for the standard wind turbine classes and is given by [24]:

$$u(z)_{pl} = u_{ref}\left(\frac{z}{z_{ref}}\right)^{\alpha_p}, \tag{2-4}$$

Where z_{ref} is a reference height and u_{ref} is mean wind speed at that height. z stands for the actual height and α_p is the empirical power law exponent.

The power exponent coefficient, α_p , is a parameter that defines how much shear it is in the wind speed at a given height. Higher shear means higher power law exponent value and thus higher wind speed at the same height [14]. For normal wind conditions, IEC gives $\alpha_p = 0.14$, but present study adjust this parameter to be site-specific. Meaning that, different values of the power law wind shear exponent will characterize the atmospheric stability. The values of α_p derived from the offshore measurements, used in this study, for different stability conditions with associated wind speed, appear in Table 2-j.

This parameter has a relation with the surface roughness length, z_0, when indicating different types of stabilities [19]. This roughness length parameter decides the height of the surface layer varying with different surfaces. Offshore, it is the sea surface roughness, due to ocean waves, which contributes to the provision of the wind speed [17]. The sea surface roughness is very low compared to the surfaces on land [25], this relates to lower turbulence offshore. To derive the roughness of the sea, Charnock expression can be used as followed [26]:

$$z_0 = \frac{\alpha_C u_*^2}{\mathrm{g}}, \tag{2-5}$$

where α_C is Charnock parameter, a dimensionless roughness (typical range: 0.01-0.03), u_* is the friction velocity and acceleration of gravity is given as g.

The roughness length dominates a momentum transfer between wind and water. The changing of roughness length depends on the wave field as B. Lange discuss in reference [27]. The wind profile dependency of the wave field can be seen in Figure 2-ii together with the other factors that affects the wind conditions.

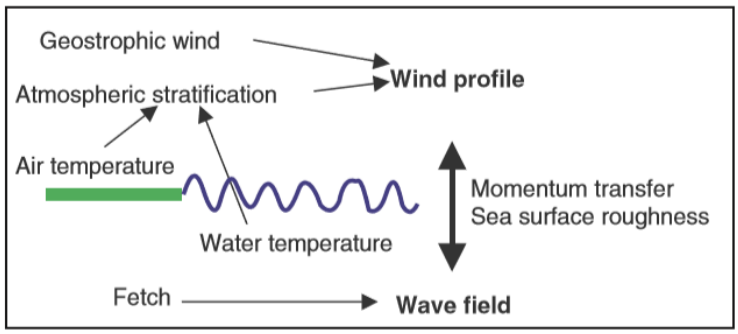

Figure 2-ii - Environmental components affecting the wind profile [27]

- Logarithmic wind profile

The logarithmic wind profile, denoted as log law, originates from a similarity theory in meteorology [17]. From zero wind speed it increases nearly logarithmically due to pressure gradient forces. In the industry they often assume neutral stability and the log law for neutral atmospheric condition which is given by [17]:

$$u(z)_{log} = \frac{u_*}{\mathrm{k}} ln\left(\frac{z}{z_0}\right), \tag{2-6}$$

Where the friction velocity u_* is divided by the Von Karman constant k, z is the considered height and z_0 represent the aerodynamic roughness parameter.

The logarithmic wind profile can be extended to non-neutral conditions by using a stability-dependent function, ψ, which gives the stability-corrected wind profile as [4]:

$$u(z)_{log} = \frac{u_*}{\mathrm{k}} ln\left(\frac{z}{z_0} - \psi\right), \tag{2-7}$$

ψ allows for a separation between the roughness and the stability effects, such that the profile is govern by the stability rather than by the roughness. As Table 2-b shows, it is zero for neutral

conditions, positive for unstable conditions and negative for stable conditions [4]. The literature gives slightly different values of the constants, but the ones in Table 2-b are typical.

Table 2-b The correction factor for all atmospheric stability conditions

Atm. Stability	Stabilit- dependent function
Neutral conditions	$\psi = 0$
Stable conditions ($\zeta > 0$)	$\psi = -4.8\zeta$
Unstable conditions ($\zeta < 0$)	$2\ln(1+x) + \ln(1+x^2) - 2\tan^{-1}(x)$

Where the stability parameter $\zeta = \frac{z}{L}$ play an important role and $x = (1 - 19.3\zeta)^{\frac{1}{4}}$ [4]. A study done by Wijk et al. [18] showed that the inclusion of the Obukhov length stability correction factor (z/L), minimized the error that the wind profile incorporates when it is applied offshore.

2.1.4 Spectral analysis

A turbulent wind field, as the once sampled with point measurements, consists of fluctuating motion occurring with different frequencies and amplitudes. A turbulent wind spectrum, also denoted as power spectral density (PSD), which is used in this thesis to show how the energy of the wind turbulence is distributed between different frequencies. In the wind industry, when measured data is insufficient to establish site-specific spectral densities, standard spectrum are often used for representing PSD [3]. In this thesis, spectral analysis is performed both from measured data and by the use of standard models.

Fourier transform is a mathematical tool to compute this information by breaking the turbulent time series in the time domain into components and transformed to a frequency domain [17]. Turbulent energy in Figure 2-iii is estimated by a power spectral density function, which shows energy distribution on frequencies.

As Nybø et al. [6] points out, this low-frequency range is important region for offshore wind turbine response due to the fact that most energy will be located here. The energy will decrease with the decaying eddies towards higher frequencies until viscosity of the fluid converts the kinetic energy into heat [28].

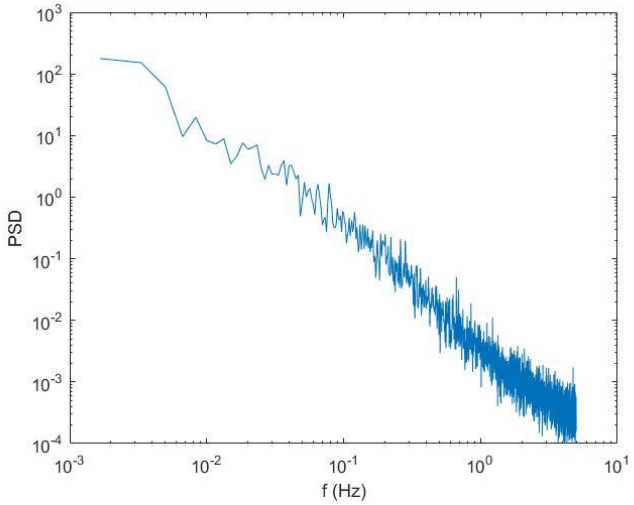

Figure 2-iii Spectra estimated by Welch's algorithm in six segments by hamming window using 50 % overlap

In wind energy, various spectrums are used as a tool to describe turbulence such as Kaimal spectrum or Von Karman spectrum. These two spectrums are incorporated in the two turbulence models used for generating standard wind fields in this thesis, section 2.4. These models provide similar spectral information at hub height, but they represent spatial characteristics differently [6]. As specified in reference [29], the wind turbine blades experiences spatial variation of turbulence, a single-point spectrum, as described above, does not represent this well enough.

Coherence, on the other hand, provides information about the spatial variation inside the wind field. Turbulent wind blows at different points in horizontal, lateral and vertical direction and between these points, the turbulent fluctuations may correlate. Thus, coherence is a function of the fluctuating period in the wind velocities [6]. Coherence measures the magnitude of correlation in the separation distance which depends on the distance between the points in space, the mean wind speed and frequency [30]. Coherence is defined by correlation functions which consist of information about the frequencies, amplitudes and phases of one time series or between two time series. The correlation terms can be describes as followed [31]:

- Cross-correlation analyse the correlation between time series operating at two different points in space, x and y, to find mutually fluctuations in the velocities. The x and y time series is placed upon each other and then one of them is shifted, in relation to the other, to find similarities. Mathematically, the two functions is multiplied with each other after each shift and then integrated over a common time axis [31].

- The auto-correlation describes the correlation of the turbulent wind velocities in one time series with itself. That is, how different random processes inside the time series will correlate with the next observed fluctuation, within the time series.

The correlation function in the time domain is difficult to interpret. In order to obtain the amplitude and phase information of the frequency components, the Fourier transform must be applied. When auto-correlation function and the cross-correlation function has been through the Fourier transformation, they are converted into the so called auto-spectral density and cross-spectral density [31].

Low coherence appears when the points is separated by a long distance. While, a closer separation distance provides higher coherence. Coherence in a general formulation, is expressed by the cross-spectra, S_{xy} at the frequency f, in an absolute form, divided by a square root of a one-sided auto-spectra, S_{xx} and S_{yy} at the frequency f. Coherence can be calculated for each of the velocity components and for x, y and z direction. The general spatial coherence model gives coherence between points x and y of the same wind components by [10]:

$$\gamma = \frac{|S_{xy}|}{\sqrt{S_{xx}S_{yy}}}. \tag{2-8}$$

Coherence can be separated into two parts [6]:

- A real part, called co-coherence
- An imaginary part, called quad-coherence

The latter is, according to Nybø et al. [6], often ignored which can cause a simplified wind structure within the turbulent wind fields. The reference [6] question how the imaginary part will affect nowadays growing rotor sizes.

2.2 Standard turbulence models

The IEC standard [1] recommends two turbulence models for wind field generation. The *Kaimal spectral and exponential coherence model* and the *Mann uniform shear model*, hereafter denoted as Kaimal and Mann, which are the two standard models used in this thesis. According to IEC, both turbulence models assumes the turbulence to be stationary. Both models are also assumed to be under the influence of neutral atmospheric conditions and is limited to the surface layer. IEC points out that in the use of these turbulence models, standard input parameters shall include effects of varying wind speed, shears and direction as well as

to allow rotational sampling through variation of shear [32]. This thesis takes the advantages of standard inputs to generate standard wind fields using Mann and Kaimal turbulence model. IEC standard has previously suggested that these standard input parameters for onshore and offshore conditions, should be equal. This year, a new contribution of standards has been published, but these are not open for this study to view. However, it has opened for adjustment of some standard parameter to be site-specific [32]. This study takes advantage of this method, by fitting turbulence intensities and wind profiles to the measurements for each stability condition and wind speed scenarios.

2.2.1 The kaimal spectrum and exponential coherence model

This is a model that combines turbulent wind spectra with turbulent structures of spatial correlation.

- *The Kaimal spectrum*

In this model, the kaimal spectrum describes the energy in the turbulent wind field. This spectrum is derived based on wind measurements done by Kaimal in 1972 [33]. IEC has adapted to that version [1] and gives the spectra for the three wind components, k = u, v , w, as followed [10]:

$$S_k(f) = \frac{\frac{4\sigma_k^2 L_k}{\bar{u}_{hub}}}{\left(1 + \frac{6fL_k}{\bar{u}_{hub}}\right)^{\frac{5}{3}}}, \tag{2-9}$$

where S_k is the PSD at a given frequency, f, in Hertz (Hz), σ_k is the standard deviation of the turbulent velocity component, k, which is derived by integrating the spectra and L_k is the site and altitude dependent length scale of the turbulent wind speed.

Key parameters for the kaimal spectrum are defined by the IEC standard [1] and are given in Table 2-c below.

Table 2-c Kaimal spectrum parameters

Parameter	**Turbulent component**		
	$\mathrm{k} = u$	$\mathrm{k} = v$	$\mathrm{k} = w$
Standard deviation σ_k	σ_u	$0.8\sigma_u$	$0.5\sigma_u$
Length scale L_k	$8.1\ \Lambda_u$	$2.7\ \Lambda_u$	$0.66\Lambda_u$

Here, $\Lambda_u$represents a turbulence scale parameter, to define the length scale of turbulence along wind u-component in the longitudinal direction at hub height. IEC standard requires the parameter to be 42 m for z > 60 m and 0.7z for z < 60 m [1] (z=hub height).

The Kaimal spectrum is used for representing the upstream wind field in front of the wind turbine. The rotation of the wind turbine blades samples the turbulent wind, hence spatial variation is needed to be represented in addition to the PSD [3]. When the blade samples the turbulence, it will experience a different wind spectrum than the single-point spectrum which makes it important to include rotationally sampled spectrum described by the coherence functions, which also account the shear effects.

- *The exponential coherence model*

Burton et al. [29] mentioned that Kaimal do not have a straightforward analytical expression for the coherence function. An empirical exponential model of coherence is used to find coherence for the velocity in the mean wind direction. Kaimal turbulence model only account for the spatial correlation of the turbulence in the longitudinal direction [1]. Kaimal do not account for coherence in the lateral- and the vertical velocity component. Spatial cross-correlation is described by coherence depending on spatial extent and separation distance between two points. The coherence function is given by [1] and is set to be real and positive.

$$\gamma = \exp\left(-12\left(\left(\frac{f\delta}{u_{hub}}\right)^2 + \left(\frac{0.12\ \delta}{L_c}\right)^2\right)^{0.5}\right), \tag{2-10}$$

where f is the frequency (Hz) and δ is the magnitude of the spatial separated points on to a plane normal to the mean wind direction, while L_c is the coherence scale parameter $(= 8.1\Lambda_1)$.

A real and positive coherence function implies a variation in along-wind velocity over the cross section, which will be in phase [6].

2.2.2 The Mann uniform shear model

J. Mann developed an algorithm commonly used in wind engineering to simulate turbulent wind fields and performed a study on wind field simulation in 1998 [35]. The Mann uniform shear model, hereafter denoted as Mann. The model is based on the spectral tensors for atmospheric surface-layer turbulence at high wind speeds [4], which origins from the Von Karman's model, introduced in 1948 [36]. The spectral tensors, Φ, are derived in the IEC standard [1], which defines the spectral properties and allows for simulation of three-dimensional fields of all components of the wind velocity fluctuations [4]. When turbulence is modelled by these tensors, coherence is provided in all three wind directions [5].

The Mann model uses the Von Karman energy spectrum and assumes that the spectral tensors is isotropic for the initial condition [1]. The spectrum is modified to account for the shear deformation, which will stretch the turbulent eddy structure and thus the flow is transformed into being an anisotropic flow [14]. The anisotropic parameter, Γ, included in the Mann model, is a non-dimensional number which parameterize the eddy lifetime [37]. The stretched eddy due to wind shear motion, is illustrated in Figure 2-iv.

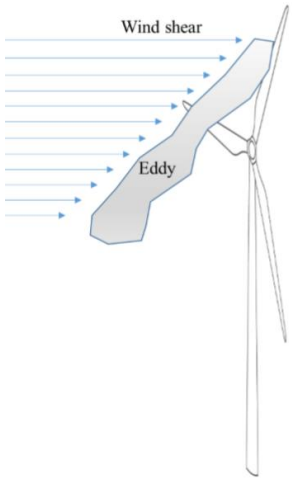

Figure 2-iv Wind shear motion affecting the turbulent eddy [14]

There are three required parameters for the Mann model, according to the IEC standard [1], illustrated in Table 2-d.

Table 2-d Required parameters in the Mann model

Parameter	Value
Γ	3.9
σ_{iso}	$0.55\sigma_u$
L_M	$0.8\Lambda_u$

Where the reference describes Λ_u to be 42 m for hub height higher than 60 m, which gives the turbulent length scale, $L_M = 33.6$. The length scale describes the eddy-size containing most energy. Γ, L_M, together the energy dissipation rate of the eddies, $\alpha\epsilon^{2/3}$, defines the three parameters of the Mann model [37]. When spectral properties are defined by the spectral velocity tensor, it is a function of the three mentioned parameters and the wave number in three dimensions [37]. These parameters are must be defined as input in the DTU Mann turbulence generator, as explained in section 2.4.1 and 2.4.6.

The information of the coherence from the Mann model is derived by the integral of the spectral tensors [1] as the below formula shows:

$$\gamma = \frac{|\int\int \Phi_{ij}(k) exp\left(-ik_y\delta_y\right) exp(-ik_z\delta_z) dk_y dk_z|}{\sqrt{\int\int \Phi_{ii}(k) dk_y dk_z \Phi_{jj}(k) dk_y dk_z}}, \quad (2\text{-}11)$$

where $j = 1,2,3$ for the longitudinal, lateral and vertical turbulent wind components. k is the wave vector, where $k_y \; and \; k_z$ is the wave number in lateral- and vertical direction. While $\delta_y \; and \; \delta_z$ is the separation distance in lateral- and vertical direction.

It is a desire to represent the coherence by a frequency spectrum instead of the wave spectrum as the formula above implies. This can be achieved by introducing the relation $f = \frac{kU}{2\pi}$, so that wave numbers are transformed into frequencies [6].

2.3 Data selection

To design wind turbines, it is important to have fundamental knowledge about meteorological aspects such as wind. When moving from shore to offshore environment, it is necessary to collect information on the offshore environmental characteristics in order to understand how the environmental components vary, to gain information about environmental generated loads, such as wind, which will affect the turbines.

2.3.1 Measurements

This knowledge starts with offshore measurements. It is difficult to get accurate measurements due to the need of good equipment in a dynamic environment. However, statistical approach can be used to assure the quality of the sampled data to exclude weirdness in the data which may occur during measurement. Ideally, one should measure at many points simultaneously, to map structures as a function of time and space.

The data used in this study is sampled at a meteorological mast located on the German research platform, FINO-1. The platform is placed in the North sea north of Borkum [38]. The meteorological mast is equipped with sonic anemometers which is an instrument for recording wind variables. Sonic anemometers are placed at the heights 40, 60 and 80 m. Instruments at heights within the rotor-swept area gives valuable environmental data to get more accurate information about the conditions in that area. Sampling frequency is set to 20 Hz for the anemometers at 40 and 80 m and 10 Hz for 60 m. In wind energy, it is normal to store samples in 10 minutes blocks due to the fact the relevant frequencies will be within this time frame. This will normally be sufficient for the natural periods for bottom fixed turbines and at the limit for the floating turbine, as this turbine have much longer natural periods.

FINO-1 has provided this study with 15 months of measured data. These data have resulted in high-quality time series by applying a processing procedure, explained by Nybø et al [9]. The steps to process these measured data will slightly be explained below and the overview of the steps is illustrated in Figure 2-v. The results from this procedure, reduced the available time series from 100 % to 26.7 % which is equal to data set of more than 6000 with 30 minutes periods [9]. The measured data provides a wide range of turbulence intensities at low wind speeds. The turbulence intensity is about five to ten percent for higher wind speeds. For further details, the referred article [9], gives a complete explanation on how the raw data undergoes a quality control with removal of disturbances that is not suitable for further analysis.

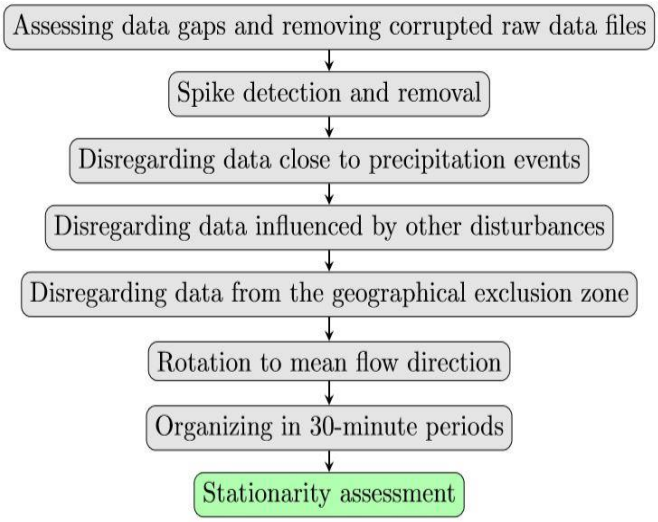

Figure 2-v - Processing procedure to obtain quality of sampled data followed by a stationarity assessment

- Data gaps:

The measured data contains some gaps of missing data due to maintenance of equipment, lightning strike, power failure or other mechanical problems. In these periods, the wind speed has not been recorded.

- Spikes:

By illustrating measured data in a time series, spikes are discovered. These are huge jumps in the wind velocity which stands out from the rest of the samples in the time series. It is considered as erroneous measurements.

- Precipitation:

Periods of precipitation disturbs the sonic anemometer sampling process. A sudden rise in the temperature measured with the sonic anemometers can be a consequence of rain, but it is observed that also the wind speed measurements are affected. The rain information measured at FINO-1 is considered not to be accurate. Droplets can stick to the anemometer transducers a while after the rain has occurred and thus the data from 10 minutes before and 50 minutes after rainfall is removed.

- Other disturbances:

Aerosol particles such as sea spray and unclear weather like fog can influence the accuracy of the sonic anemometers and are therefore excluded when periods of high temperature

fluctuations occur in the measurements. There are wind farms placed nearby FINO-1- Wind blowing from that direction, or from land to sea, is affected by either the wind turbines itself or other obstacles on land. The wind might also blow through the mast before reaching the sonic anemometers, which makes the flow influenced by the meteorological mast before it is measured. After these steps, the measured data should now only contain undisturbed, offshore wind.

- Rotation of the wind:

The three wind components sampled with the sonic anemometer are rotated into mean wind speed in the mean flow direction.

- Stationarity

When analysing the wind speed, it is important that time series possess stationarity, which means that mean and standard deviation is invariant over time. This is desired due to more predictable fluctuations within a stationary time series. A stationarity test is recommended by Nybø et al. [9] and is performed under a selection process of time series as described in the next section.

2.3.2 Selection process

After the processing of data, available wind speeds with associated atmospheric stability and turbulence intensity (TI) at the hub height, is found. The time series (the coloured dots) in Figure 2-vi have the duration of 30 minutes and are a result of combining the 10 minutes blocks from the measurements. The different colours represent the stability of the time series and the TI is based on an average of six 10-minutes intervals of 1 Hz, where standard deviation is assumed to be constant upwards from 80 m, where it is calculated [6].

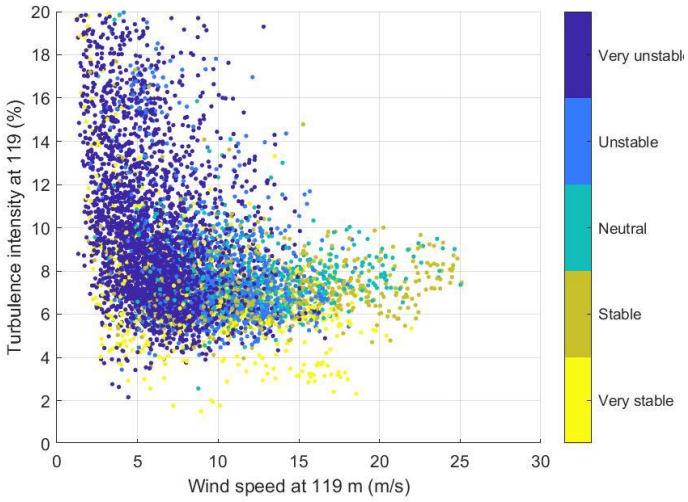

Figure 2-vi - Available turbulence intensity as a function of wind speed at 119 m with associated atmospheric stability (30-minutes periods)

Wind speed at 119 m is found from the point measurement at 80 m by using this height as a reference height and then the desire height is derived with the logarithmic wind profile, showed in equation (2-6). The roughness length included in the log law are calculated from 40 and 80 m wind speeds.

The stability is calculated by using data at 40 m. This boundary layer height is assumed to be within the surface layer, since the Obukhov length stability classification is only valid within this lower part of the boundary layer. To be able to get the stability information at 119 m, the classified stabilities are lifted to hub height from 40 m, with the assumption that it will be representative for the complete rotor area [6]. For further use, the 30 minutes time series were paired together into 60 minutes time series before generating wind fields. The reason for this, is the output length of the wind fields, which will have a favourable length when analysing wind turbine response in SIMA.

This study aimed to select untypical cases with high TI together with stability situations located outside its “normal region”. To exemplify it, one want to choose the time series with stable conditions (yellow dots in Figure 2-vi) located above the swarm of stable situations with high TI. The selected time series in the stable, unstable and neutral atmospheric conditions are scenarios from below rated, close to rated and above rated, which is relative to wind turbine rated wind speed. It is the minimum wind speed at hub height when the turbines rated power is achieved, which correspond to the wind speed of 11.4 m/s. The 90^{th} percentile was used as a limit for selecting the time series. Between the limits, the time series represent the normal occurring behaviour of the offshore wind. Therefore, the chosen time series is located outside the limit as the circle around the time series illustrates in Figure 2-vii.

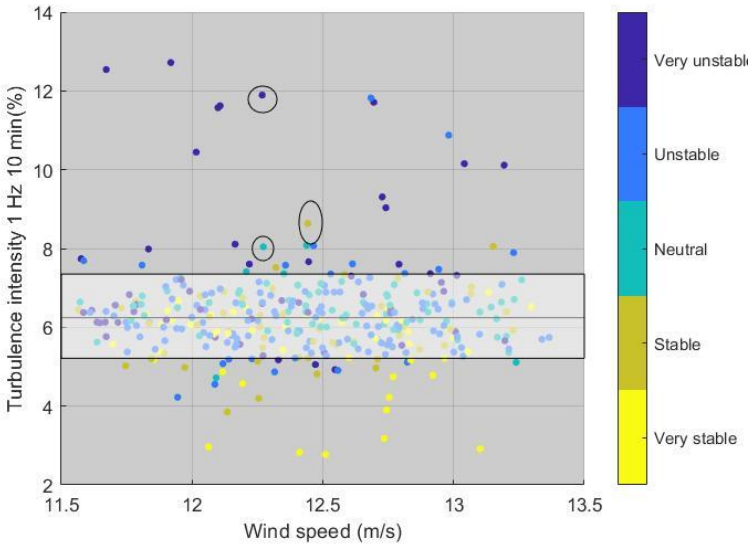

Figure 2-vii 90th percentile for selecting time series

The selection process was an iterative process. At first, yhe cases where chosen based on the figure above and then, the stationarity of the time series was evaluated. The two-step process of the stationarity test is described by Nybø et al. [9] and is a tool to evaluate the linear trend and the moving statistics of the time series. The chosen time series has been double checked with a manual inspection to exclude unexpected behaviours that has found its way past the processing procedure. Throughout this study, the temperature measured by sonic anemometer, shows that it might be erroneous. Yet, the errors are assumed to be small. These temperatures have been used in the stability calculations and may therefore be a contributor to stability uncertainties. However, by considering time series situated far inside the stability ranges, as shown in Table 2-a, it is assumed to be negligible. The nine chosen time series to be used in wind field simulation is presented in Table 2-e.

Table 2-e Selected time series for generating turbulence wind fields

BELOW RATED	Neutral	Stable	Unstable
Measuring time:	4 July 02:00	25 October 11:00	10 June 23:30
Wind speed:	7.92 m/s	7.47 m/s	6.81 m/s
Turbulence intensity:	7.53 %	8.21 %	14.95 %
MOL:	-1013.28	344.81	-359.08
RATED	Neutral	Stable	Unstable
Measuring time:	2 July 22:00	12 November 04:30	15 February 09:00
Wind speed:	12.44 m/s	13.15 m/s	11.67 m/s
Turbulence intensity:	8.08 %	8.05 %	12.54 %
MOL:	-1640.27	235.48	-44.09
ABOVE RATED	Neutral	Stable	Unstable
Measuring time:	13 November 14:00	23 December 13:30	22 November 19:00
Wind speed:	16.79 m/s	17.61 m/s	18.00 m/s
Turbulence intensity:	7.58 %	7.58 %	8.77 %
MOL:	-1816.10	387.86	-305.49

In Table 2-e, some of the stable conditions is formed during the day. Stable boundary layers can be formed during the day, when the sea surface is colder than the air. Reasons may be advection of warm air over a colder surface [17] or due to low-level jets (LLJs), which is fast moving ribbon of air in the low levels of the atmosphere [39], and is often located 100 to 300 m over the ground [17]. As reference describes [40], LLJs affects stable conditions by increasing the shear flow. For the means of a wind turbine, this might create more persistent wakes and increase loads. It can also occur under neutral conditions. Yet, for both stabilities, LLJs is a rare phenomenon.

Turbulence stable boundary layer may occur sporadically and be patchy, which allows the upper portions of the boundary layer to decouple from the surface regions [17]. The study performed by H. J. Breedt [41] aimed to describe neutral and non-neutral wind flow and found that turbulence increases during unstable conditions, which corresponds with the dominant unstable conditions with high TI in Figure 2-vi. Nybø et al, [6], showed that increasing the wind speed offshore, gives a more frequent, neutral atmospheric stability. Yet, variation in

atmospheric stability is expected to exist at high wind speeds due to low friction of the water surface, which Obukhov length represents by the term friction velocity shown in the eq. (2-3).

2.4 Wind field simulation

2.4.1 TurbSim

National renewable energy laboratory (NREL) has developed TurbSim [42] which is a tool to simulate stochastic, full-field, turbulent wind fields. This simulation tool origins from a program, called SNLWIND, written by Paul Veers in 1988. This program also generated full-field turbulent wind, but it was limited to only generate the flow for the longitudinal component [43]. However, NREL have added several spectral models to the program and modified it to generate the lateral and vertical velocity components as well [10]. TurbSim generates a two-dimensional turbulent flow field by combining a chosen spectral model and coherence model as the Figure 2-viii below illustrates. Variables of these models are given in an input file, together with specifications of the desired wind field such as spatial and temporal resolution.

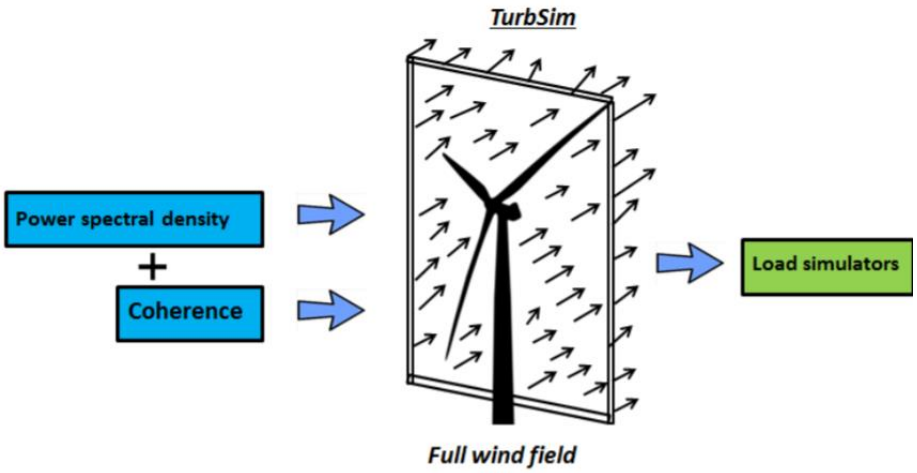

Figure 2-viii By combining spectral and coherence models, TurbSim creates a full wind field for load simulation for offshore wind turbines [44]

A code incorporates several optional spectral models and important fluid dynamic features with the purpose of simulating turbulence environments that is known to affect the turbine response and loading [10]. The overview of the TurbSim simulation method is shown in Figure 2-ix below. The processes influenced by parameters from the input file is indicated by blue lines, while the black lines correspond to processes performed by internal variables [10]. TurbSim is often used in conjunction with the recommended turbulence model, Kaimal. This study used TurbSim to generate turbulent wind fields by Kaimal and by an option called TIMESR, both cases are in more detailed in section 2.4.4 and 2.4.5

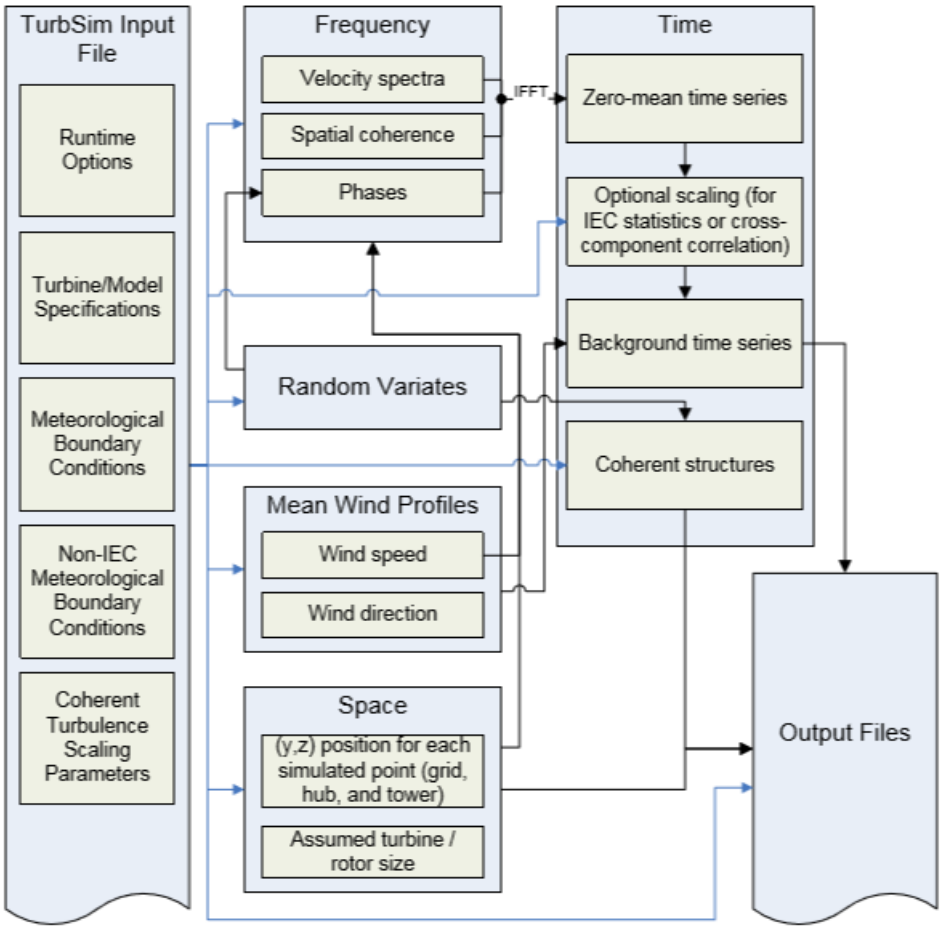

Figure 2-ix Flow chart of the simulation by TurbSim [10]

2.4.2 DTU Mann generator

The simulation of a synthetic wind field by using the Mann turbulence model can be performed by the DTU Mann generator [14]. As with TurbSim, this code is made for the intention of calculating wind turbine response in time domain [45]. The development of the code starts in 2003 and expanded further the following years. It was initially developed to be used with HAWC2, a low-fidelity wind turbine analysis tool. The Mann turbulence generator, provides a wind box containing fully coherent 3D-turbulence structures [45]. The wind box generated from turbulence generator is illustrated by Figure 2-x. Mann creates a wind box that is in principle a wind field in volume at a given time. This field is then ''pushed'' through the turbine. The field uses the «frozen turbulence» assumptions.

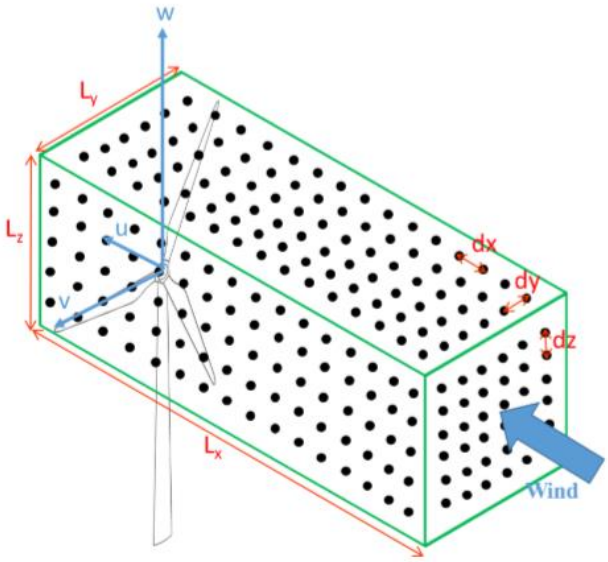

Figure 2-x Three-dimensional turbulent wind box simulated by DTU Mann generator. Where $d_{x,y,z}$ is the distance between simulated points and $L_{x,y,z}$ is the length scale of the turbulent eddies [14]

The user-defined input parameters in the generator, depends on how the user want to characterize the flow. The required input parameters for the DTU Mann turbulence generator is shown in Table 2-k, section 2.4.6.

2.4.3 Simulation cases

Several standard wind fields have been run using the recommended IEC turbulence models, Kaimal and Mann [1], varying in wind speed and stability. These are compared to close to realistic offshore generated wind fields, TIMESR. For this study, the wind turbine simulation uses these three different wind field generation techniques to compare the dynamical load response. TIMESR is created based on the measurements from FINO-1 while kaimal and Mann uses standard parameters. Yet, some of the standard parameters are adjusted to achieve the same shear profile, wind speed and turbulence intensity at hub height as the selected time series from measurements. This is to exclude the dominating effects from these input parameters, which can impact the dynamic response of the wind turbine [6], mainly because we want to see how different simulating methods provide turbulent flow characteristics, such as coherence and stability dependence of turbulent structures. The results by using these simulation tools, is twenty-seven wind fields for the three wind speed scenarios, with different atmospheric stabilities as Table 2-f, Table 2-g, Table 2-h shows.

Table 2-f Below rated wind speed generated wind fields

Scenario 1: Below Rated	**Wind field simulator:**
Case 1: Neutral	Mann generator
Case 2: Neutral	TurbSim: Kaimal
Case 3: Neutral	TurbSim: TIMESR
Case 4: Stable	Mann generator
Case 5: Stable	TurbSim: Kaimal
Case 6: Stable	TurbSim: TIMESR
Case 7: Unstable	Mann generator
Case 8: Unstable	TurbSim: Kaimal
Case 9: Unstable	TurbSim: TIMESR

Table 2-g Rated wind speed generated wind fields

Scenario 2: Rated	**Wind field simulator:**
Case 10: Neutral	Mann generator
Case 11: Neutral	TurbSim: Kaimal
Case 12: Neutral	TurbSim: TIMESR
Case 13: Stable	Mann generator
Case 14: Stable	TurbSim: Kaimal
Case 15: Stable	TurbSim: TIMESR
Case 16: Unstable	Mann generator
Case 17: Unstable	TurbSim: Kaimal
Case 18: Unstable	TurbSim: TIMESR

Table 2-h Above rated wind speed generated wind fields

Scenario 3: Above Rated	**Wind field simulator:**
Case 19: Neutral	Mann generator
Case 20: Neutral	TurbSim: Kaimal
Case 21: Neutral	TurbSim: TIMESR
Case 22: Stable	Mann generator
Case 23: Stable	TurbSim: Kaimal
Case 24: Stable	TurbSim: TIMESR
Case 25: Unstable	Mann generator

Case 26: Unstable	TurbSim: Kaimal
Case 27: Unstable	TurbSim: TIMESR

All the simulations have a simulation length, T, of 3800 seconds, where 200 seconds correspond to a transient period (free vibration period). The latter is a type of excitation caused by a sudden force loading, which, in this thesis, is the effects occurring in the initial time of the wind turbine simulations from the applied aerodynamic loading. It is a desire that these effects will die out within the first 200 seconds, in order to have one hour left for wind turbine simulation. However, during the wind field simulation it was found, that for some cases, the transient time should have been increased.

All cases are generated with the same grid height of 220.5 m, which is the distance between the bottom and the top of the field. The TurbSim guide [10], sets the requirement of ½ Grid height < hub height in order to have all points in the wind field above ground level. The grid width is set to be equal to the height. The user manual further recommends both to be at least 10% greater than the rotor diameter, DTU 10 MW is 178.3 m. Since the wind turbine simulation includes a floating wind turbine, which will move a lot during simulation, the grid size is set to be larger than this recommendation.

The wind fields are generated at 64 grid points in both lateral- and vertical direction with a spacing of 3.5 m. The time step in TurbSim is recommended to be 0.05 s for most simulations [10], but this recommendation is developed for smaller wind turbines. As this thesis studies larger wind turbines, a time step of 0.1 s is used. We expect this time step to be sufficient to cover all interesting eigenfrequencies of the wind turbine. The Mann model is run with a corresponding similar time step as explained in section 2.4.6. The turbine hub height, 119 m, is defined in the simulation to set the centre of the grid at this position.

2.4.4 Wind field simulation: TIMESR

As mentioned, the so-called TIMESR option in TurbSim are used to generate a wind field based on measurements of FINO-1. Time series of u-, v- and w- velocity components measured by the sonic anemometer at the points 40, 60 and 80 m, are specified directly by using an additional input file in TurbSim. First, TurbSim rotates all velocity points into the mean direction and the mean values are then removed so that the time series only contains fluctuations. Thereafter, a Fourier transformation is performed on the zero-mean time series to calculate the spectral amplitudes and the phase angles of the frequency components. In the frequency domain, values of the spectral amplitude for the simulated grid points in the y-z plane, is obtained by linear interpolation or by using the nearest-neighbour extrapolation [10].

By using Veers method in the numerical simulation, random phases are generated at each simulation point, dependent on chosen seed in the input file. These random phases are correlated with the phase angles of the time series from a reference point. The reference height is chosen to be 80 m, since it is the closest point to the hub, this height may provide more important phase information for the rotor swept area than lower heights [6]. The specified coherence model is used to ensure proper coherence between the simulated points and the input time series. The TurbSim guide, points out, that coherence between the simulated points and the input time series of other heights is not guaranteed [10]. For the same reasons as explained by Nybø et al. [6], the Davenport coherence model is chosen in the TIMESR wind field generations to ensure coherence between the simulated points and the time series from 80 m. The Davenport coherence model is similar to the IEC Kaimal coherence function, though simpler. When the terms b=0 and CohExp = 0 in the TurbSim input file, the general coherence model becomes the Davenport coherence model [10], which is given by:

$$\gamma = \exp\left(-C \cdot \frac{f \cdot \delta}{\bar{u}_m}\right), \tag{2-12}$$

Where f is the frequency, δ is the separation distance between the points x and y and $\bar{u}_m$ is the mean wind speeds of these two points. C is the decay coefficient which is calculated from measurements by finding the coherence between points in the vertical direction for the distance between 40-60 m, 40-80 m and between 60-80 m. The obtained decay coefficient values are shown in Table 2-i, which are implemented in TurbSim to calculate the coherence for the wind fields. As highlighted by Nybø et al. [6], by using several distances, the statistical uncertainty of the coherence are reduced. We can further expect that more distances and longer periods would reduce the uncertainty even more.

Table 2-i The decay coefficient obtained from measurements and used as input in TIMESR

Wind speed (m/s)	**Atm. stability**	**Decay coeff.** C_u	**Decay coeff.** C_v	**Decay coeff.** C_w
7.5	Unstable	18.0	10.3	4.0
7.5	Stable	19.5	8.8	4.3
7.5	Neutral	10.4	7.7	3.8
12.5	Unstable	8.0	6.0	3.9
12.5	Stable	12.1	8.5	4.4
12.5	Neutral	11.4	7.8	4.8
17.5	Unstable	13.2	9.4	5.7
17.5	Stable	17.9	10.8	5.5
17.5	Neutral	12.3	8.5	4.9

As shown by the cases of Table 2-i, the coherence coefficients are largest in the longitudinal direction and lowest in the vertical. This is in correspondence with the findings of Etienne et al. [46], also studying the coherence at FINO1. It means that the coherence decays faster with reduced frequency (definer) in the longitudinal direction. We may also observe that the stable cases have larger coherence coefficients, also consistent with Etienne.

The wind profile input file is derived by using a logarithmic wind profile, defined by equation (2-6). The wind speed is calculated for each height for the 64 grid points in the wind fields before using it as an input parameter in TurbSim. The logarithmic wind profiles are dependent on stability. The profile is added to the wind field after the turbulent structures are simulated and the mean wind speeds from the measurements at 80 m are also re-introduced. This way of profiling the wind speed is dependent on the roughness length, which is calculated from 40 and 80 m.

2.4.5 Wind field simulation: Kaimal

The program, TurbSim, starts the simulation in the frequency domain where the velocity spectra and spatial coherence is defined before an inverse Fourier transform is applied to produce the time series [42]. By using the IEC Kaimal in TurbSim, the velocity spectra and standard deviations is assumed to be invariant across the grid. The only variation is the standard deviation of the u velocity component occurring due to the inclusion of the spatial

coherence model [10]. As for TIMESR, the coherence function calculates neighbouring points' variation in the field depending on the separation distance [14].

As mentioned under simulation cases in section 2.4.3, it is a desire that all simulated wind fields have the same hub height wind speed, shear profile as well as the same turbulence intensity at hub height. These factors can dominate the results, which is wanted to be excluded.

The wind profile is scaled by the power law as recommended by the IEC standard [24]. The power law shear exponent, α_p, is adjusted to fit the measurement situations. It is derived using the wind speeds from the selected time series, thus the atmospheric stability is included, as shown in Table 2-j. This makes it possible for TurbSim to reproduce the exact wind speed at hub height. The turbulence intensity is also derived from these time series by averaging six 10 minutes 1 Hz blocks, as mentioned in section 2.1.1.

Table 2-j Power law exponent (α_p) derived for neutral, stable and unstable atmosphere.

	Neutral	Stable	Unstable
Below Rated	0.0561	0.0211	-0.0267
Rated	0.0589	0.0759	0.0045
Above Rated	0.0596	0.0844	0.0125

2.4.6 Wind field simulation: Mann

Mann is generated as a three-dimensional wind box, which requires a definition of several grid points in the x direction as well, denoted as N_x. The DTU software requires the grid points for the turbulent box to be 2^n [14], where n is an integer. To obtain a similar time step as TurbSim, an integer of 15 is chosen. The time step is given by dividing the simulation length of 3800 seconds by N_x, which results in a time step of 0.116 s. Each grid point in the box represent a spatial location as well as providing information about the local wind speed for *u*, *v* and *w* components [14]. As with TurbSim, the wind field is created to have enough grid points to cover the whole rotor swept area of the wind turbine. The spatial resolution between points in the longitudinal direction varies for each simulation case and is found as followed,

$$d_x = \frac{T \cdot \overline{u_x}}{N_x}, \tag{2-13}$$

where T is the simulation time (3800 s) and $\bar{u}$ is the mean speed at hub height in the longitudinal direction.

The "energy dissipation of eddies" parameter, $\alpha\epsilon^{2/3}$, varies for each selected time series. This is a way to include the same turbulence intensity at hub height as from the measurements. Hence, the same TI as Kaimal and TIMESR for the same wind speed and atmospheric stability simulation run. It is calculated as follows [1]:

$$\alpha\epsilon^{2/3} = \frac{55}{18} \cdot 0.4754 \cdot \sigma_{iso}^2 \cdot l^{-\frac{2}{3}}. \quad (2\text{-}14)$$

and the IEC standard describes the isotropic variance as [1]:

$$\sigma_{iso} = 0.55 \cdot \sigma_u, \quad (2\text{-}15)$$

where the standard deviation σ_u, is the one including characteristics from measurements. The input parameters to simulate the Mann wind field is included in Table 2-k.

Table 2-k Input parameters for simulating Mann turbulent wind field.

Description	Fixed simulation parameters
Number of grid points in the longitudinal direction (x-direction)	$N_x = 32768$
Number of grid points in the lateral direction (y-direction)	$N_y = 64$
Number of grid points in the vertical direction (z-direction)	$N_z = 64$
N provides the wind field size:	$2^{15} \cdot 2^6 \cdot 2^6 = 32768 \cdot 64 \cdot 64$
Spacing between grid points (x-dir.). This varies for each simulation case, equation (2-13).	d_x
Spacing between grid points (y-dir.)	$d_y = 3.5$
Spacing between grid points (z-dir.)	$d_z = 3.5$
The length scale of the turbulent box	$L = 33.6$
A non-dimensional shear distortion parameter	$\Gamma = 3.9$
Dissipation rate of turbulent eddies	$\alpha\epsilon^{2/3}$

After the Mann generator simulation, the files from the generated wind fields, are adjusted manually using a MATLAB routine, adding a mean wind profile. Here, the mean wind speed in the field is scaled using the power law wind profile, eq. (2-4), with the same shear exponent as used in Kaimal. In the scaling procedure, the standard deviation is adjusted to get the same standard deviation as Kaimal and TIMESR (by including the TI in $\alpha\epsilon^{2/3}$, we obtain a wind field with a TI similar to the desired one but not equal to). The scaled wind speed for each grid height is defined manually in the wind turbine simulation software, SIMA.

3 Offshore wind turbine characteristics

3.1 DTU 10 MW RWT

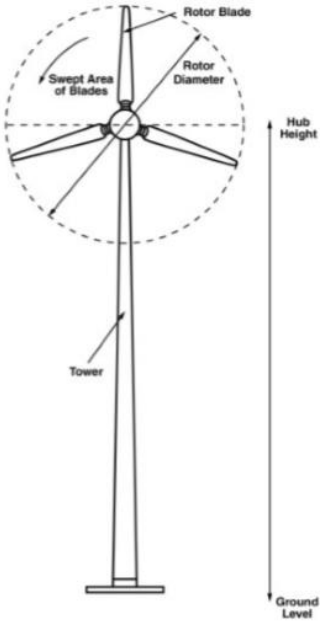

Figure 3-i HAWT wind turbine

The two wind turbines used in this study is based on the DTU 10 MW reference turbine [12]. Except for the blades, the whole turbine is a upscaled version of the NREL 5 MW reference wind turbine [47]. Figure 3-i illustrates a horizontal axis wind turbine (HAWT) from the bottom to the tower top, including the hub height and the rotor swept area of the blades. Behind the hub component, there is a motor house called nacelle, housing the gear, brake, generator and the control system. The latter is important for controlling the turbine by pitching the blades under aerodynamic loading in relation to get maximum power output. These two turbines are similar, except for the substructure, which is connected to the tower bottom. The bottom fixed turbine has a monopile substructure and the other one represents the floating offshore wind turbine with a Spar buoy. The key parameters for the DTU 10 MW RWT is shown in Table 3-a [12].

Table 3-a Key parameters of the 10 MW reference turbine [12]

Parameter	**DTU 10 MW RWT**
Wind regime	IEC Class 1A
Rotor Orientation	Clockwise rotation - Upwind
Control	Variable speed Collective pitch
Cut in wind speed	4 m/s
Cut out wind speed	25 m/s
Rated wind speed	11.4 m/s
Rated power	10 MW
Number of blades	3
Rotor diameter	178.3 m
Hub diameter	5.6 m
Hub height	119 m
Drivetrain	Medium speed, Multiple stage gearbox
Minimum rotor speed	6.0 rpm

Maximum rotor speed	9.6 rpm
Maximum generator speed	480.0 rpm
Gearbox ratio	50
Maximum tip Speed	90 m/s
Hub overhang	7.1 m
Shaft tilt angle	5.0 deg
Rotor pre-cone angle	-2.5 deg
Blade pre-bend	3.332 m
Rotor mass	227.962 kg
Nacelle mass	446.036 kg
Tower mass	628.442 kg

3.2 Support structures

There are several designs of the wind turbine substructure, as Figure 3-ii illustrates.

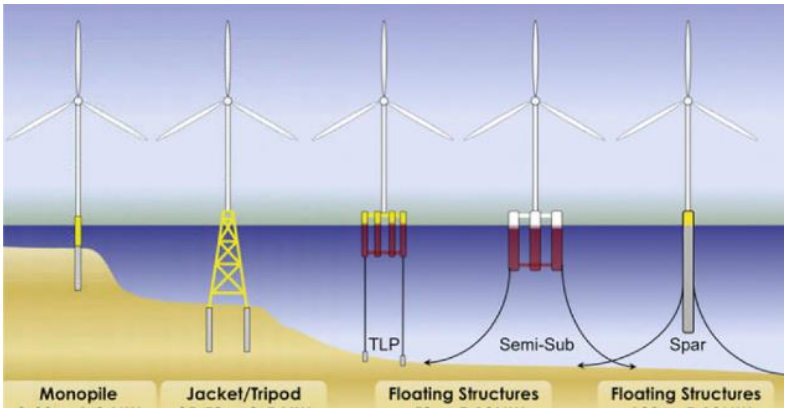

Figure 3-ii Offshore wind turbines with different substructures (https://www.windpowerengineering.com/projects/offshore-wind/foundations-that-float/)

The monopile to the left and the floating structure, spar to the right, are the two sub-structures considered in this study. They both support the tower.

3.2.1 Monopile

The monopile is a frequently used sub-structure for the bottom-fixed wind turbines. It is connected to the tower through a transition piece. From the tower bottom and down to the seabed, it continues into the soil, with its tabular structure and constant diameter. The task of the bottom fixed structure is to transfer the weight and the environmental loads to the seabed

[48]. As the latter reference describes, the loads appearing at the rotor due to the wind, will be transferred downwards causing bending loads in the support structure. The structure is used in shallow waters and DNV-GL recommends a water depth of 0 – 25 m [49].

The DTU 10 MW RWT with monopile substructure used in this study, is described in reference [11]. The monopile is designed for 30 m water depth and is extended with 42 m below the mudline. The transition piece (TP) extends from 10 m below the sea water level (SWL) to 11.5 m above SWL. The outer diameter of both the monopile and the TP is 9m [11]. Sørum et al.[11] have studied the DTU 10 MW RWT with a monopile foundation and as this is the bottom fixed turbine used in this study, we assumes that the model is acceptable for wind turbine simulation.

3.2.2 Spar

A floating sub-structure is needed in larger water depths such as 120 to 300 m. In this study, a spar sub-structure is considered and according to Skaare et al. [50], a slender deep draft hull make static stability requirements easy to fulfil. This floating body can move as a rigid body in six degrees of freedom (DOF), also denoted as modes [48]. A cartesian coordinate system is used. The x-y plane is at the mean water level, x pointing in the mean wind direction and z is positive upwards.

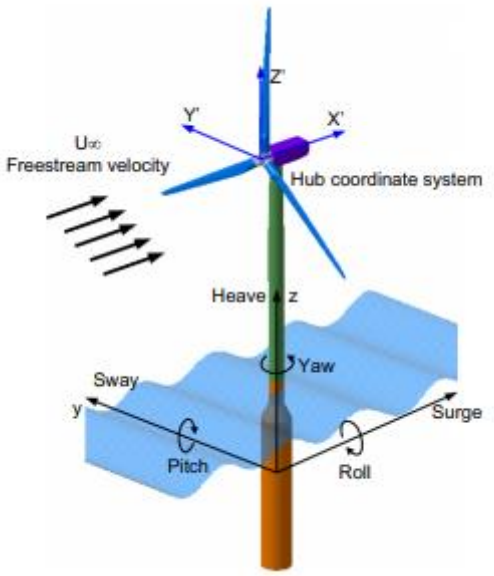

Figure 3-iii The degrees of freedoms of a floating sub-structure [51].

As Figure 3-iii shows, the movements consist of three translation modes and have three possible ways to rotate. It is defined as surge, sway, heave, roll, pitch and yaw, which Table 3-b give an overview of.

Table 3-b The modes of motion for a floating sub-structure

Degrees of freedom	
Surge:	Translation in the mean wind direction, x-axis. (Longitudinal direction)
Sway:	Translation along the y-axis (Lateral direction)
Heave:	Translation along the z-axis (Vertical direction)
Roll:	Rotation about the x-axis
Pitch:	Rotation about the y-axis
Yaw:	Rotation about the z-axis

These motions are a response to the environmental loads. To keep the spar sub-structure in position, a mooring system is needed. This consist of chains and anchors. As the chains keeps it in place, they also contribute to dampen the motions of the floater [3]. The spar floater, received for use in this thesis, is described by reference [52] and the main dimensions of the sub-structure is given in Table 3-c.

Table 3-c Structural properties of the spar floater [52].

Spar body	**dimensions**
Draft	120 m
Elevation to platform top	10 m
Depth to top of taper below SWL	4 m
Depth of bottom of taper below SWL	12 m
Platform diameter above taper	8.3 m
Platform draft diameter below taper	12 m
Platform mass	1.17e07 kg

The tower bottom is connected to the elevation of the spar platform 10 m above SWL. The top of the platform is connected with the deep draft by a linearly tapered conical region, which extends from 4 m to 12 m below the SWL. As reference describes [52], the purpose is to reduce hydrodynamic loads near the surface. The dimension of the spar shows that the diameter of the main hull is larger than the cylinder at the water line. The correct ratio between these two will obtain the heave natural period [48]. The large draft is the reason for large moment of inertia in roll and pitch modes which, as reference [48] states, makes it easier to obtain large natural periods in these motions. The latter reference also describes how proper ballasting

can control the moment of inertia in roll/pitch, such that desire natural periods in these modes can be obtained. The mooring lines for a spar body is normally equipped with a crow-foot configuration (delta line) as illustrated in Figure 3-iv below. The meaning behind this configuration is to let the mooring line system take up the forces instead of the structure. The mooring system avoids that the structure drift from its location and secure required stiffness in the yaw motion of the overall structure. It has an important task to withstand wind induced mean yaw forces as well as tuning the yaw natural period [53].

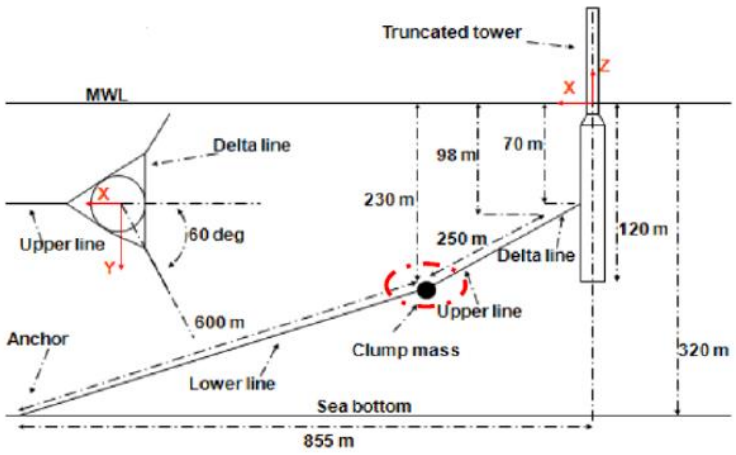

Figure 3-iv Example of at mooring system with crowfoot configuration for a spar sub-structure [52].

The mooring system is changed in order to simplify the modelling and analysis. The changes are explained by W. Xue [52] like this:

"First, the delta connection is eliminated, which means that an additional linear yaw stiffness should be added to the system to achieve the sufficient yaw restoring force. Second, all the catenary lines with multiple segments are replaced by a uniformly distributed line, with average values of the mass, weight, and stiffness. Third, all the damping of mooring system is neglected. To be honest, these simplifications are suitable for static analysis, but may not be appropriate in all dynamical conditions" (p.46).

Therefore, an inclusion of damping in the yaw mode had to be considered. The main properties of the mooring system used in this study, is given by [52] and are summarized in Table 3-d.

Table 3-d Properties of the mooring system [52].

Number of mooring lines	3	
Angel between adjacent lines	120	deg
Water depth	320	m
Depth to fairleads below SWL	70	m
Radius to fairleads from spar centerline	6.5	m
Radius to Anchors from spar centerline	855.17	m
Unstretched mooring line length	902.2	m
Mooring line diameter	0.09	m
Equivalent mooring line mass density	233.1198	kg/m
Equivalent mooring line axial stiffness	384,243,000	N
Additional yaw spring stiffness	147,510,000	Nm/rad

3.3 Modification of the spar floater

To achieve the best dynamic starting point for the spar floater before simulation, it has been modified. The reason for the modification is due to development of simulation tool over the last years and wind turbine evolvement. As well as the desire to have two identical turbines, except for the controller, for the simulation and for comparison of results. The floating wind turbine is adjusted with the same specifications as the 10 MW bottom fixed turbine[11], which is based on the DTU 10 MW RWT, except for the monopile support structure. Some modifications are performed to fit the turbine into a floating system and explained in the following sections. The new 10 MW spar floating wind turbine is composed of tower, rotor, hub and nacelle, borrowed from the bottom fixed turbine. This excluded the differences within foil modelling.

3.3.1 Tower adjustment

The tower needed a smaller adjustment due to different mounting with the spar sub-structure. The transition piece from the original tower was removed and the extension of spar, 10 m above SWL, worked as a connecter with the tower. To compensate for the missing tower length due to removal of TP, the tower length was adjusted, such that the turbine corresponded to the actual turbine height. The new tower mounted on spar, was heavier than the previous tower. Therefore, a mass reduction of the sub-structure was performed in order to float at correct draft. The amount of weight removal is performed by calculating the difference of the properties above the SWL between the previous and the new turbine. A heavier tower also led to slightly improper value of the centre of buoyancy (CB), which is

placed on the spar body above centre of gravity (CG). CB is an opposite force to CG and provides vertical displacement to support the weight of the turbine. A large distance between CG and CB together with the displacement signify large enough restoring forces in roll/pitch to ensure a small static roll/pitch [48]. The corrected values are listed in Table 3-e.

Table 3-e Adjustment on the spar sub-structure

Corrected component	Old value	New value
Spar weight	1.18e07 kg	1.17e07 kg
Buoyance force	131.5 MN	13.156 MN

3.3.2 Controller adjustment

Both turbines have used the basic DTU 10 MW controller [54], but it has been modified for the spar floater with some adaptions to avoid controller-induced instabilities of the overall system. When the DTU 10 MW RWT is mounted onto the spar platform, it may experience some pitch resonant motion in the above rated wind speed region, which is caused by negative damping from the blade pitch controller, as shown by reference [55].

The controller is based on the classical proportional-integral control theory [12] and Jonkman et al. [47] explains that the full-span rotor-collective blade-pitch-angle commands are computed using gain-scheduled proportional-integral (PI). The goal of a blade-pitch control system is to regulate the generator speed [47] and is obtained for the floating wind turbine by reducing the proportional-integral gains. The blade pitch controller natural frequency will then be lower than the platform pitch frequency (0.025 Hz) and is more likely to avoid resonance with the eigenfrequency of the floater. The original blade-pitch control system had a natural frequency of 0.06 Hz (DTU 10 MW RWT) as specified in the first row in Table 3-f. There is a special need of active damping in the turbine in wind speeds above rated. If one uses the control algorithms for a bottom fixed turbine, the system will be unstable. The originally spar floater had modified the blade pitch natural frequency to 0.02 Hz [52], shown in the second row in Table 3-f. As we thought this was to close to the pitch eigenfrequency, we reduced it to 0.01 Hz. This was to eliminate negative damping, which can cause a build-up of resonance in platform pitch. The thought was that a lower frequency in the controller would improve the platform pitch response, since the controller would pitch the blades such that the system would experience faster damping. This is a primitive way of solving the problem, which may cause additional loads at higher frequencies due to the slow regulation.

To derive the controller response natural frequency, it follows the equation of motion for the rotor speed error and is explained by Jonkman et al. [47]. The values of the original and reduced gain constants are included in Table 3-f.

Table 3-f Modification of the PI gain constants of the DTU blade pitch controller.

Wind turbine	**Proportional gain of pitch controller [rad/(rad/s)]**	**Integral gain of pitch controller [rad/rad]**	**Blade pitch controller natural frequency [Hz]**
10 MW RWT	0.524484	0.262243	0.06 Hz
10 MW spar from [52]	0.174828	0.0156993	0.02 Hz
New 10 MW spar	0.087414	0.003924825	0.01 Hz

Example of the pitch mode response when the blade pitch controller natural frequency is changed from 0.02 Hz to 0.01 Hz in Figure 3-v and Figure 3-vi below. Full test in Appendix C.

.

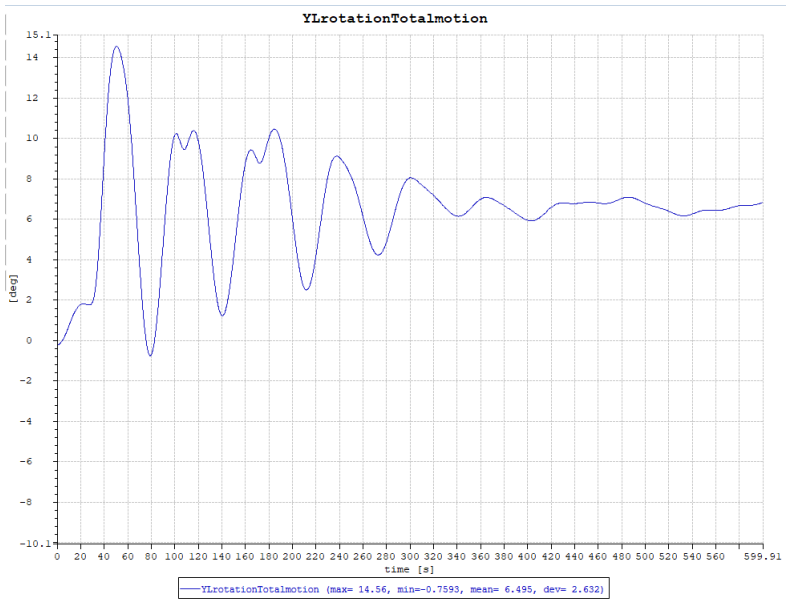

Figure 3-v The pitch motion response to uniform 12 m/s wind test (0.02 Hz)

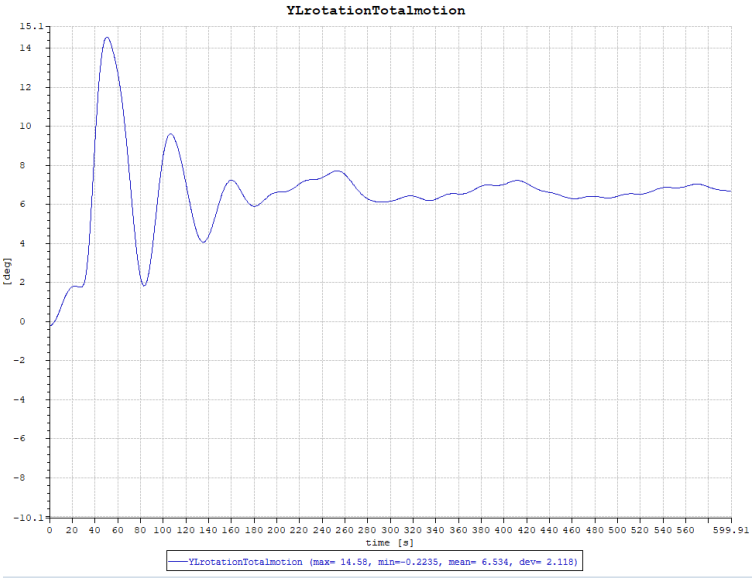

Figure 3-vi The pitch motion response to uniform 12 m/s wind test (0.01Hz)

Wind velocities can provide overload in the generator due to increasing load when the rotor speed fluctuates. A second modification is made to the controller to avoid these fluctuations. Thus, control switch in the controller input file is changed from a constant generator power to a constant generator-torque control strategy.

The simulation in SIMA crashed after 2000 s with the above rated wind speed scenarios. Some tests due to this problem can be seen in Appendix D, which showed that it occurs build-up of oscillations in the yaw rotation before the simulation fails. It seems like that instabilities did not occur due to classical negative damping in the pitch motion. It looks like a motion in the y-(rotor) plane triggers an unstable behaviour.

We could try to make the blades stiffer, but this makes the blades different from the bottom fixed wind turbine. The time step in dynamic analysis could be lowered to 0.005 s or 0.0025 s, which could solve the problem if it is caused by numerical reasons. It was tested with 0.005 s, which fulfilled the simulation run but the build-up of oscillations towards the end of the simulation was still present. Yet, it was concluded that this only shifted the problem.

The system may become physical unstable due to the controller and the controller functionality to reduce the yaw-motion should be studied more. In this study, we used a so-called “sledgehammer method” which dampen the yaw motion such that the system has a stable behaviour.

3.3.3 Decay tests

If the structural properties are changed, the natural frequency of the structure, mass and damping also changes [4]. Therefore, decay tests have been performed to see how the system reacts and to evaluate the damping level. These tests were performed by interacting the tower top with a ramp force which was released after 100 s. The wind turbine structure will then oscillate around its initial position and the movements will be damped within a natural period. This leads the system back into initial position. The aim of the first test is to find the natural periods of all six DOF. The natural periods obtained from these tests are shown in Table 3-g.

Table 3-g Natural periods of the spar floater obtained by decay tests

Mode	Natural period (seconds)
Surge	134.4 s
Sway	135 s
Heave	31.5 s
Roll	40 s
Pitch	40 s
Yaw	10.2 s

The natural period of the translation modes of surge and sway are larger than 100 s, which is expected, as these movements are normally large. This is due to the limited restoring stiffness from the mooring system [52].

The second decay test had an aim to find the correct damping ratio for the movements of the spar floater. As mentioned earlier, the mooring lines was simplified and thus it was necessary to insert the system with damping to compensate for this. The damping level of the system is solved mainly by quadratic drag, which is defined in SIMA under hydrodynamic properties of the spar platform. Only a small value of linear drag was implemented to reduce vibrations, this to prevent numerical problems in the dynamic analysis. This was a challenging «back and forth»-process, which consisted with a lot of tuning to find sensible decay. This is due to the coupling between the degrees of freedom. More details in Appendix C.

When the decay test was performed, logarithmic decrement was used to estimate the system damping ratio. The logarithmic decrement, δ, is found by dividing the initial amplitude, x_0, by the second amplitude, x_n, as equation (3-1) below shows.

$$\delta = \ln\left(\frac{x_0}{x_n}\right). \tag{3-1}$$

The logarithmic decrement can then be divided by 2π to find the damping ratio, ζ, as it appears below.

$$\zeta = \frac{\delta}{2\pi}. \tag{3-2}$$

The decay test results with chosen damping ratio for the global motion of the spar sub-structure are shown by Figure 3-vii, Figure 3-viii, Figure 3-ix and Figure 3-x.

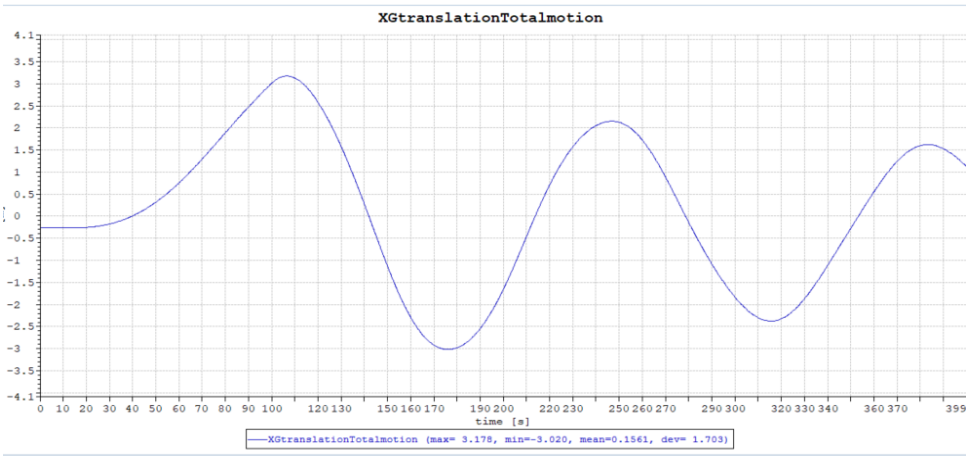

Figure 3-vii Performed decay test to investigate the damping ratio of the surge motion.

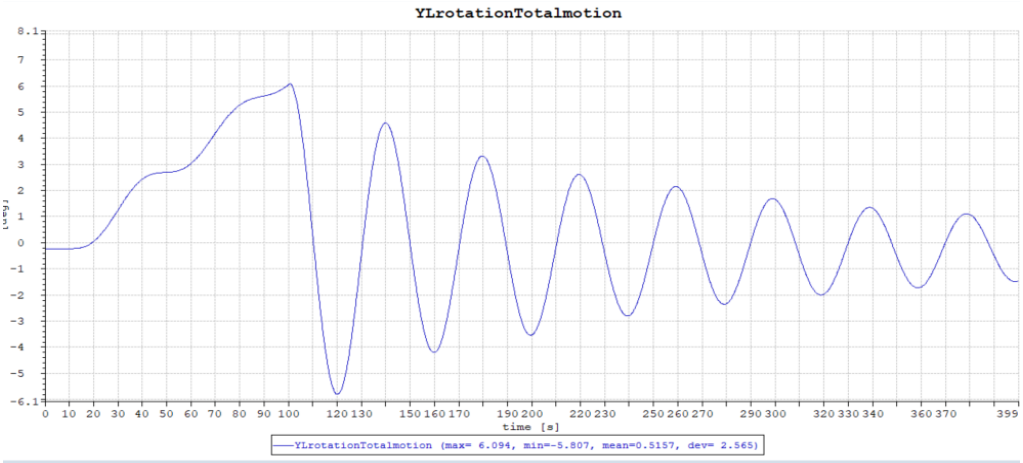

Figure 3-viii Performed decay test to investigate the damping ratio of the pitch motion.

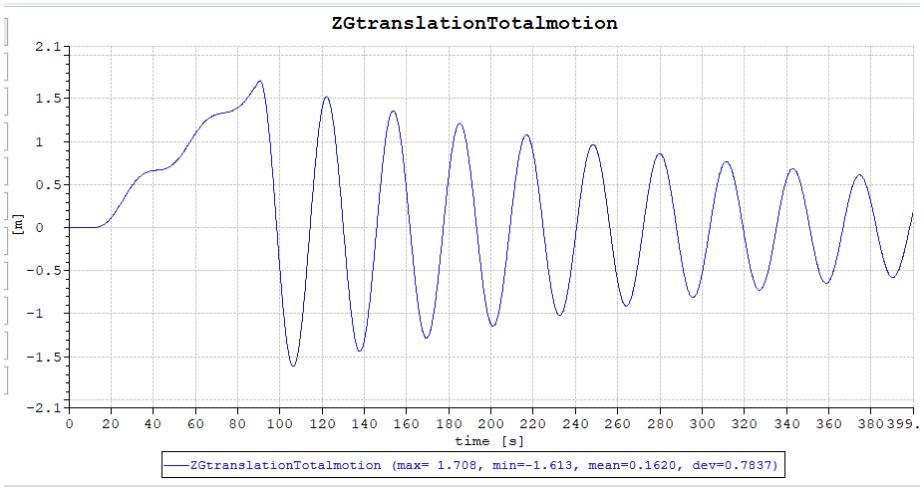

Figure 3-ix Performed decay test to investigate the damping ratio of the heave motion.

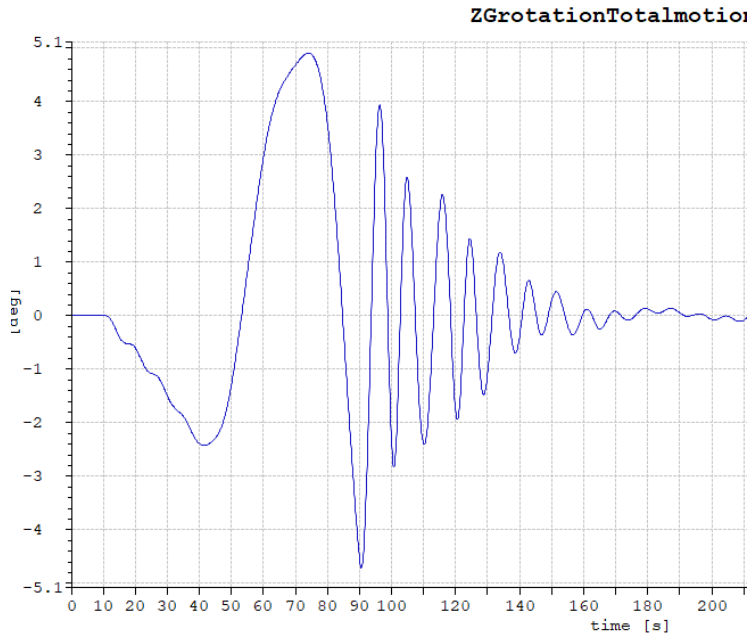

Figure 3-x Performed decay test to investigate the damping ratio of the yaw motion.

Since surge and sway gives about the same result in the tests, as well as pitch and roll, only surge and pitch are presented. It is also worth mentioned that the yaw decay tests were performed before the "sledgehammer method" was applied.

3.4 Dynamic analysis

The turbine dynamics depends on the excitations from wind (and waves), which are acting on the structure as well as its natural frequencies [14]. For the floating wind turbine, excitations from the six global modes also affect the dynamics. Offshore wind turbines are continuously exposed to dynamic and cyclic loads due to wind and operation forces. The turbulent wind

from various wind field formulations are used in this study as aerodynamic loading to analyse components that are subjected to bending stress. This is important to study since a wind turbine may lead to fatigue damages due to cracks in the components that are exposed to the dynamic loads over a longer period. Igwemezie et al. [56] describes the loads impacting the turbine and lists the various sources as:

- Steady loads from high winds
- Wind shear
- Yaw error and motion
- Stochastic loads from turbulence
- Transient loads from gust events
- Operational start and stop of the turbine
- Resonance-induced loads from vibration of the wind turbine structure

3.4.1 Simulation tool

SIMA (Simulation of Marine Operations) is a software for simulation of marine operation from modelling to dynamical analysis results. This software can perform simulations with coupled effect of waves, winds and currents for structural or mooring analysis. The complex floating offshore wind system need efficient calculations, and computations in SIMA are based on the well-known and efficient solvers, SIMO and RIFLEX [57], which is programs that will run in the background under the control of SIMA, when performing dynamical analysis. RIFLEX can perform calculations on flexible structural components, while SIMO is suited for study of multiple rigid bodies with various non-linear connections.

3.4.2 Input parameters for load analysis

The only environment used in this study, is the wind, but the wave conditions had to be included in order to run the program, with the small wave height of 0.0001 m. All runs have a simulation length of 3800 s. The Kaimal and TIMESR inflow fields is simulated with a time step of 0.01 seconds, while Mann is specified with a time step of 0.016 seconds. More specifications directly in SIMA are needed when Mann is used as the environmental input. All inputs in SIMA are given with more details in Appendix B.

3.4.3 Turbine control systems

Skaare et al. [50] points out that the combined wave and wind loads, and the choice of blade-pitch control strategy, stands for the main challenges for the floating wind turbine. This study is focusing on aerodynamical loading, which is defined by the IEC as the static and dynamic load caused by airflow. This interacts with the stationary and the rotational parts of the wind

turbine. The cut in and cut out speed, is the start and stop of the blade rotation for wind harvesting, as illustrated in Figure 3-xi.

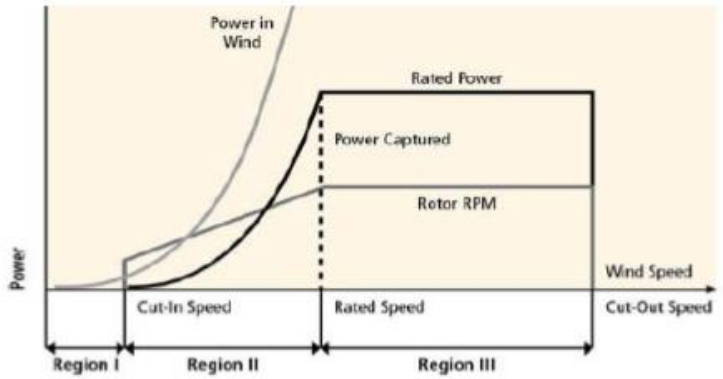

Figure 3-xi Diagram of captured wind power.

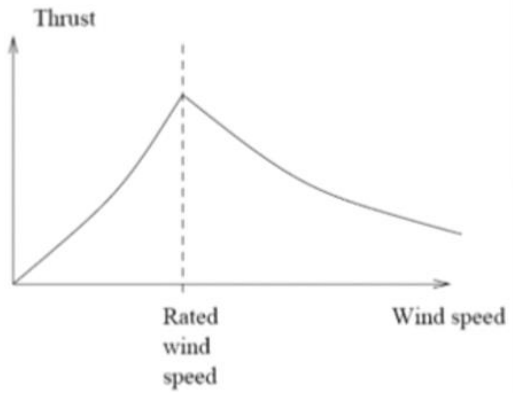

Figure 3-xii Wind turbine thrust force at different wind speeds

The different regions of occurring wind speed is explained below:

- Below rated wind speed:

The wind speed inside the partial load region is the region two, as illustrated in Figure 3-xi. The blade has a constant pitch angle and the rotational speed is increasing for capturing as much energy as possible from the wind flow. In this region, the thrust force is increasing towards rated wind speed as Figure 3-xii shows. This side of the curve is implying a positive damping for the wind turbine system [58]. Meaning that a build-up of oscillations due to the systems displacements is not occurring.

- Rated wind speed:

Wind speed about 11.4 m/s is considered as rated wind speed. This is when the turbine experiences maximum thrust force, thus maximum power output. This region lies between region two and three in Figure 3-xi.

- Above rated wind speed:

High wind speed stream in region 3. This is a region where the system strives to operate in a constant power regime. The rotational speed is kept constant and the blades is controlled to achieve the constant power output by variable pitch angles, which will minimize structural loads. As illustrated at the right side in Figure 3-xii, the turbine loses thrust force when the blades pitch due to increased wind speed. This region may imply negative damping [59], which can cause build-up of oscillations, in particular platform pitch. This is a problem for the floating wind turbine because the wind will give more energy around the natural period in pitch, in this region [50]. The reference [53] describes how this must be controlled by active damping implemented in the controller and further explains how they take advantage of individual pitching of the blades to also control the platform roll and yaw motions.

3.4.4 Natural frequency assessment

The natural frequency, also referred to as the Eigen-frequency, is the frequencies of the structural behaviour due to loading. The aerodynamic loading will cause many components in the wind turbine to vibrate. The natural frequency of these vibrations, depends on structural dimensions [56]:

- The height of the tower
- Wall thickness of the tower
- Diameter of the support structure

These are the eigenfrequencies for the elastic deformations. For the floating platform, the eigenfrequencies of the platform movements must also be considered. The natural frequency also depend on structural materials, which is often steel [56]:

- The top mass (weight), which includes: rotor blade, hub and nacelle.
- Installation and maintenance platform on the wind turbine.
- For the bottom fixed: soil-structure and water depth.

The first natural frequency of the tower movement, is important to assess when performing structural analysis and as reference [60] points out, wind spectrum, wave spectrum and operational intervals of the rotor is the forcing frequencies that also must be considered. The frequency ranges for the different described dependencies are illustrated in Figure 3-xiii.

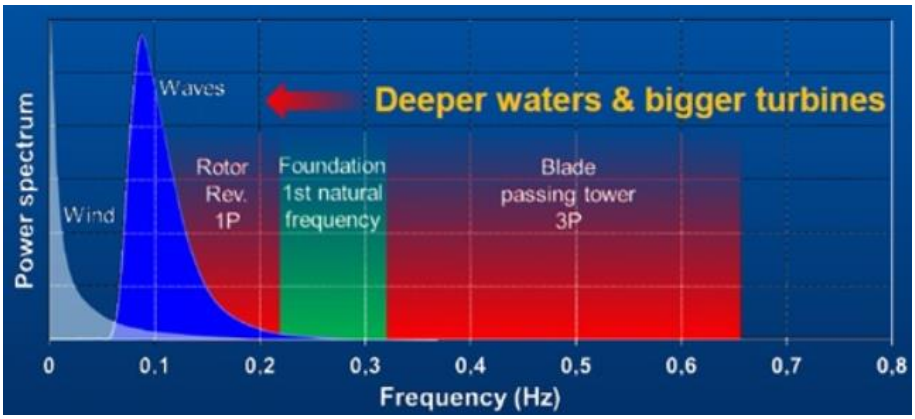

Figure 3-xiii Power spectrum as function of frequency [60]

As Figure 3-xiii illustrates, wind spectrum has lower frequency range compared to the frequencies of the rotor operation. Sørum et al. [11], have studied and tested the functionality of the bottom fixed turbine, used in this study, and has for instance reduced the natural period by increasing the wall thickness of the tower by 20%. Reference [56] points out that an reduction of natural frequency may bring it closer to the low frequency forcing of the wind, which increases the risk of occurring resonance. Resonance may enhance structural stress due to combination and build-up of maximum amplitudes [56]. The offshore turbines have a shape as a long slender column with a heavy mass on top as well as a rotating mass. Bhattacharya et al. [61] states that such shape has a natural frequency close to the excitation frequencies imposed by environmental and operational loads and thus, are dynamically sensitive. One of the important parameters to determine the dynamic response of the offshore wind turbines, are the rotational frequency of the blades [14]. This is referred to the 1P and 3P frequencies. The 1P is the constant rotor rotational speed, varying with different types of wind turbine speed mechanisms [61]. The excitation frequency, due to rotational speed of the DTU 10 MW RWT has the operational range between 6 RPM and 9.6 RPM, i.e. 0.1-0.16 Hz. When the blade is in front of the turbine tower, during operation, it will cause vibrations due to the wind shade effects as illustrated to the right in Figure 3-xiv. As seen in the figure, the wind loading on the tower is reduced, yet the structure will experience additional dynamical loading, referred as the excitation frequency, 3P load.

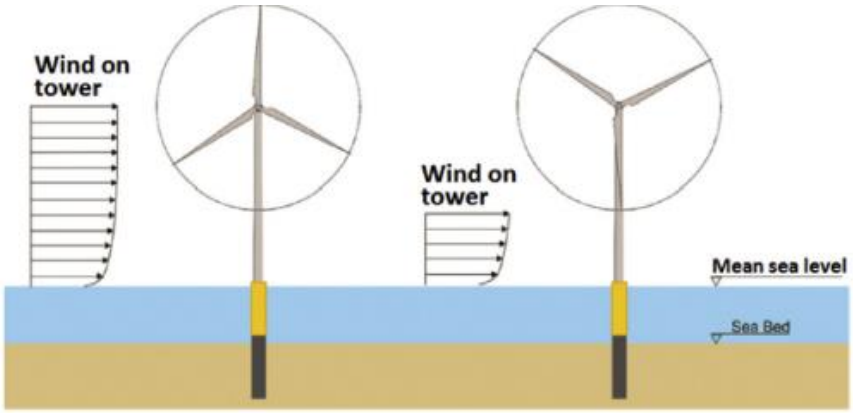

Figure 3-xiv Undisturbed wind forces on the tower to the left and 3P load on the right due to blade shadowing effects [56]

Similar to 1P, 3P has a frequency band which is found by multiplying the limits of 1P by the three blades [61]. This gives a band of 0.3 Hz – 0.48 Hz for the DTU 10 MW RWT. The sub-structure frequency, which is the overall wind turbine global frequency, has a range which lies outside the frequency range of 1P, 3P and wind spectrum to avoid resonance [56]. Skaare et al. [59] points out that the main focus in design of the support structure is to avoid natural periods within the range the 1st and 3rd harmonics of the rotor period. The natural frequency of the support structure should not fall into 1P or 3P range, but rather lie on the outside or in between, depending on the flexibility of the structure. It is important to mentioned that a separate eigen-frequency analysis of the whole structure, aside for the decay test of the spar platform, are not performed in this study. However, an eigenvalue analysis performed in SIMA by Sørum et al. [11] shows the natural frequency of the bottom fixed turbine, used in this study. The natural frequency of the first modes are given in Table 3-h.

Table 3-h Natural frequency of the whole bottom fixed wind turbine obtain with SIMA by Sørum et al.[11] .

Mode	**Natural frequency [Hz]**
1st Tower side-side mode	0.227
1st tower fore-aft mode	0.228
1st blade asymmetric flapwise (yaw)	0.564
1st blade asymmetric flapwise (pitch)	0.594
1st collective flap mode	0.624
1st asymmetric edgewise1	0.951
1st asymmetric edgewise2	0.957
2nd tower side-to-side	1.303
2nd tower fore-aft	1.189
2nd asymmetric flapwise (yaw)	1.460
2nd asymmetric flapwise (pitch)	1.682

The findings of the bottom fixed natural frequencies are closely related to the eigenvalue analyses of the DTU 10 MW RWT [12].

3.4.5 Tower bottom bending moment

Bending loads in the tower bottom origin from the horizontal aerodynamic loads on the rotor, which is transmitted to the nacelle. The tower structure has a conical shape due to the increase of bending moments downwards from the nacelle towards the sub-structure [48]. These loads may travel through the sub-structure of the bottom fixed wind turbine proceeding into the soil. Sørum et al. [11] have studied the response of the monopile foundation from different load cases with simulations from different programs, SIMA among others. The spar floater will respond with pitch motion to environmental factors, which will cause additional bending moment in the tower due to gravity and acceleration effects. This shows that the bending moment of the tower is largely influenced by the pitch motion of the platform. Since this study are comparing the results from two different wind turbines with similar rotor and tower, but dissimilar sub-structure, the load response is studied in the tower bottom, along the wind direction.

3.4.6 Flapwise bending moment

Flapwise bending moment is a result from aerodynamic loads on the blades. As reference describes [62], this load is generated by lift and drag of the aerofoil section of the blades, which is depending on velocities of the wind and blades as well as blade surface, angle of attack and yaw motion, as illustrated in Figure 3-xv. Blade pitch and twist decide the angle of attack. The results from the aerodynamic lift and drag is thrust in the direction of rotation, which will be absorbed by the generator. Aerodynamic forces acting on the blades can be calculated in order to give the overall blade reaction and thrust loads [62]. The wind forces (shear) normal to the rotor plane, as seen in Figure 3-xv, will contribute to the bending of the blade. This creates compressive and tensile stresses in the blade cross section.

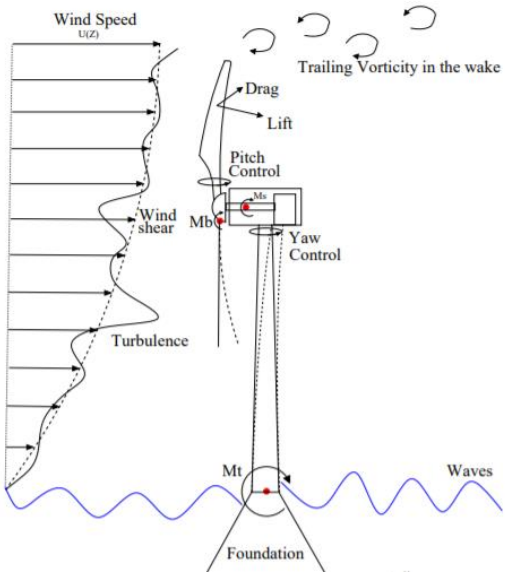

Figure 3-xv Contribution of the wind forces to flapwise bending moment in the blade root (Mb) and tower bottom bending moment (Mt) [63].

The reaction in the blade root from the various wind field formulations is calculated in SIMA, where the wind fields are simulated on the turbine. The occurring stresses in the blade increases towards the rotor, thus the most critical bending moments is in the blade root. The aerofoil is therefore designed to increase in thickness towards the hub to uphold the structural integrity [62]. A study of the flapwise bending moment in the blade root, in blade 1, is performed for both turbines assessed in this thesis.

4 Simulation results & discussion

The simulation results will be presented in two parts; wind field simulation and load simulation. Three wind field generation methods are used in this study. Two methods given by the wind industry standards and one based on offshore measurement at FINO-1. The standards are originally used with standardized parameters and generated with neutral stratification. As described under the wind field simulation in section 2.4, it has been a goal to achieve the same hub height wind speed, shear profile and hub height turbulence intensity, for both the standard wind fields and the wind fields generated from the measurements. The standard deviation is also matched at hub height across the simulators. This is to avoid its dominance on the results as we want to study the influences of turbulent wind and spatial coherences. The standard wind fields are also generated for stable and unstable atmospheric conditions due to the site-specific parameters used in the simulation runs, as described in section 2.4.5 and 2.4.6. The standard generated wind fields are thus fitted to the measurements and can be generated by other stabilities than neutral. TIMESR generated wind fields also have inputs of realistic offshore time series defined at a reference height in the simulator, which are the same height as the point measurements (80 m). As mentioned in the introduction of this thesis, TIMESR are not representing a true offshore wind field. This is due to the simplified method of creating a wind field from point measurements, using Davenport coherence model. Yet, it is assumed, in this thesis, to represent a closer to realistic wind field than the standard wind fields. Mann and Kaimal are therefore evaluated in relation to TIMESR. The simulated wind fields are used in the wind turbine simulations to investigate the different wind field generation methods effect on the wind turbine load. Both approaches have used a simulation length of 3800 seconds, where only 1 hour is used when investigating the load response. The results will focus on:

- Comparing the generated wind fields by their wind profile and by investigating turbulent wind and spatial coherences across various wind field generation methods and atmospheric stabilities. These results are presented in section 4.1.
- Present output from wind turbine simulations performed with the turbulent wind input from pre-generated wind boxes. The load response analysis focus on the tower bottom fore-aft and blade root flapwise bending moments for both the bottom fixed and the spar floating wind turbine. The wind inflow impact on the turbine response will be evaluated by investigating the performance of Kaimal and Mann relative to TIMESR. As well as investigate the load output across different atmospheric stabilities. Turbulence and coherence along with forces leading to dynamical load response will be discussed. These results are presented in section 4.2

4.1 Wind field simulation results

4.1.1 The wind profiles

The wind profile for all simulated wind fields is used to ensure that that the cross-comparison between the generated wind fields are valid. As mentioned earlier, the power law wind profile is used for Kaimal and Mann scaling (solid line in Figure 4-i) where the empirical exponent is fitted to the measurements. It is a minor difference (hardly visible in the plots) between the standard wind profiles and TIMESR (dotted line). Figure 4-i show some differences in the stable situations (red). This can be explained by the different wind profile method used, as logarithmic law is used for TIMESR. The stars represent the input measurements at 40, 60 and 80 m. Figure 4-i verifies that between the simulated flows, in each atmospheric stability, they all have matching profile at hub height (119 m).

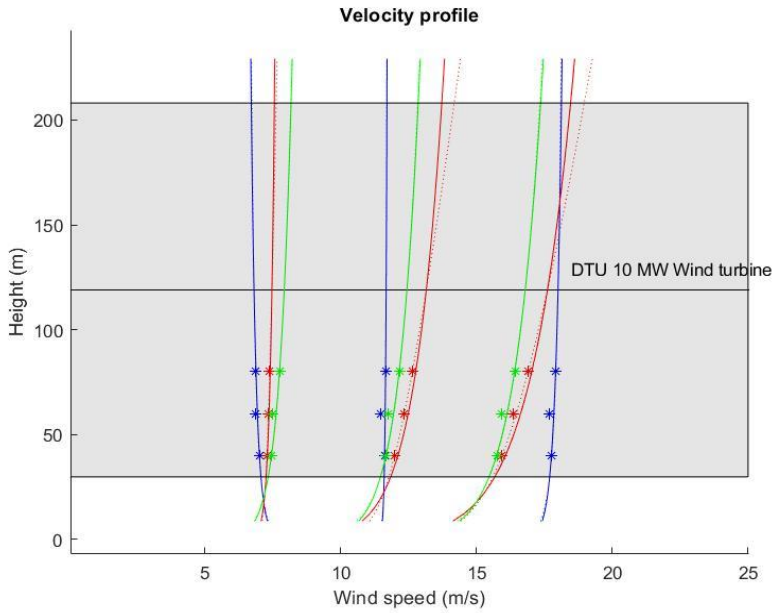

Figure 4-i The wind profiles of the simulated wind fields for the below, close to and above rated selected scenarios. Blue: unstable situations, red: stable situations and green: neutral situations.

4.1.2 The generated wind turbulence

The generated wind fields, Kaimal, Mann and TIMESR are performed with matching TI from the FINO-1 measurements. For the same reason as Doubrawa et al. [7], it is important to verify that the turbulent energy content integrated along the frequency spectrum is matched across the three wind field generation techniques. The fluctuation within the different simulated flows are analysed by the power spectral density. The spectra of the wind speed time series at hub height are computed using Welch's power spectral density estimate found using six segments with 50 % overlap and a hamming window. The length of each time series is 3600 seconds. The results, plotted at double logarithmic scale are presented in Figure 4-ii, Figure 4-iii and Figure 4-iv.

TIMESR is assumed to represent a more realistic wind condition, than those of the standard simulated wind fields. This means that the turbulence defined by Kaimal or/and Mann is considered realistic if the level of the wind spectrum is similar to TIMESR. However, if the level is above or beneath TIMESR, it corresponds to an overestimation or underestimation of the energy level in the turbulence. Yet, it is important to specify that we can not know if TIMESR gives a better performance at the generated points that lies outside the measurement points, where the offshore measurements were sampled.

Figure 4-ii covers the below rated simulated wind fields of the three generation techniques, Figure 4-iii covers the close to rated, while Figure 4-iv covers the above rated simulated wind fields. All spectrums are illustrated by the wind from either neutral, stable or unstable atmospheric conditions. Mann field is shown with blue, Kaimal is red and TIMESR are represented by yellow.

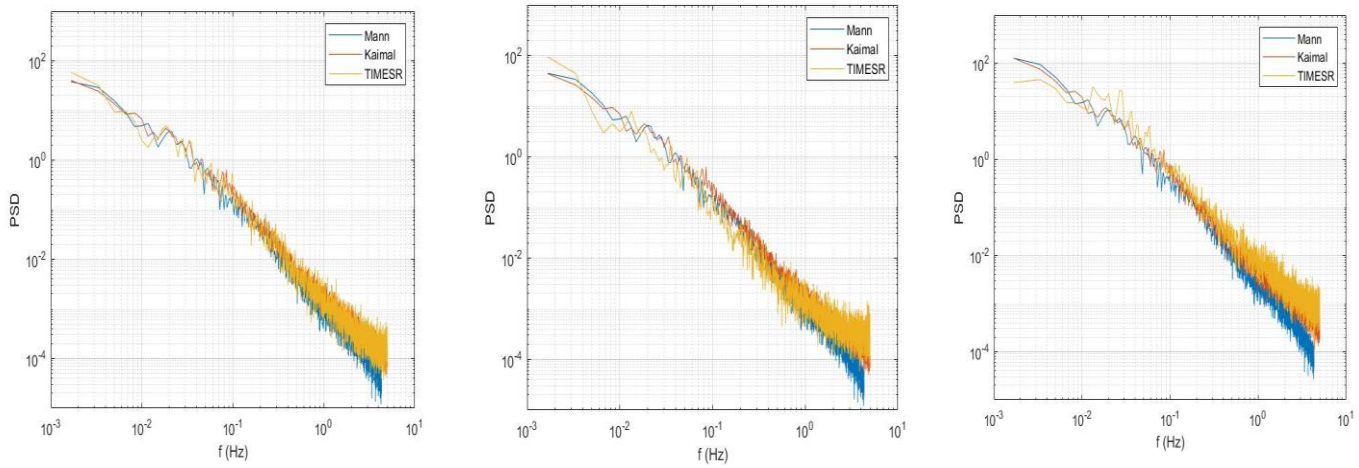

Figure 4-ii The PSD at hub centre provides the energy spectrum for the below rated simulated wind fields in neutral (left), stable (centre) and unstable (right) atmosphere.

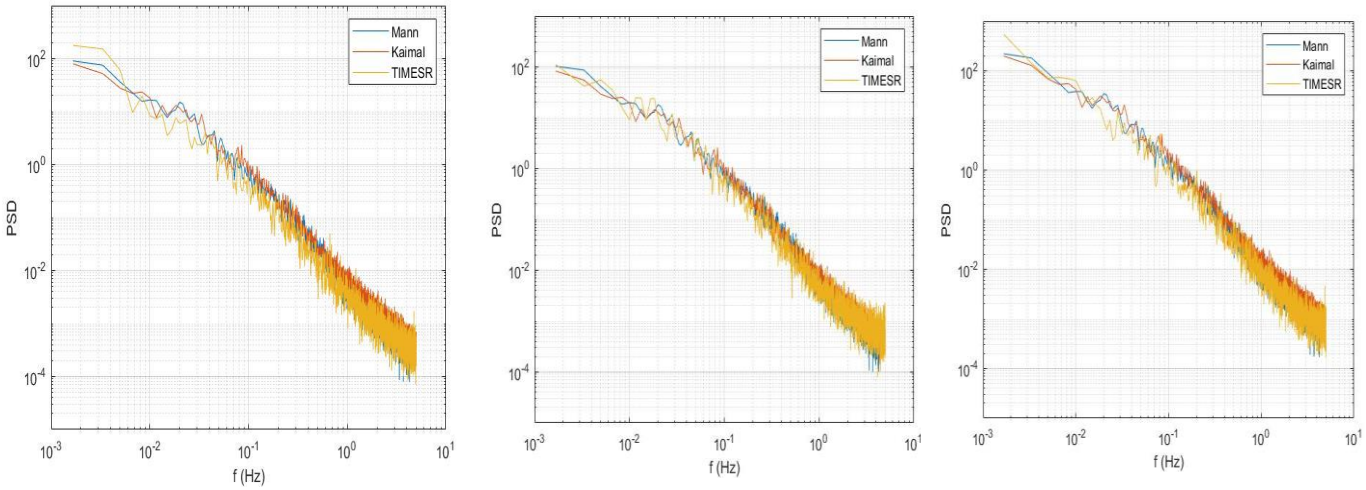

Figure 4-iii The PSD at hub centre provides the energy spectrum for the close to rated simulated wind fields in neutral (left), stable (centre) and unstable (right) atmosphere.

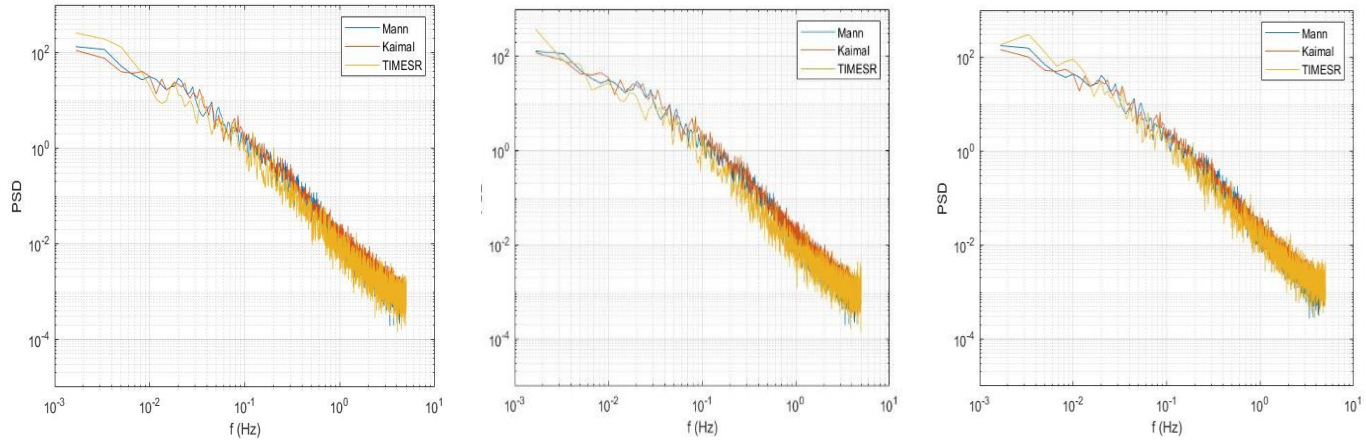

Figure 4-iv The PSD at hub centre provides the energy spectrum for the above rated simulated wind fields in neutral (left), stable (centre) and unstable (right) atmosphere.

Consistently with Nybø et al. [6], the variance of the standard wind fields and TIMESR show similarities in all wind speed scenarios, which verifies that the wind fields have the same characteristics at hub height within the same atmospheric stability. Note that the spectra are plotted on a logarithmic scale, which makes it harder to see the differences in the energy level, but advantageously illustrates the whole frequency range. As shown in Figure 4-ii, Figure 4-iii and Figure 4-iv, the standard wind fields follow each other, but deviates slightly from TIMESR. Except for the below rated scenarios (Figure 4-ii), where Mann are shifted towards lower energy at higher frequencies relative to Kaimal and TIMESR, but this is not the most important frequency range for neither of the turbines studied in this thesis. The most variance in the

energy spectrum is at the frequency range f < 0.1 Hz. As mentioned in the introduction, the lowest relevant frequency for the bottom fixed turbine is about 0.16 Hz and the lowest relevant frequency for the spar floater is about 0.01 Hz. These are frequencies corresponding to the nominal rotor frequency and the natural period of the surge mode. At the lower frequencies for all scenarios, Mann and Kaimal varies by slightly over- and underestimate the energy spectrum, in relation to TIMESR. In the low frequency range, the wind generation methods vary in content of turbulent kinetic energy in the range of large eddy sizes. The time series from the measurements are directly used in TIMESR to generate the spectrum, while the standard methods are creating time series from Kaimal and Mann spectra. Those spectra are described in section 2.2.1 and 2.2.2. Due to the large variation in the mean wind speed in the time series used as input in TIMESR, we see high energy level at the low frequency range. A lower level of energy at this range is observed from the standard simulations due to stationary methods with low variation in mean. Figure 4-ii show that the turbulent energy level is lower for the below rated wind speed than for the rated and above rated wind speed in Figure 4-iii and Figure 4-iv.It is observed that the wind fields have a better match in the midrange, which is an important range for the bottom fixed turbine.

Even though the spectra show quite similar behaviour, there might be significant differences in the spatial distribution of turbulence. It is therefore important to investigate and to compare the effects of coherence across the three wind field generations methods. Kaimal and TIMESR (Davenport model) ignore the quad-coherence (the imaginary part of coherence). Co-coherence, meaning only the physical oscillations, are thus only considered in this study. Nybø et al. [6] describes that the coherence will affect the load pattern along the wind turbine blades, when, as seen in Figure 4-v, values are below zero. This implies an opposite phase of the turbulent velocity components [6]. As seen from the same figure, the co-coherence of TIMESR (Davenport model) is forced towards zero, which means that the opposite phases are not accounted for under the wind turbine simulation.

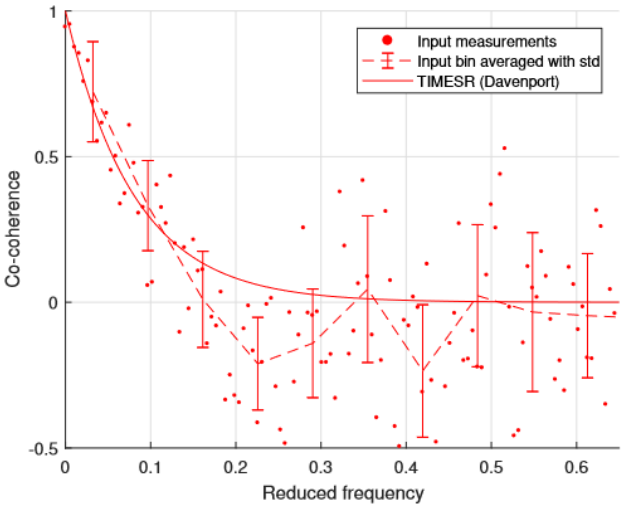

Figure 4-v Vertical co-coherence of uu-component of measurements between 40 and 80 m with the velocities of 12.5 m/s in neutral condition [6]

The spatial co-coherence is only considered for the uu-component in this thesis, due to the longitudinal velocity component limitation of the Kaimal exponential coherence model. It is evaluated for both vertical and lateral direction at the height of the turbine hub. The spatial coherences are illustrated by Figure 4-vi, where the vertical coherence is represented by point AB and lateral coherence is express by the points CD [14]. The reference [14] describes that the vertical coherence is hypothesised to influence the fore-aft/pitch, while the lateral coherence is hypothesised to influence the yaw motion of a spar floater.

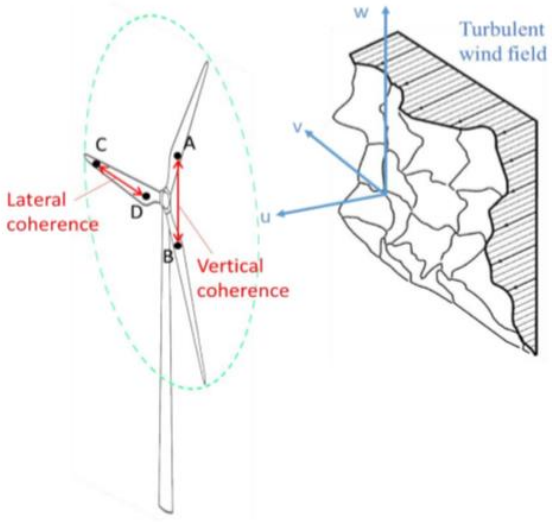

Figure 4-vi The lateral and vertical coherence of the turbulent wind field [14].

The Figure 4-vii below shows a comparison between the co-coherence of the longitudinal wind component for the standard turbulence models and the offshore measurements from the FINO-1 mast. The standard models are not able to represent co-coherence differently for each stability conditions and they are therefore represented as single curves. The co-coherence estimated based on the measurements performed by TIMESR (Davenport), depend on atmospheric stability condition through the varying decay coefficients as shown in Table 2-i.

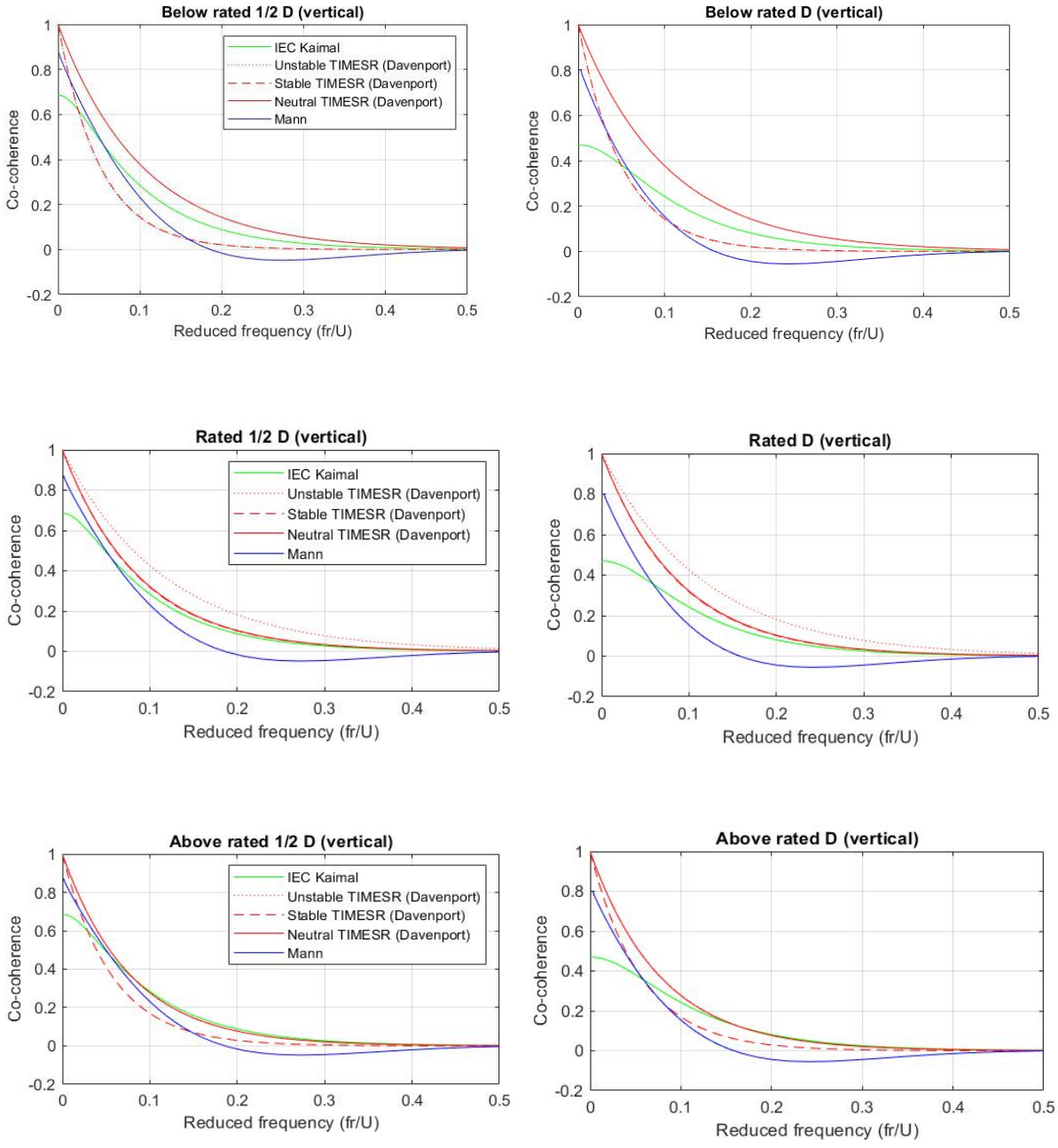

Figure 4-vii Co-coherence of the longitudinal wind component (u) at points with vertical separation distance of ½ D (89.15 m) to the left and 1 D (178.3 m) to the right. The co-coherence is illustrated for the wind speeds a) below rated, b) close to rated and c) above rated.

The Figure 4-vii illustrate the co-coherence, in the vertical direction, for the longitudinal wind component (u) with wind velocities of below rated, close to rated and above rated. The uu-co-coherence is assessed for both vertical and lateral direction at two different separation distances (δ) between two points, defined by the rotor diameter of the wind turbine: ½ D and 1D. This is the separation distances of 89.15 m and 178.3 m, respectively. Coherence from TIMESR is driven by the decay coefficients and is not affected by the separation distances. Thus, both ½ D and 1D is only implemented in this study to investigate the differences in coherence from the standard models. As shown in the Figure 4-vii, the co-drastically with the reduced frequency in all flow cases and as reference states [6], reduced frequencies above 0.5 will be insignificant. All curves of TIMESR starts at unity due to the application of Davenport coherence model. The first part in the Kaimal coherence equation (2-10(2-10), will not be accounted for at zero frequency, and thus will the Kaimal curve start at a level dependent on the chosen separation distance.

It is worth noticing that TIMESR cases have similar characteristics, seen for the unstable and stable cases at below rated scenario, where both curves decrease steeply and. In this wind speed scenario, neutral has the highest co-coherence, which might be explained by an atmosphere containing larger eddies. Neutral and stable conditions are acting similarly in the close to rated scenario and the highest co-coherence are created in the unstable atmosphere, which is more consistent with the study of Nybø et al. [6]. The latter co-coherence case is the highest, relative to the other wind speed scenarios. While neutral and unstable conditions are similar in the above rated scenario as well as moving into the same curve pattern as Kaimal. This wind speed scenario stands for the lowest co-coherence of the TIMESR cases. The similarities in the curves can be explained by the small differences in the decay coefficient obtained from the measurements as shown in the Table 2-i in section 2.4.4. Based on the Figure 4-vii, the decay rate seems to be equal for some TIMESR curves within all wind speed scenarios. However, by zooming in, the plot shows that they are not completely identical.

Co-coherence from the wind fields generated by the standard turbulence models show the dependency of the separation distance by representing lower co-coherence in the 1D figure (right side). The Mann model have high co-coherence at low reduced frequencies and then decreases rapidly. While Kaimal starts with a lower co-coherence level, but has a lower decay rate. This is consistent with the findings of Nybø et al. [6]. Kaimal shows a more similar co-coherence to the neutral TIMESR runs, especially at the close to rated and above rated scenarios, for both separation distances. The Figure 4-vii illustrate how Mann and Kaimal crosses each other at the reduced frequency close to 0.05 Hz. Mann is generally closer to the TIMESR runs in the lower frequency range, but the largest similarities is with the stable run for the largest separation distance at below rated and above rated scenarios. Mann is also the only curve representing the negative values in the vertical direction.

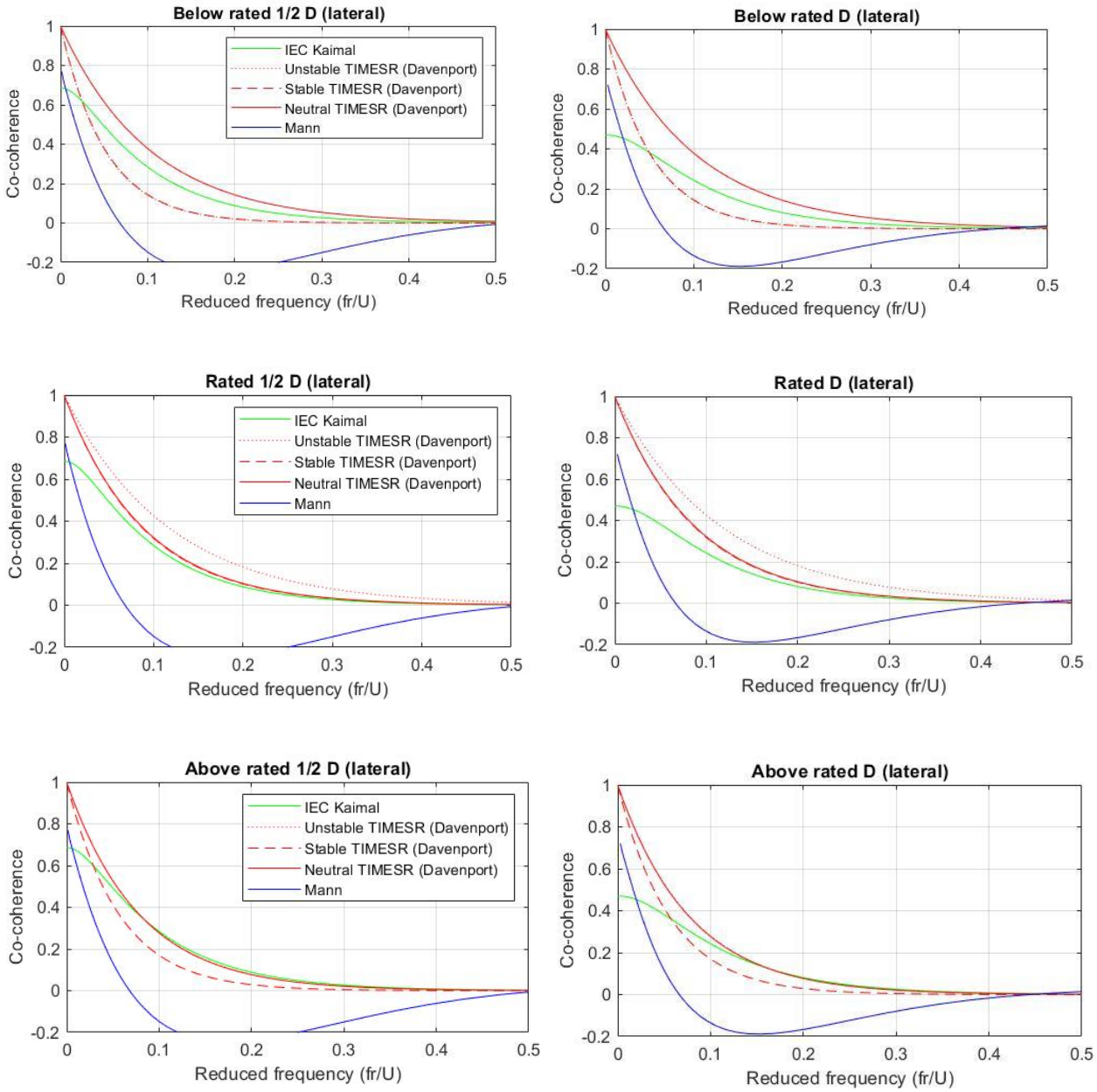

Figure 4-viii Co-coherence of the longitudinal wind component (u) at points with lateral separation distance of ½ D (89.15 m) to the left and 1D (178.3 m) to the right. The co-coherence is illustrated for the wind speeds a) below rated, b) close to rated and c) above rated.

As the Davenport model is independent of the direction, as seen in Figure 4-viii, the TIMESR co-coherences are the same in the lateral direction as the vertical direction. Figure 4-viii illustrate the co-coherence, in the lateral direction, for the longitudinal wind component (u) with wind velocities of below rated, close to rated and above rated. We see the same trends as in the vertical co-coherence with steeply decreasing coherence with reduced frequencies, and lower coherence at higher distances. Compared to the vertical direction, the co-coherence of Mann decreases faster and goes straight to negative values, which illuminates that the phase shifts are not negligible. Both directions and separation distances show that

the coherence are most pronounced at the lower frequencies ($\frac{fr}{U} < 0.2$) and between the three wind field generation methods, differences in how coherence is represented is clearly seen.

4.2 Results of simulated loads

Aerodynamic loads were carried out to test the DTU 10 MW wind turbine mounted on the monopile platform as well as to test the one mounted to the spar platform. Comparison between the simulations of Kaimal, Mann and TIMESR on the turbine response is presented in the four following sections, where the relative wind speed of the inflow fields was about 7.5 m/s, 12.5 m/s and 17.5 m/s. This corresponds to the below rated, rated and above rated wind speed of the turbine. These wind speeds were simulated with neutral, stable and unstable atmospheric situations. Altogether twenty-seven simulations are thus performed.

The result parts will include the investigation of an under- or overestimation of the loads performed by the standards, relative to the TIMESR runs. The simulation was carried out with SIMA and the software computed the turbine responses. Each simulation had a duration of 1 hour and 200 seconds. This study has focused on the results of the tower bottom fore-aft bending moments (TBBM) and the blade root flapwise bending moments (FBM). An investigation of TBBM is important for tower design and represents a typical global load, while investigation of FBM is important for the design of the blades and represents a typical local load. These bending moments are important to examine in the mind of overload and fatigue, which may be represented by the mean load and the standard deviation load for the bending moments.

The presentation of the load results from the simulation of the bottom fixed wind turbine comes first. The tower bottom bending moment are presented in section 4.2.1 and the blade root flapwise bending moment results are presented in section 4.2.2. Further, the TBBM and FBM for the spar floater are presented in section 4.2.3 and 4.2.4. These results include an overview of the load response values, load presentation by bar graphs and the atmospheric stability sensitivity to the wind turbine response is discussed. This is performed by comparing stable and unstable condition in relation to neutral stratified load simulations. Only 3600 seconds of the simulation length of 3800 seconds are analysed. The response results are transferred to MATLAB by using the output files from SIMA (sima_elmfor.bin and results.tda).

The TBBM and FBM results are extracted from those files to compare the responses in the frequency domain. The power spectral density (PSD) estimate of the bending moments was found using Welch's estimate method using six segments with 50% overlap. The segments are windowed with a hamming window. The power spectral density is performed to examine the excitation forces that govern the bottom fixed and the spar floating turbine. It is plotted by logarithmic scale, which are visualized by a frequency range (x-axis) of 0.001 – 3 Hz. Since all

important natural modes of the blades and of the tower, for both turbines are occurring at frequencies below 3 Hz. The power spectral density of the bending loads is performed for each atmospheric stabilities and wind speed scenarios, which will give an insight of which frequency of the wind turbine that collects most activity due to the load forces. The load spectra provide information about the dynamic characteristics of structural elements vibration, which gives a better understanding of the behaviour of those elements. Sim et al. [64] points out that this is forces that will be revealed as distinct spectral peaks. The peaks are sharper the lower the damping of the mode of associated frequency. The energy of these peaks comes from the turbulent wind and related to natural frequency of the modes described in section 3.4.4. Linearly load spectra are also considered since this show the differences more clearly for certain frequency ranges.

The complete results from the wind turbine analysis can be seen in Appendix E, which includes tower top and bottom yaw moments, edgewise bending moments in the blade root, as well as axial forces acting towards the mooring lines and the global responses of the spar platform.

4.2.1 Tower bottom fore-aft bending moment – Bottom fixed turbine

The resulting tower bottom fore-aft bending moment is presented in this section for the 10 MW bottom fixed wind turbine.

The pre-generated wind boxes: Kaimal, Mann and TIMESR are all used in the simulation of the bottom fixed wind turbine. The tower bottom fore-aft bending moment is investigated for the various flow-simulation techniques: Kaimal, Mann and TIMESR, performed for neutral, stable and unstable atmospheric conditions. In total, twenty-seven simulations, where the below rated, close to rated and above rated wind speed scenarios were considered. The inflow fields and the dynamical calculation parameters are shown in Table 4-a below. The values presented by Table 4-b, Table 4-c and spectral analysis can be used to quantify the standard generated inflows performance relative to TIMESR.

Table 4-a Simulation input in SIMA

Environmental load	Simulation time (s)	Time step (s)	Time increment
Kaimal/TIMESR/Mann	3800	0.01/0.01/0.0116	0.1/0.1/0.116

The results extracted from the SIMA output file is represented by the mean value and the standard deviation of the tower bottom bending moment. The TBBM presented by the computed mean load (MNm) are shown in Table 4-b. We observe no large differences in the mean values in the bending moment between the different simulation techniques. It is seen that the mean load also tends to increase with increasing wind speed and reduced at the above rated scenario.

Table 4-b Statistics of the mean (MNm) for the load of the tower bottom fore-aft bending moment. Results from below rated, close to rated and above rated inflow fields for the bottom fixed wind turbine. Various atmospheric stabilities and wind field simulation techniques are considered.

	Below rated			**Rated**			**Above rated**		
	Neutral	*Stable*	*Unstable*	*Neutral*	*Stable*	*Unstable*	*Neutral*	*Stable*	*Unstable*
Kaimal	98.67	86.97	73.08	127	116.8	139.2	87.09	84.26	79.30
TIMESR	99.78	88.57	72.22	130.3	118.5	137.3	87.70	85.95	79.84
Mann	97.72	85.87	71.18	127.5	116.8	142.5	87.06	84.23	79.23

The mean TBBM load can cause overload in the component, over time, and must thus be considered. It is relevant to investigate whether the TBBM is mostly due to mean load or due to standard deviation load. The latter stands for a variability that may contribute to fatigue. These are important values to estimate the effect on the tower bottom and to investigate the different load response across the simulation techniques.

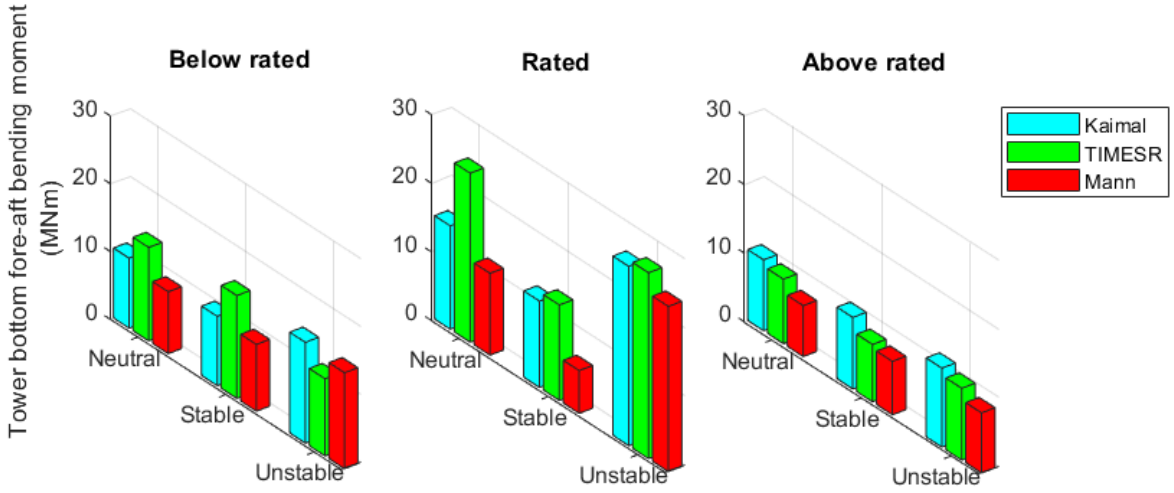

Figure 4-ix Standard deviation of tower bottom fore-aft bending moment. Results from below rated, close to rated and above rated inflow fields for the bottom fixed wind turbine. Various atmospheric stabilities and wind field simulation techniques are considered.

The computed std of the tower bottom fore-aft bending moment loads is illustrated by Figure 4-ix. The load is presented by bar graphs. Kaimal is represented by a blue bar, TIMESR is represented by green and the bending moment from Mann inflow field have a red bar. The Figure 4-ix illustrates some load increase with increasing wind speed, but as clearly as seen in the mean load in Table 4-b. The low increase of the load is most especially visible in the stable condition at the close to rated scenario, where the opposite is true for the std of Mann, which show a reduction in the computed std load. As expected, the above rated scenario shows a reduction of the load, which is seen in the context of the blade pitching to achieve constant power output. A comparison between the loads, as illustrated in Figure 4-ix, show that the result from the standard generated inflow fields gives a similar bending moment in the below rated scenario, they agree on a lower impact on the tower bottom than for the TIMESR case in the rated scenario, while in the above rated scenario, Kaimal is consistently producing a higher bending moment load than the other inflow options.

Table 4-c Statistics of the standard deviation (MNm) for the load of the tower bottom fore-aft bending moment. Results from below rated, close to rated and above rated inflow fields for the bottom fixed wind turbine. Various atmospheric stabilities and wind field simulation techniques are considered. Green indicates an underestimated load and blue indicates an overestimated load.

	Below rated			**Rated**			**Above rated**		
	Neutral	*Stable*	*Unstable*	*Neutral*	*Stable*	*Unstable*	*Neutral*	*Stable*	*Unstable*
Kaimal	10.32	10.22	14.86	15.06	12.58	26.13	10.33	10.42	11.51
TIMESR	13.78	15.16	11.39	24.63	13.91	27.08	9.404	8.365	10.46
Mann	9.125	9.844	14.14	11.92	6.234	24.06	7.428	7.789	8.760

An overview of the values from the load standard deviation (MNm) is implemented in Table 4-c. The color codes included in Table 4-c is an overview of either an underestimation and/or an overestimation of the bending moment performed by the standard inflows relative to TIMESR. Green indicates that the loads are underestimated, and blue indicates that the loads are overestimated.

Table 4-c indicates a good agreement between the estimated loads between Mann and Kaimal, except for the above rated scenario where they give opposite results, as shown by the color codes. A comparison between the two standards, show that they slightly differ in the computed standard deviation load, where Mann generally generates lower loads than Kaimal. Table 4-c show that all the simulation techniques provide highest bending moment load in the unstable atmospheric condition, which can be seen in the context of higher turbulence level in these situations. It is also interesting to investigate the bending moment across atmospheric stabilities, as the the wind industry typically simulate with neutral atmospheric inflow. A comparison of the load response from the unstable and stable conditions relative to the neutral conditions are thus performed.

The effect of different atmospheric stratification on the bottom fixed tower bottom bending moment was found to be rather large in some cases. It is observed higher loads for the unstable stratification scenarios, especially with Kaimal and Mann, which exeeds 50%, 70% and 100% higher loads, relative to the neutral conditions. It is seen that TIMESR inflow cases also generate higher bending loads in the unstable condtions than those of neutral in both rated and above rated scenarios. This might have a connection with typically larger turbulence level in the unstable stratification and due to coherence, as Nybø et al. [6] found significant coherent structures in the unstable situations. For the rated scenario, all load cases with stable stratification relative to the neutral condition. The differences between atmospheric

stabilities, represented by TIMESR, is not that pronounced, exept for the rated scenario, where stable are 43.5% lower than the neutral case. Yet, all TIMESR cases exceeds above 10% differences.

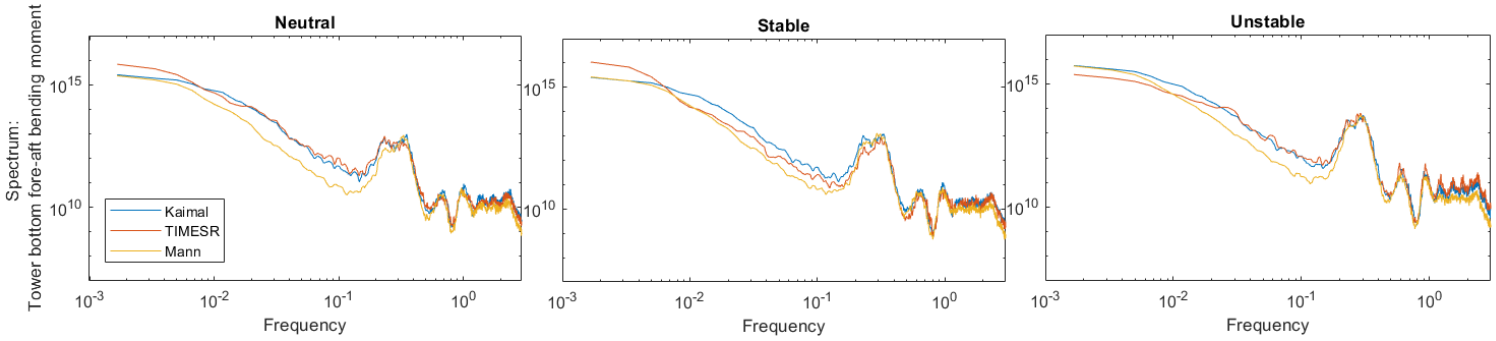

Figure 4-x Comparison of the bottom fixed wind turbine response in terms of load spectra for the three flow-simulation methods [Kaimal (blue), TIMESR (red) and Mann (yellow)] and various atmospheric conditions: neutral (left), stable (middle) and unstable (right). Given for the tower bottom fore-aft bending moment in the below rated wind-speed scenario.

Figure 4-x show the load spectra of the reconstructed tower bottom fore-aft bending moment of the bottom fixed wind turbine, given for the below rated scenario. As mentioned earlier, the lowest important frequency for the bottom fixed is the rotational frequency at about 0.1-0.16 Hz.

We observe highest spectral peaks in the unstable situation, illustrated in Figure 4-x. The load spectra also show that a high respone from the low-frequency range due to low-frequency signals, this is the range of the energetic turbulent wind. It is found a peak at about 0.23 Hz, whichi is, according to Table 3-h in section 3.4.4, the 1st tower natural frequency. Kaimal and TIMESR seems to mostly agree on the load response in the neutral and in the stable condition. The largest differences are seen in the low-frequency range. In that range, Mann show a trend of providing lower load response. All cases seems to match the spectral peaks in the unstable condition. Sim et al. [64] points out that the peak of the natural frequency of the first tower fore-aft bending mode is important for the overall energy content. A deficit from this spectral peak may lead to errors in tower load estimation. Load from the blade passing frequency show an spectral peak of the so-called 3P, about 0.3 Hz. This peak occur at a lower frequency than for the close to rated and the above rated scenarios due to lower rotational speed in the below rated scenario. The reason for the differences in the spectral peaks may be that frequencies of the roational sampling of the inflow turbulence does not match perfectly across the flow-simulation techniques and will result in variation of energy transferred to the rotor thrust and thus in loads. As seen in the Figure 4-x, the standard deviation of the tower bottom bending moment is dominated by the tower motion and load variation of the 3P excitation.

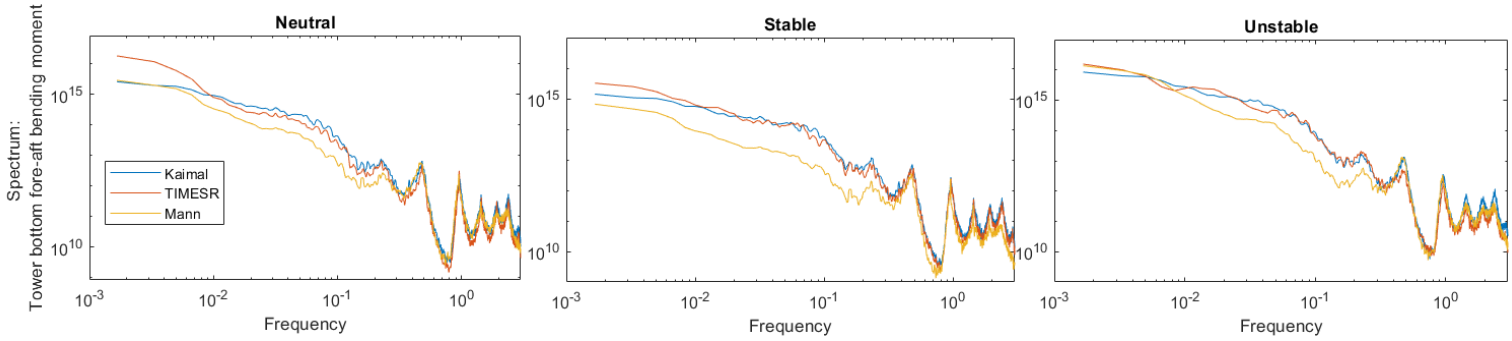

Figure 4-xi Comparison of the bottom fixed wind turbine response in terms of load spectra for the three flow-simulation methods [Kaimal (blue), TIMESR (red) and Mann (yellow)] and various atmospheric conditions: neutral (left), stable (middle) and unstable (right). Given for the tower bottom fore-aft bending moment in the close to rated wind-speed scenario.

Figure 4-xi show the load spectra of the reconstructed tower bottom fore-aft bending moment of the bottom fixed wind turbine, given for the close to rated scenario.

As for the below rated scenario, we observe the load variation to be consistently higher for TIMESR and Kaimal than for Mann, most pronounced in the lowest part of the frequency range. Except for the first tower bending natural frequency, which occur at 0.23 Hz, the different inflow options seems to have matching peaks. The load response due to the blade passing roational frequency, 3P, occur at about 0.48 Hz. This occur at higher frequency than the below rated scenario due to higher rotational speed. A third peak is clearly seen at about 0.96 Hz. This might be due to the 1st blade bending edge mode as both Sørum et al. [11] and the DTU 10 MW RWT [12], describes this mode at this particular frequency. As the close to rated scenario computes the largest standard devations for the TBBM, the load responses are illustrated with a linearly y-axis to see the differences in the response between the three methods more clearly.

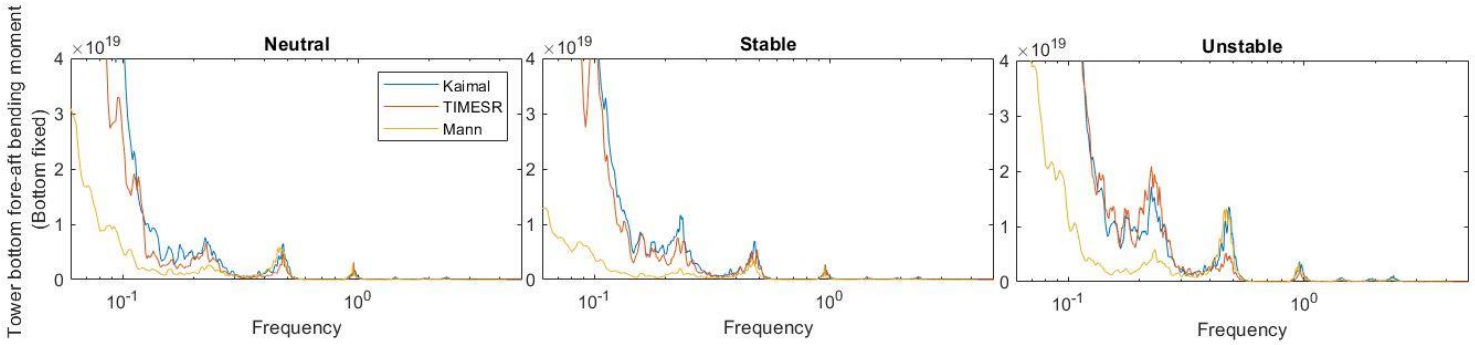

Figure 4-xii The load spectra of tower bottom fore-aft bending moment, with a logarithmic x-axis (0 – 3 Hz) and a linear y-axis. Given for the bottom fixed wind turbine in the close to rated wind speed scenario.

Figure 4-xii, show the large contributor from the wind to the TBBM, as well as the differences between the three flow-simulation methods. Mann genereally provides less variation to the bending load, and Kaimal and TIMESR are quite similar, except for the 3P peak in the unstable situation, where TIMESR is much lower than the loads generated from the standard inflow.

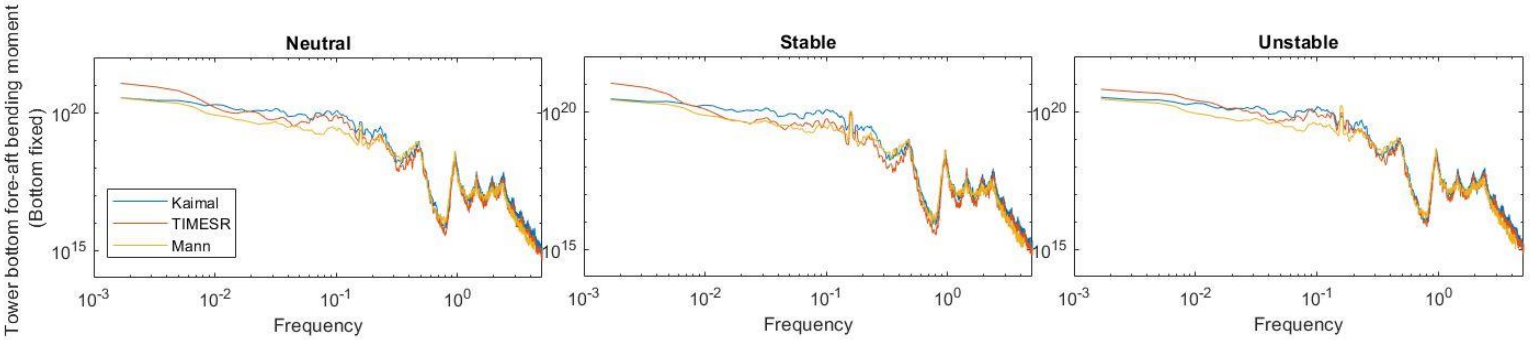

Figure 4-xiii Comparison of the bottom fixed wind turbine response in terms of load spectra for the three flow-simulation methods [Kaimal (blue), TIMESR (red) and Mann (yellow)] and various atmospheric conditions: neutral (left), stable (middle) and unstable (right). Given for the tower bottom fore-aft bending moment in the above rated wind-speed scenario.

Figure 4-xiii show the load spectra of the reconstructed tower bottom fore-aft bending moment of the bottom fixed wind turbine, given for the close to rated scenario.

We observe that the load response from Mann is closer to the two other simulation techniques, compared to below rated and close to rated inflow scenarios. In the above rated wind speed scenario, the largest differences between the methods are also seen in the lowest part of the frequency range. For this scenario, the load from the rotational frequency gets more conspicuous, which give an load variation at about 0.16 Hz. For the 1P variation, TIMESR gives lowest results in neutral, Kaimal gives lowest peak in the unstable situation, while the three methods give about the same peak in the stable situation. The are also some differences in the 1st tower fore-aft mode, at about 0.23 Hz, where Kaimal provide highest response in all atmospheric situations. This is a major contributor to the overestimation of the loads relative to TIMESR, as explained earlier. As for the below rated and close to rated scenarios, the 3P blade passing frequency at 0.48 Hz is shown with a distinct peak, but contributes with higher energy to the tower bottom for-aft bending moment in the above rated scenario. The next peak revealed in Figure 4-xiii is at about 0.95 Hz and are most likely from the blade edge mode as shown in Table 3-h.

4.2.2 Flapwise bending moment in the blade root – Bottom fixed

The resulting flapwise bending moment in the blade root is presented in this following section for the 10 MW bottom fixed wind turbine. The FBM is investigated for one of the three blades, blade 1.

The pre-generated wind boxes: Kaimal, Mann and TIMESR are all used in the simulation of the bottom fixed wind turbine. The turbulent wind impacts the wind turbine and have consequences for the loads in the wind turbine components. The FBM in the blade root is investigated for the various flow-simulation techniques performed for neutral, stable and unstable atmospheric conditions. In total, twenty-seven simulations, where the below rated, close to rated and above rated wind speed scenarios were considered. The inflow fields and the dynamical calculation parameters are shown in Table 4-d below. The values presented by Table 4-e, Table 4-f and spectral analysis can be used to quantify the standard generated inflows performance relative to TIMESR.

Table 4-d Simulation input in SIMA

Environmental load	Simulation time (s)	Time step (s)	Time increment
Kaimal/TIMESR/Mann	3800	0.01/0.01/0.0116	0.1/0.1/0.116

The results extracted from the SIMA output file is represented by the mean value and the standard deviation of the flapwise bending moment. The FBM in the blade root presented by the computed mean load (MNm) are shown in Table 4-e. The mean bending load values in Table 4-e shows quite similar values between the simulation techniques within the same atmospheric stability condition. However, by the look on the mean values across atmospheric conditions within the same simulation techniques, they are not as similar. Yet, it does not show significant differences.

Table 4-e Statistics of computed mean (MNm) load of the flapwise bending moment in the blade root. Results from below rated, close to rated and above rated inflow fields for the bottom fixed wind turbine. Various atmospheric stabilities and wind field simulation techniques are considered.

	Below rated			**Rated**			**Above rated**		
	Neutral	*Stable*	*Unstable*	*Neutral*	*Stable*	*Unstable*	*Neutral*	*Stable*	*Unstable*
Kaimal	17.79	16.05	14.00	21.23	19.30	23.63	14.01	13.20	12.81
TIMESR	17.96	16.27	13.85	21.75	19.51	23.32	14.04	13.58	13.09
Mann	17.68	15.91	13.75	21.37	19.39	24.26	14.15	13.49	13.26

The mean FBM are results from loads that may create overload in the component, over time, and must thus be considered. It is relevant to investigate whether the FBM is mostly due to mean load or due to standard deviation load. The latter stands for a variability that may contribute to fatigue. These are important values to estimate the effect on the blade root and to see the different load response across the simulation techniques.

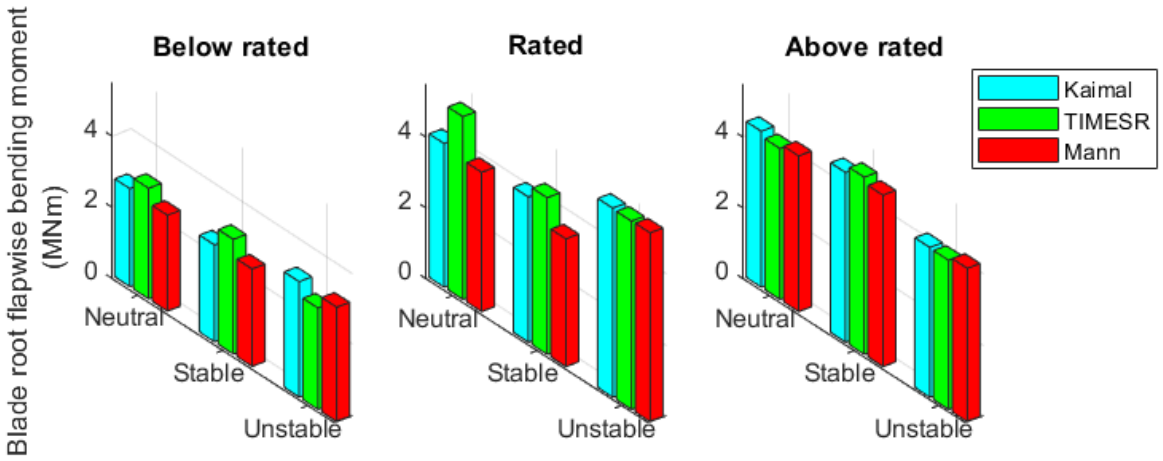

Figure 4-xiv Standard deviation of the flapwise bending moment in the blade root. Results from below rated, close to rated and above rated inflow fields for the bottom fixed wind turbine. Various atmospheric stabilities [(neutral, stable and unstable)] and wind field simulation techniques are considered.

The computed std load of the flapwise bending moment is illustrated by Figure 4-xiv. The load is presented by bar graphs. Kaimal is represented by a blue bar, TIMESR is represented by green and the bending moment from Mann have a red bar. Figure 4-xiv show a increase of std load with increasing wind speed, this is related to a higher average load in the rated wind speed scenario. Oposite to the TBBM loads in the previous section, the above rated standard deviation are not reduced. Yet, if the total bending moment (mean + std) were to be computed, it is seen that the close to rated scenario generates highest bending loads, as expected. Since the std loads are not reduced with the blade pitch angle, it may be a huge contributor to fatigue damage in the blade root.

Figure 4-xiv show similarities in the bending moment results across flow-simulation techniques, most pronounced in the below rated and above rated scenarios. Where, especially the standard generated load cases follow each other. The bars illustrate, in general, very similar behaviour in the computed std in the unstable condition for all simulation techniques, for the close to rated and above rated wind-speed scenarios. The unstable condition in the close to rated scenario show similar performance between the three simulated cases.

Table 4-f Statistics of the standard deviation (MNm) for the load of the flapwise bending moment in the blade root. Results from below rated, close to rated and above rated inflow fields for the bottom fixed wind turbine. Various atmospheric stabilities and wind field simulation techniques are considered. Green indicates an underestimated load and blue indicates an overestimated load.

	Below rated			**Rated**			**Above rated**		
	Neutral	*Stable*	*Unstable*	*Neutral*	*Stable*	*Unstable*	*Neutral*	*Stable*	*Unstable*
Kaimal	2.758	2.726	3.248	4.059	4.104	5.344	4.406	4.797	4.232
TIMESR	3.111	3.230	2.852	5.165	4.429	5.322	4.264	5.009	4.216
Mann	2.697	2.741	3.220	3.938	3.612	5.334	4.401	4.846	4.333

An overview of the values from the load standard deviation (MNm) is implemented in Table 4-f. The color codes included in Table 4-f is an overview of either an underestimation and/or an overestimation of the bending moment, performed by the standard inflows relative to TIMESR. Green indicates that the loads are underestimated, and blue indicates that the loads are overestimated.

Table 4-f points out that the differences between load response by Kaimal and Mann is not that pronounced for the std given for the flapwise bending moment. This means that the load output by the simulation of the standard flow-simulations were closer to the loads resulting from TIMESR, especially seen for the unstable condition in the close to rated scenario where Kaimal and Mann only overestimate the load by 0.4% and 0.2%. Table 4-f show a trend of underestimation of the load response relative to TIMESR in stable situations. While unstable situations show the opposite result. The differences in flapwise bending moment across atmospheric stability conditions are present, but not as significant as for the TBBM load. The greatest effect of atmospheric stratification on the flapwise bending moment in the blade root are found for the unstable condition in the close to rated scenario, where Kaimal and Mann exceed 30% higher loads than those of neutral. The overall findings show variation of computed loads across atmospheric stabilities.

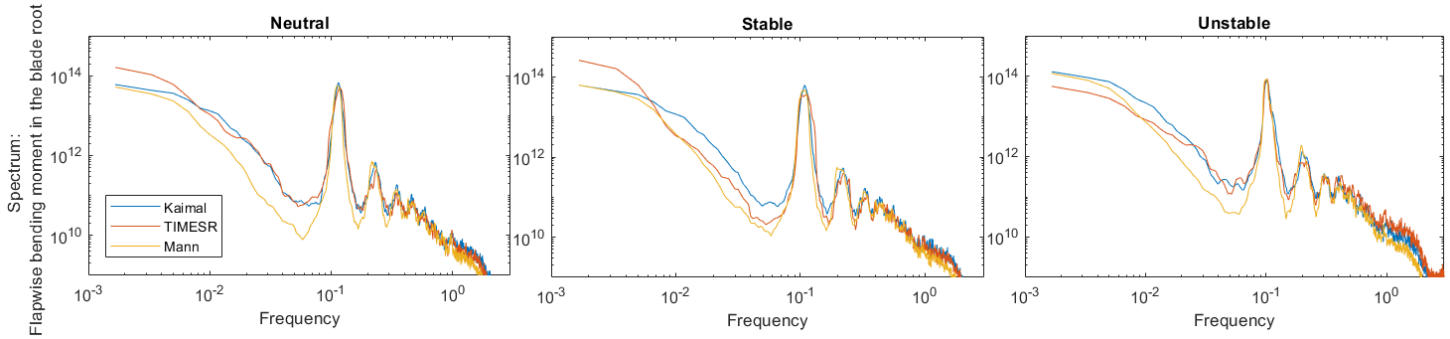

Figure 4-xv Comparison of the bottom fixed wind turbine response in terms of load spectra for the three flow-simulation methods [Kaimal (blue), TIMESR (red) and Mann (yellow)] and various atmospheric conditions: neutral (left), stable (middle) and unstable (right). Given for the flapwise bending moment in the blade root for the below rated wind-speed scenario.

Figure 4-xv show the load spectra of the reconstructed flapwise bending moment in the blade root, for the below rated scenario. As mentioned earlier, the lowest important frequency for the bottom fixed is the rotational frequency at about 0.1-0.16 Hz.

We observe that Mann respond with a lower energy compared to the other in frequencies below 0.1 Hz, but it is closer to TIMESR in the stable condition. In the neutral case, Kaimal and TIMESR follow each other. While the performance of all flow-simulation techniques seems to match the responses shown as spectral peaks. The peaks occur in a frequency range, which are more important for the bottom fixed turbine. When the wind turbine blades rotate, they will sample the inflow turbulence and give a response. This is the 1P load, shown as the first peak in Figure 4-xv at about 0.11 Hz. Beside the energy from the turbulence, this seems to dominate in the response, in all the atmospheric conditions. The next peak is found at 0.22 Hz and is according to Table 3-h closest to the 1st tower mode. The third peak observed, at about 0.3 Hz, might correspond to the blade passing frequency, 3P load. The fourth peak have the same energy content as the 3P in the unstable condition. This is found at about 0.45 Hz and is most likely due to the 1st blade asymmetric flapwise mode.

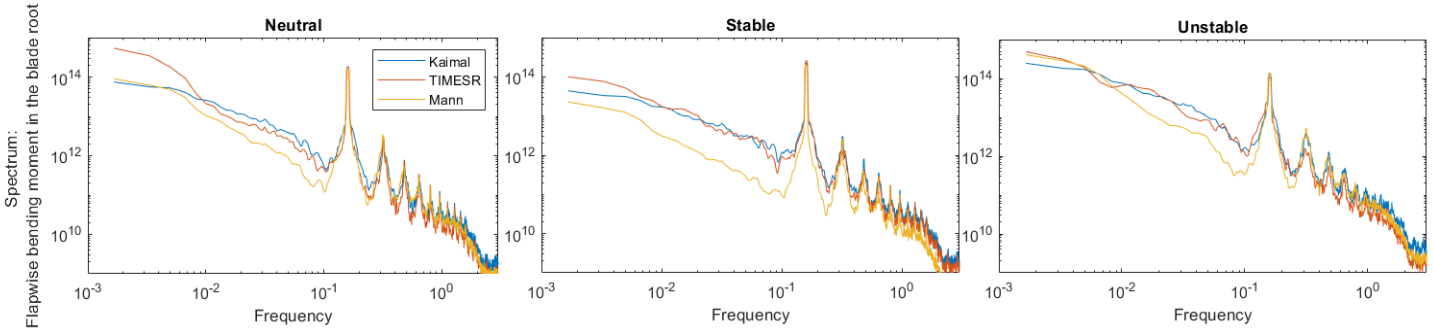

Figure 4-xvi Comparison of the bottom fixed wind turbine response in terms of load spectra for the three flow-simulation methods [Kaimal (blue), TIMESR (red) and Mann (yellow)] and various atmospheric conditions: neutral (left), stable (middle) and unstable (right). Given for the flapwise bending moment in the blade root for the close to rated wind-speed scenario.

Figure 4-xvi show the load spectra of the reconstructed flapwise bending moment in the blade root, for the close to rated scenario.

In the close to rated scenarios, the turbulent wind forcing affect the bending moment with most energy in the low frequency range, below 0.1 Hz. This frequency region shows most pronounced differences across the flow simulation-methods, where Mann model once again tends to give a lower load response lower energy level, especially pronounced in the stable situation, than those of Kaimal and TIMESR. The two latter flow-simulation techniques seem to follow each other. All methods seem to match the occurring spectral peaks. The load due to rotational frequency, 1P, is at about 0.16 Hz and show largest impact on the flapwise bending moment in the stable situation. The next dominating peak is due to the blade passing frequency of two blades at 0.32 Hz, which may be the response due to the 1st tower mode. The 3P spectral peak is shown at 0.48 Hz. The two last mentioned frequencies have highest load in the unstable situation. According to Table 3-h, the peak at about 0.6 Hz is in between the natural frequencies of the 1st asymmetric flapwise mode and the 1st collective flap mode.

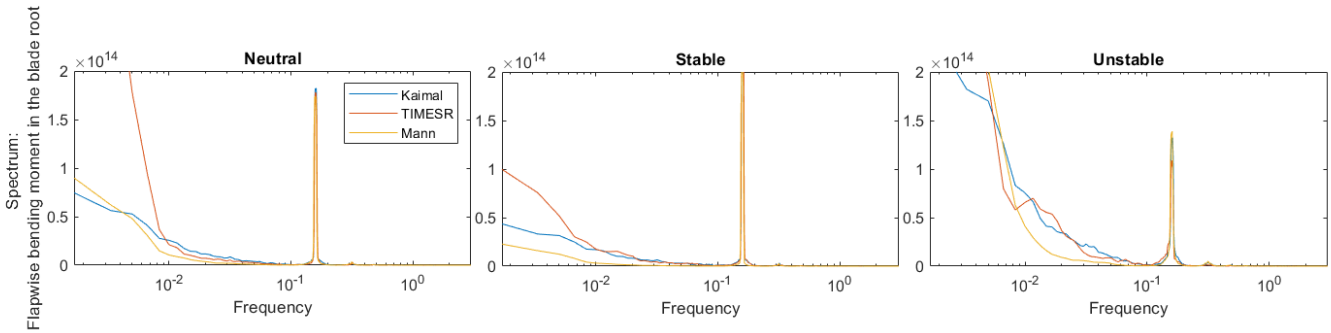

Figure 4-xvii The load spectra of flapwise bending moment, with a logarithmic x-axis (0 – 3 Hz) and a linear y-axis. Given for the close to rated wind speed scenario.

The load spectra with a linear y-axis is shown in Figure 4-xvii, which better illustrates the differences more clearly. It shows the dominance of the low-frequency signals and the rotational frequency. Figure 4-xvii show the same performance for all flow-simulation techniques where they all match the 1P load.

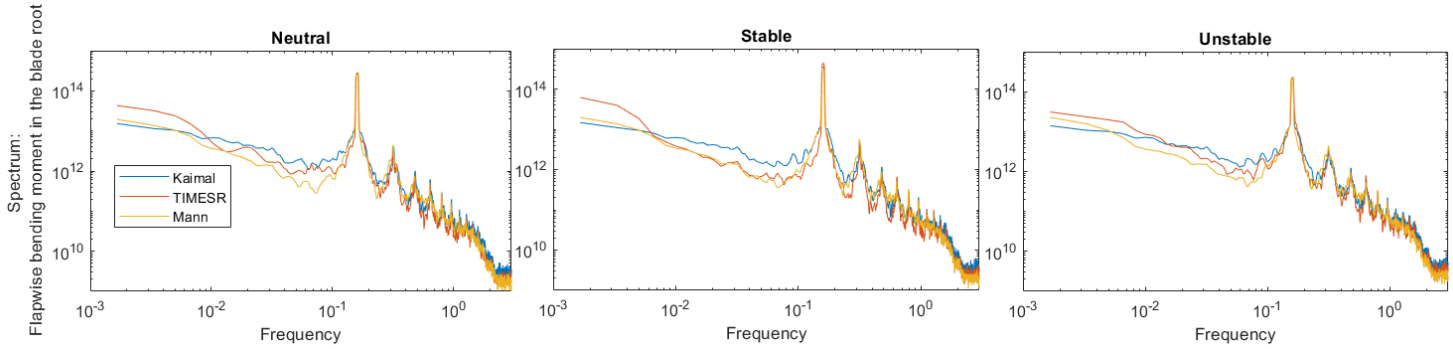

Figure 4-xviii Comparison of the bottom fixed wind turbine response in terms of load spectra for the three flow-simulation methods [Kaimal (blue), TIMESR (red) and Mann (yellow)] and various atmospheric conditions: neutral (left), stable (middle) and unstable (right). Given for the flapwise bending moment in the blade root for the above rated wind-speed scenario.

Figure 4-xviii show the load spectra of the reconstructed flapwise bending moment in the blade root, for the above rated scenario. Once again, we observe differences between the flow-simulation techniques at low-frequency range. In this wind speed scenario, Mann follow TIMESR in the stable situation. The 1P load is found to dominate the load response and is highest within the stable condition. All flow-simulation techniques seem to match the spectral peaks in Figure 4-xxvii. The most likely 1st tower mode is found at 0.32 Hz, while blade passing frequency is shown with a spectral peak at about 0.48 Hz. The fourth peak, at about 0.64 Hz is closest to the natural frequencies of the 1st collective flap mode.

4.2.3 Tower bottom fore-aft bending moment – Spar floater

The tower bottom fore-aft bending moment is found for the spar floater by simulating the pre-generated wind boxes, Kaimal, Mann and TIMESR as the wind input, in SIMA. In total, twenty-seven simulations, where the below rated, close to rated and above rated wind speed scenarios were considered. The various stability conditions were included to each wind field simulation techniques. The inflow fields and the dynamical calculation parameters are shown in Table 4-g below. The values presented by Table 4-h, Figure 4-xix and Table 4-i, can be used to quantify the standard generated inflows performance relative to TIMESR.

Table 4-g Simulation table

Environmental load	Simulation time (s)	Time step (s)	Time increment
Kaimal/TIMESR/Mann	3800	0.01/0.01/0.0116	0.1/0.1/0.116

TBBM load responses for the spar floater is expected to be higher than for the bottom fixed turbine due to the contribution of the weight. The tower bottom fore-aft bending moment presented by the computed mean load are shown in Table 4-h. As seen in Table 4-h, the significance in the computed mean, across the simulation techniques, are not as pronounced as the differences across the atmospheric stability situations. Note that Kaimal in the below rated unstable scenario is considered as erroneous.

Table 4-h Statistics of the mean (MNm) for the load of the tower bottom fore-aft bending moment. Results from below rated, close to rated and above rated inflow fields for the bottom fixed wind turbine. Various atmospheric stabilities and wind field simulation techniques are considered.

	Below rated			**Rated**			**Above rated**		
	Neutral	*Stable*	*Unstable*	*Neutral*	*Stable*	*Unstable*	*Neutral*	*Stable*	*Unstable*
Kaimal	180.2	159.5	-9.475	241.4	220.2	256.1	162.7	157.9	148.7
TIMESR	182.2	162.4	133.2	245.7	224.7	254.4	163.9	160.3	149.9
Mann	178.6	157.7	131.3	242.1	219.6	266.8	163.1	157.5	149.0

The mean TBBM are responsible for loading and must thus be considered, as the mean part of the TBBM may contribute to overloading, over time, of the turbine component. It is relevant to see if the main TBBM load comes from the mean load or are due to the standard deviation load. The std load stands for a variability that may contribute to fatigue.

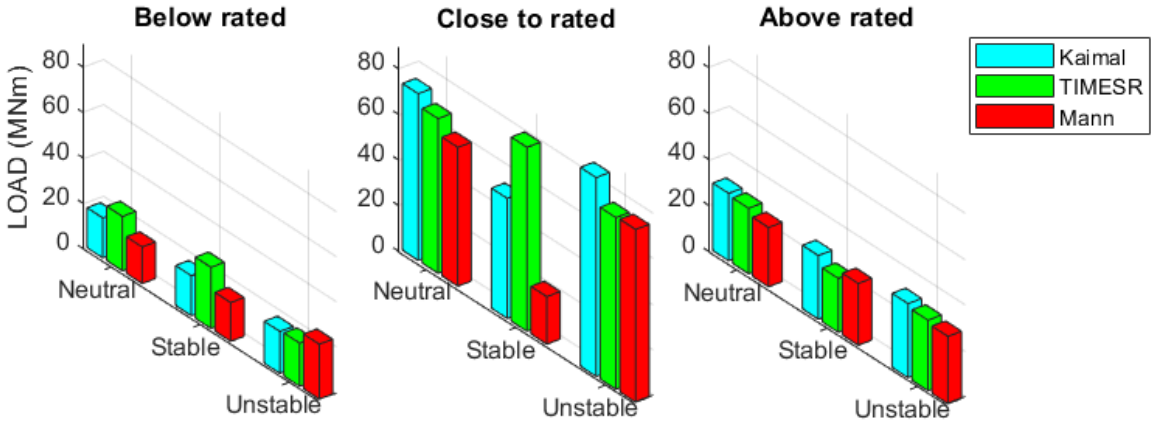

Figure 4-xix Standard deviation of tower bottom fore-aft bending moment. Results from below rated, close to rated and above rated inflow fields for the spar floating wind turbine. Various atmospheric stabilities and wind field simulation techniques are considered.

The computed standard deviation of tower bottom fore-aft bending moment load is illustrated by Figure 4-xix. The load is presented by bar graphs, where Kaimal is represented by a blue bar, TIMESR is represented by green and the bending moment from Mann inflow field have a red bar. The Figure 4-xix clearly show that the loads are increases with increasing wind speed with the result of higher TBBM in the close to rated scenario for all inflow options. The loads are seen to reduce in the above rated scenario, which are most likely due to the blade pitching to achieve constant power output. The bars also indicate the difference within the various atmospheric stability conditions across the wind field simulation techniques.

An overview of the values of the load standard deviation (MNm) is implemented in Table 4-i. The color codes included is an overview of either an underestimation and/or an overestimation of the bending moment, performed by the standard inflows relative to TIMESR. Green indicates that the loads are underestimated, and blue indicates that the loads are overestimated.

Table 4-i Statistics of the computed standard deviation (MNm) load for the tower bottom fore-aft bending moment. Results from below rated, close to rated and above rated inflow fields for the bottom fixed wind turbine. Various atmospheric stabilities and wind field simulation techniques are considered. Green indicates an underestimated load and blue indicates an overestimated load.

	Below rated			**Rated**			**Above rated**		
	Neutral	*Stable*	*Unstable*	*Neutral*	*Stable*	*Unstable*	*Neutral*	*Stable*	*Unstable*
Kaimal	17.64	17.61	18.48	73.15	52.67	87.24	29.32	27.71	32.23
TIMESR	23.95	26.96	19.00	67.87	80.72	75.33	28.51	23.43	30.69
Mann	16.14	17.08	24.15	60.92	20.87	75.77	25.78	26.88	29.29

Table 4-i show that Mann and Kaimal does not follow each other as closely in this load response as they did for the bottom fixed turbine TBBM. The only exception is for the stable stratified load case for below rated wind speed scenario. The largest differences for the stable computed std load are in the close to rated scenario, where Mann are underestimating the TBBM relative to TIMESR by 70%. In general, Kaimal underestimates in the below rated scenario, while overestimates for the higher wind speed scenarios, with the exception in the stable condition for the close to rated scenario. The largest overestimation of the TBBM is observed for the unstable Mann inflow, by 27% relative to TIMESR. Table 4-i show that Kaimal yields consistently larger loads than Mann.

The Table 4-i also show that unstable and stable situations are different than the neutral situations. The close to rated scenario, for the stable Mann inflow, gives about 65% lower computed std load than the neutral situation. Kaimal gives about 40% higher loads than the neutral condition, in the below rated scenario. The differences of stabiltites in TIMESR are not as pronounced as for the other load cases. Yet, the loads are both lower and higher than the neutral cases, with values between 10 – 20%.

The Figure 4-xx, Figure 4-xxi and Figure 4-xxiii shows the load spectra for below rated, close to rated and above rated scenarios. The various flow-simulation methods covering neutral, stable and unstable situations are included in the spectra.

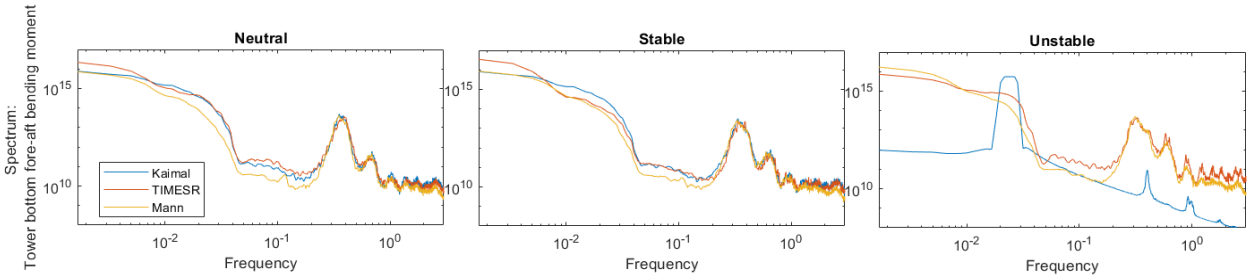

Figure 4-xx Load spectrum of tower bottom fore-aft bending moment given for the spar floater – BR

The load spectra in Figure 4-xx show most differences between the three models in the frequencies lower than 0.2 Hz. As mentioned earlier, there seems to be an error in the unstable condition by Kaimal, shown in Figure 4-xx, and is thus not included in the discussion. Also mentioned earlier, the low-frequency range is an important range for the spar floater since the loads will be impacted by the rigid motion of the platform. No sharp peaks due to the motion of the spar platform is observed. In general, in the low frequency range, Kaimal show closer match to TIMESR than the loads by Mann in the neutral case. While the standard models swithces between being the matching part with TIMESR in the stable situation.

The spectral peaks shown in Figure 4-xx is obsereved to match quite well across the flow-simulation methods. The most pronounced peak is due to the blade passing frequency, the 3P load at about 0.32 Hz, which as greatest impact in the neutral and stable atmospheric conditions. While the next peak at abot 0.6 Hz more dominant in the unstable situation.

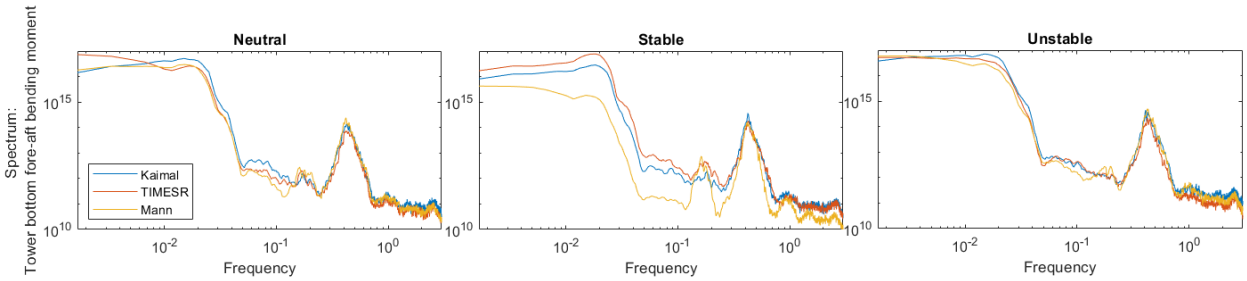

Figure 4-xxi Load spectrum of tower bottom fore-aft bending moment given for the spar floater – R

The results in Figure 4-xxFigure 4-xxi show once more differences in the low frequency range, most substantial in the stable situation. The turbulent wind forcing are impacting the TBBM moment with most energy with its low frequency signals. A small bump is observed at about 0.018 Hz (i.e. time scale of 55 seconds), which is closest to the pitch motion. In neutral stratified load spectra within the range of 0.05 – 0.1 Hz, Kaimal tend to be higher than the two others. A small peak are seen for the 1P load, while the most dominating peak is observed at about 0.42 Hz and referred to the 3P load. The peak is well mathced across the flow-simulation techniques and it has largest impact on the TBBM in the unstable case.

The differences at the low-frequency range illustrated in with an linear y-axis. This show the difficulty to obsereve the differences in a logarithmic scale. The peak that appear in, is the one discribed above at about 0.018 Hz. The fig show clear differences in the effects that affct the TBBM load across the flow-simulation methods.

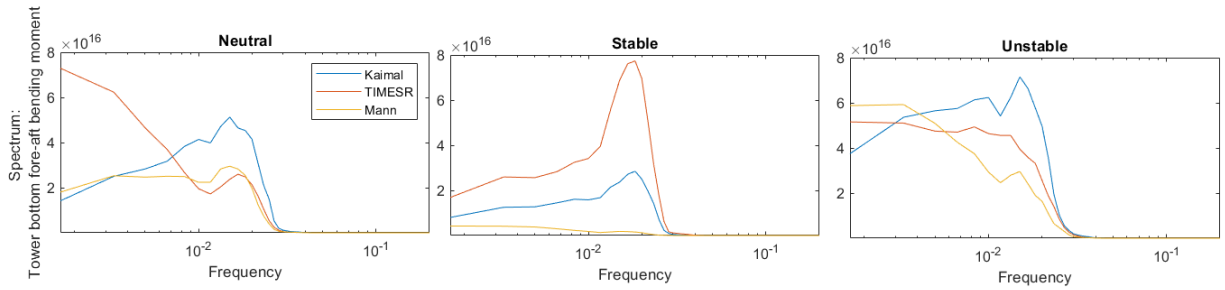

Figure 4-xxii Load spectrum of tower bottom fore-aft bending moment, with a logarithmic x-axis (0 – 0.2 Hz) and a linear y-axis.

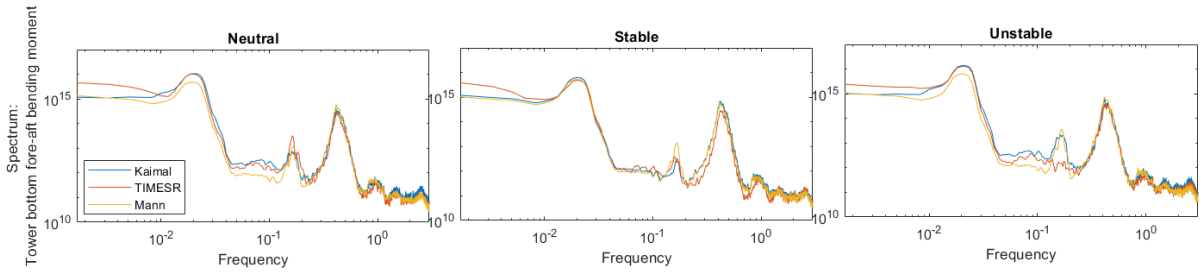

Figure 4-xxiii TBBM AR

The load spectra for the above rated scenario is shown in Figure 4-xxiii. The peak around 0.02 Hz is more visible in this spectrum, but with less energy than the close to rated scenario. There seems to be more agreement between Kaimal, Mann and TIMESR in the above rated scenario. Kaimal performance is generally closer to TIMESR. Interestingly, TIMESR misses the 1P load in the unstable situation. The 1P load occur at about 0.16 Hz and we observe it to have larger energy content than for the peak in the close to rated scenario. The 3P is a more dominant peak, which are well matched across the flow-simulation techniques and gives greatest effect in the unstable atmospheric condition.

4.2.4 Flapwise bending moment in the blade root – Spar floater

The resulting flapwise bending moment in the blade root is presented in this section for the 10 MW spar floating wind turbine. The FBM is investigating for one of the three blades, blade 1.

The pre-generated wind boxes: Kaimal, Mann and TIMESR are all used in the simulation of the spar floating wind turbine. The turbulent wind impacts the turbine, which react with platform global motions. Both wind and platform movements have consequences for the loads in the wind turbine components. The flapwise bending moment in the blade root is investigated for the various flow-simulation techniques performed for neutral, stable and unstable atmospheric conditions. In total, twenty-seven simulations, where the below rated, close to rated and above rated wind speed scenarios were considered. The inflow fields and the dynamical calculation parameters are shown in Table 4-j below. The values presented by Table 4-l and spectral analysis can be used to quantify the standard generated inflows performance relative to TIMESR.

Table 4-j Simulation input in SIMA

Environmental load	Simulation time (s)	Time step (s)	Time increment
Kaimal/TIMESR/Mann	3800	0.01/0.01/0.0116	0.1/0.1/0.116

The flapwise bending moment in the blade root presented by the computed mean load are shown in Table 4-k. There are not significant differences in the mean load of FBM across the three wind field simulation techniques. There is a slightly more variation in the results across the atmospheric stabilities.

Table 4-k Statistics of the mean (MNm) load of the flapwise bending moment. Results from below rated, close to rated and above rated inflow fields for the bottom fixed wind turbine. Various atmospheric stabilities and wind field simulation techniques are considered.

	Below rated			**Rated**			**Above rated**		
	Neutral	*Stable*	*Unstable*	*Neutral*	*Stable*	*Unstable*	*Neutral*	*Stable*	*Unstable*
Kaimal	18.63	16.81	16.80	23.76	21.34	25.53	15.33	13.90	13.97
TIMESR	18.82	17.06	14.48	24.10	22.05	25.24	15.03	14.18	13.32
Mann	18.52	16.70	14.40	23.68	21.26	26.82	15.40	13.72	14.55

The mean FBM are results from loads that may create overload in the component, over time, and must thus be considered. It is relevant to investigate the FBM is mostly due to mean load or by standard deviation load. The latter stands for a variability that may contribute to fatigue.

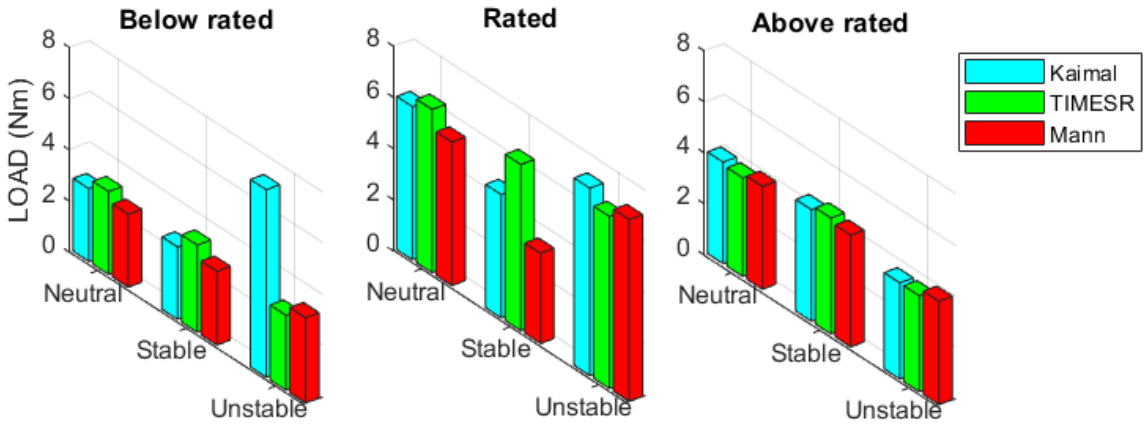

Figure 4-xxiv Standard deviation of tower bottom fore-aft bending moment. Results from below rated, close to rated and above rated inflow fields for the spar floating wind turbine. Various atmospheric stabilities and wind field simulation techniques are considered.

The computed standard deviation load of the flapwise bending moment is illustrated by Figure 4-xxiv. The load is presented by bar graphs. Kaimal is represented by a blue bar, TIMESR is represented by green and the bending moment from Mann have a red bar. Figure 4-xxiv clearly show that the loads increases with increasing wind speed. This results in higher FBM in the close to rated scenario, except for the stable condition, where both Kaimal, but especially Mann does not increase as much as TIMESR. In the above rated scenario, the standard flow-simulation techniques closely match the computed std for TIMESR.

An overview of the values of the load standard deviation (MNm) is implemented in Table 4-l. The color codes included is an overview of either an underestimation and/or an overestimation of the bending moment, performed by the standard inflows relative to TIMESR. Green indicates that the loads are underestimated, and blue indicates that the loads are overestimated. Once again, the unstable condition for Kaimal, in the below rated scenario, might be erroneous.

Table 4-l Statistics of the computed standard deviation load (MNm) for the flapwise bending moment in the blade root. Results from below rated, close to rated and above rated inflow fields for the bottom fixed wind turbine. Various atmospheric stabilities and wind field simulation techniques are considered. Green indicates an underestimated load and blue indicates an overestimated load.

	Below rated			**Rated**			**Above rated**		
	Neutral	*Stable*	*Unstable*	*Neutral*	*Stable*	*Unstable*	*Neutral*	*Stable*	*Unstable*
Kaimal	2.843	2.826	7.324	5.986	4.812	7.324	3.982	4.380	3.769
TIMESR	3.231	3.402	2.925	6.377	6.486	6.719	3.867	4.553	3.763
Mann	2.847	2.880	3.328	5.604	3.526	7.100	4.035	4.383	4.052

Table 4-l show that both Kaimal and Mann underestimate the computed std load in the stable situations, while they overestimate in the unstable situations relative to TIMESR, for all wind speed scenarios. The below rated and above rated scenarios show some agreement of the load estimation between the standard load cases, except for the unstable Kaimal in the below rated scenario, which overestimates the load by 150%, which may be assumed to be incorrect.

The sensitivity of the load response due to atmospheric stability is observed in Table 4-l, where the largest differences is seen in the close to rated scenario. Both standard wind field techniques generate lower loads in the stable conditions relative to neutral, while TIMESR generates a slightly higher load. The opposite is true for the unstable situation, where the standards cause higher loads than the neutral case.

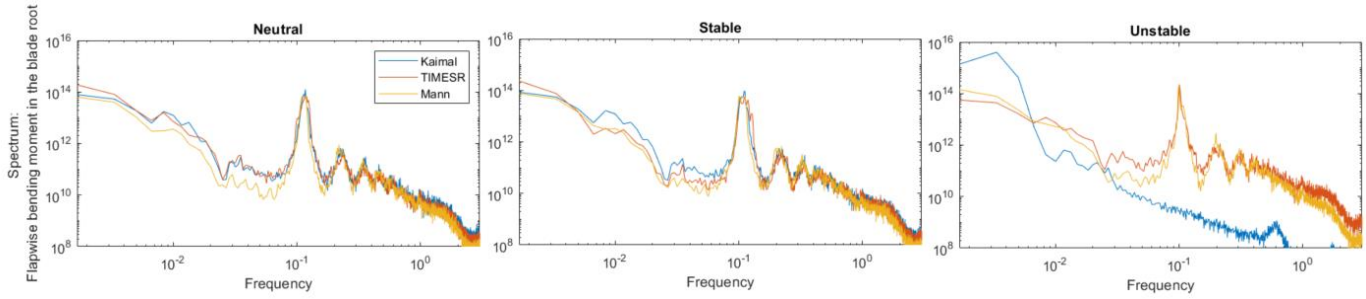

Figure 4-xxv Comparison of the spar floating wind turbine response in terms of load spectra for the three flow-simulation methods [Kaimal (blue), TIMESR (red) and Mann (yellow)] and various atmospheric conditions: neutral (left), stable (middle) and unstable (right). Given for the flapwise bending moment in the blade root for the below rated wind-speed scenario.

Figure 4-xxv show the power spectral density of the reconstructed flapwise bending moment in the blade root, for the below rated scenario. Note that Kaimal is considered as an error and are not included in the discussion.

We observe effects on the response from the platform movements in Figure 4-xxv, as the low frequency responses are shown at the surge eigenfrequency, at about 0.01 Hz. This is shown to be higher for the Kaimal method in neutral and stable situations. It is observed a well performance of Kaimal in the neutral atmospheric stability, as it follows TIMESR closely. Mann have lower energy, and the figure show that loads are not excited from the platform movements. The rotational frequency is dominant for the flapwise vibrations of the blade. The 1P load is observed at about 0.1 Hz and contribute significantly to the response at all cases. The peak found at the range of 0.2 Hz is most likely due to the tower frequency. The 3P is also visible and is found at about 0.3 Hz. All the dominating peaks are well matched across the flow-simulation techniques.

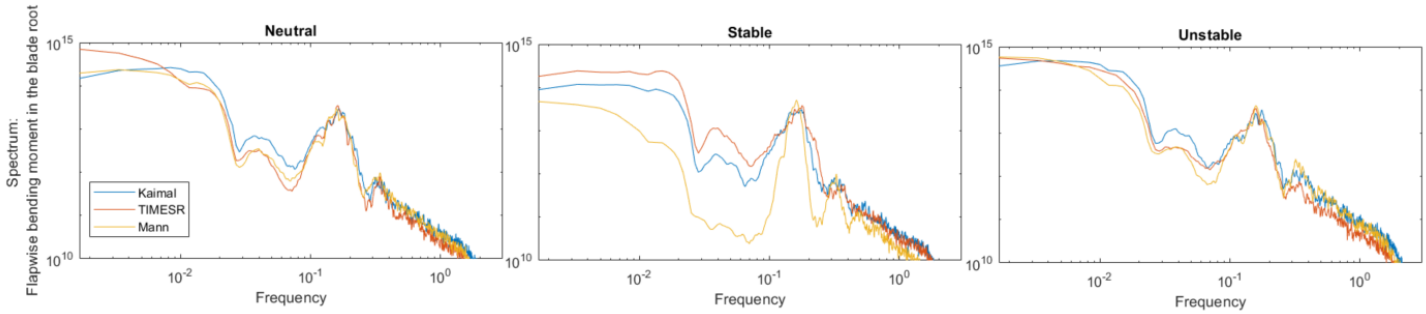

Figure 4-xxvi Comparison of the spar floating wind turbine response in terms of load spectra for the three flow-simulation methods [Kaimal (blue), TIMESR (red) and Mann (yellow)] and various atmospheric conditions: neutral (left), stable (middle) and unstable (right). Given for the flapwise bending moment in the blade root for the close to rated wind-speed scenario.

Figure 4-xxvi show the power spectral density of the reconstructed flapwise bending moment in the blade root, for the below rated scenario. There is a higher energy level around the surge eigenfrequency mode, at about 0.015 Hz, compared to the below rated scenario. Kaimal is observed to have higher response at the lower frequencies in the neutral and the unstable conditions. TIMESR has the highest visible response in the stable condition, while Mann seems to completely miss it. The greatest differences across the flow-simulation techniques are observed within this stability. A peak is visible in the range of 0.04 Hz for all cases, which is closest to the heave eigenfrequency. The 1P load occur at about 0.16 Hz for all cases, but is observed to be less dominant than the response at lower frequencies.

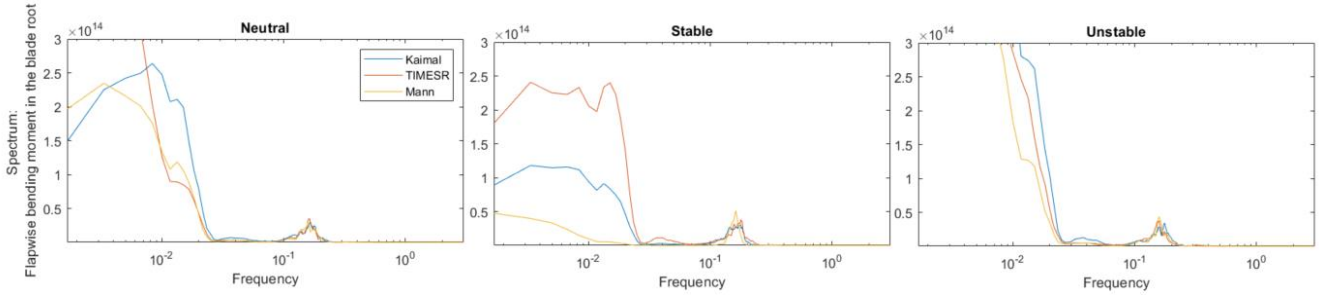

Figure 4-xxvii Load spectrum of flapwise bending moment, with a logarithmic x-axis (0 – 3 Hz) and a linear y-axis.

The load spectrum with a linear axis is shown by Figure 4-xxvii and illustrates the differences at the lower frequencies more clearly. As well as to show how dominant the response is in this region, where the six rigid body movements of spar impact the response. The Figure 4-xxvii also show the well matched 1P load across the flow-simulation techniques.

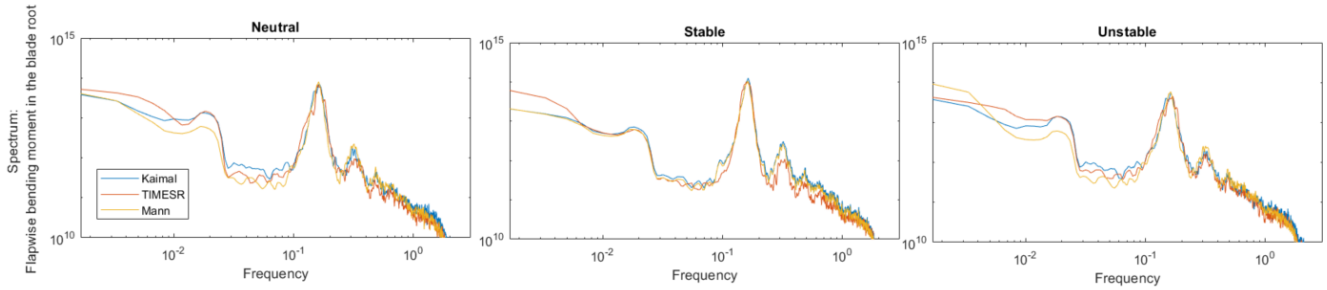

Figure 4-xxviii Comparison of the spar floating wind turbine response in terms of load spectra for the three flow-simulation methods [Kaimal (blue), TIMESR (red) and Mann (yellow)] and various atmospheric conditions: neutral (left), stable (middle) and unstable (right). Given for the flapwise bending moment in the blade root for the above rated wind-speed scenario.

Figure 4-xxviii show the power spectral density of the reconstructed flapwise bending moment in the blade root, for the above rated scenario. The observed peak in the low frequency range is shifted towards 0.02 Hz. This is in between the surge and the pitch frequencies. Unlike the close to rated scenario, the flow-simulation techniques seem to have the same performance in the stable situation. Once again, Mann is shown to give the lowest response in the low frequency range for neutral and unstable conditions. Like the below rated scenario, the 1P variation have a larger impact on the response than the excitations from the spar platform. The 3P load is visible at about 0.32 Hz and is found to have the lowest peak for the TIMESR flow field.

5 Summary & conclusion

The overall aim of this study was to perform wind turbine simulations with turbulence inflow from different wind field simulation techniques, to explore structural load response of a bottom fixed and a spar floating wind turbine.

Wind turbine simulations are performed with SIMA to investigate structural loads in response to the environment. The environment used in this study, is turbulent wind. As the wind turbine design actively becomes larger, the importance to model realistic offshore environments increases. The recommended wind fields used in the industry, the Kaimal spectral and exponential coherence model and the Mann spectral tensor model, have not developed in line with the increasing offshore wind turbines structures. Nor are they expanded to represent the full stability range in an offshore environment. When wind fields with different wind model techniques are generated, they will yield different loads. There is a need to reduce uncertainty by reproduce realistic offshore turbulent structures that include all atmospheric conditions.

In this study, the standard generated wind fields are compared to the wind fields generated by the TIMESR method. The latter have been implemented with time series from the point measurements sampled at the offshore mast FINO-1, which are assumed to represent a closer to realistic wind environment. The standard generated wind fields are adjusted with site-specific parameters to represent stable and unstable atmospheric conditions. The wind fields have matching characteristics such as standard deviation, turbulence intensity and mean wind speed to exclude their dominance on the load response. The reason is that we wanted to investigate load response due to turbulence and coherence.

Efficient offshore wind turbine is needed to perform simulations. A spar floating wind turbine is modified to be identical with the bottom fixed turbine assessed in this study, except for the sub-structure. There are some factors in the spar model that needs further investigation, such as to study the instabilities due to the yaw motion. The application of the controller used for the spar floater should also be further analysed.

The analysis of the load response given for the bottom fixed and the spar floater includes wind flow surrounding the whole wind turbine rotor. This flow is the pre-generated wind boxes from the three wind field generation techniques. The results from the simulations has been presented in chapter 4 where the turbulent wind fields analysed and compared. The loads that the turbulent wind flow produce on the rotor and the tower, in terms of flapwise bending moment and tower bottom bending moment, is explored. The performance of Kaimal and Mann is investigated relative to TIMESR. Finally, the stable and unstable condition is evaluated relative to the neutral condition to see the impact of assuming neutral atmospheric stability when the standard methods are used to represent the offshore turbulent structures.

The findings of the simulated wind fields showed that it is possible to create wind fields with matching characteristics at hub height from measurements, which is verified with the wind profile and the wind spectrum. The most energetic variation of the turbulent wind across the simulation methods is in the frequency range below 0.1 Hz. The turbulent wind spectrum show that the standard models represent turbulent wind similarly, while TIMESR vary in representing turbulence higher or lower than Kaimal and Mann. Several wind fields should be generated with different seeds to get less uncertainty.

Temporal distribution of coherence was investigated, where co-coherence as function of reduced frequency was considered. The standard models nor TIMESR have matching co-coherence. The co-coherence is found to be most significant at low frequencies and will therefore have a large effect on the floating turbine. The Davenport model is used to represent co-coherent time series for TIMESR. This might not be acceptable or representative for the measurements as this simple coherence model cannot fully characterize coherence in different directions nor over a distance. This might be crucial for the large offshore wind turbines. Quad coherence (represents the phase shifts of the coherence structure) only represented by Mann and limited for the others. This is a limitation, since the phase shift can have an impact on the loads. It is recommended to further strive to find and use methods to better represent the measurements.

Based on the various turbine load studied, it is concluded that is difficult to state which wind field simulation techniques that performs the load prediction best. Yet, the analysis showed that Mann tends to underestimate the computed standard deviation, especially in the tower bottom fore-aft bending moment for both turbines. As seen from the load spectra, Kaimal generally matches TIMESR more closely. These differences may be related to the differences seen in the lateral co-coherence, where Mann behaved quite different than the others. The load response showed that it is sensitive to atmospheric stability, which show that neutral might be a poor assumption, especially with increasing rotor sizes.

6 Further work

- Run the same wind fields with different seeds to verify the findings
- Snapshots of turbulence with varying atmospheric stability to see the different eddy sizes
- Proper decomposition modes to illustrate coherent structures in the turbulent flow
- Analyse the distribution of the load response, which can give insight into relatively extreme values in each simulation [7]
- Further use the standard deviation values to perform a fatigue analysis
- Investigate the controller functionality to reduce the yaw-motion
- Use/develop routines to systematically test the functionality of turbine components
- Stress test of turbine components
- Further investigate the load response illustrated in Appendix E

References

[1] IEC, 'Wind Turbine—Part 1: Design Requirements, IEC 61400-1', vol. 3, p. 60, 2005.

[2] BSI, 'BSI British Standards- BS EN 61400-3:2009- Wind turbines - Part 3: Design requirements for offshore wind turbines', in *BSI British Standards- BS EN 61400-3:2009*, British Standards, 2009.

[3] DNV, 'DNV-OS-J101 Design of Offshore Wind Turbine Structures', *Det Nor. Verit. As*, no. May, pp. 1–238, 2014.

[4] Det Norske Veritas Germanischer Lloyd, 'DNVGL-RP-C205: Environmental Conditions and Environmental Loads', *DNV GL Recomm. Pract.*, 2017.

[5] L. Eliassen and E. E. Bachynski, 'The effect of turbulence model on the response of a large floating wind turbine', in *Proceedings of the International Conference on Offshore Mechanics and Arctic Engineering - OMAE*, 2017.

[6] A. Nybø, F. G. Nielsen, J. Reuder, M. Churchfield, and M. Godvik, 'Evaluation of different wind fi elds for the investigation of the dynamic response of offshore wind turbines', pp. 1–24.

[7] P. Doubrawa, M. J. Churchfield, M. Godvik, and S. Sirnivas, 'Load response of a floating wind turbine to turbulent atmospheric flow', *Appl. Energy*, vol. 242, no. October 2018, 2019.

[8] L. Eliassen and C. Obhrai, 'Coherence of Turbulent Wind under Neutral Wind Conditions at FINO1', in *Energy Procedia*, 2016.

[9] A. Nybø, F. G. Nielsen, and J. Reuder, 'Processing of sonic anemometer measurements for offshore wind turbine applications', *J. Phys. Conf. Ser.*, 2019.

[10] B. J. Jonkman, 'TurbSim User's Guide v2. 00.00', *Natl. Renew. Energy Lab.*, no. October 2014, 2014.

[11] S. H. Sørum, J. T. H. Horn, and J. Amdahl, 'Comparison of numerical response predictions for a bottom-fixed offshore wind turbine', *Energy Procedia*, vol. 137, pp. 89–99, 2017.

[12] M. H. Christian Bak, Frederik Zahle, Robert Bitsche, Taeseong Kim, Anders Yde, Lars C. Henriksen, Anand Natarajan, 'Design and performance of a 10 MW wind turbine', 2013.

[13] J. Mur-Amada and A. Bayod-Rujul, *Variability of Wind and Wind Power*, no. June 2010. 2010.

[14] R. M. Putri, 'A Study of the Coherences of Turbulent Wind on a Floating Offshore Wind

Turbine', no. June, p. 166, 2016.

[15] L. M. Bardal, A. E. Onstad, L. R. Sætran, and J. A. Lund, 'Evaluation of methods for estimating atmospheric stability at two coastal sites', *Wind Eng.*, 2018.

[16] J. A. Businger and A. M. Yaglom, 'Introduction to Obukhov's paper on "turbulence in an atmosphere with a non-uniform temperature"', *Boundary-Layer Meteorol.*, 1971.

[17] R. B. Stull, *An introduction to Boundary Layer Meteorology*. Kluwer academic publishers, 1988.

[18] A. J. M. Van Wijk, A. C. M. Beljaars, A. A. M. Holtslag, and W. C. Turkenburg, 'Evaluation of stability corrections in wind speed profiles over the North Sea', *J. Wind Eng. Ind. Aerodyn.*, 1990.

[19] S. Emeis, 'Current issues in wind energy meteorology', *Meteorological Applications*. 2014.

[20] M. Ragheb, 'Energy and power of the wind', 2012.

[21] A. Sathe, J. Mann, T. Barlas, W. A. A. M. Bierbooms, and G. J. W. Van Bussel, 'Influence of atmospheric stability on wind turbine loads', *Wind Energy*, 2013.

[22] Sø. E. Larsen, S.-E. Gryning, N. . Jensen, H. . Jørgensen, and J. Mann, 'Mean Wind and Turbulence in the Atmospheric Boundary Layer Above the Surface Layer', p. 5, 2007.

[23] S. E. Gryning, E. Batchvarova, B. Brümmer, H. Jørgensen, and S. Larsen, 'On the extension of the wind profile over homogeneous terrain beyond the surface boundary layer', *Boundary-Layer Meteorol.*, 2007.

[24] 'BSI British Standards. Wind turbines -', 2009.

[25] B. Lange, S. Larsen, J. Højstrup, and R. Barthelmie, 'Importance of thermal effects and sea surface roughness for offshore wind resource assessment', *J. Wind Eng. Ind. Aerodyn.*, 2004.

[26] A.-S. Smedman *et al.*, 'Towards a fundamentally new understanding of the marine atmospheric boundary layer', in *16th Symposium on Boundary Layers and Turbulence*, 2004.

[27] B. Lange, 'Offshore Wind Power Meteorology', in *Wind Energy*, 2007.

[28] A. Borovik, 'Kolmogorov's "5/3" Law | Mathematics under the Microscope'. [Online]. Available: https://micromath.wordpress.com/2008/04/04/kolmogorovs-53-law/. [Accessed: 11-Jun-2019].

[29] T. Burton, N. Jenkins, D. Sharpe, and E. Bossanyi, *Wind Energy Handbook, Second*

Edition. 2011.

[30] P. K. Manne, 'The importance of wind turbulence and coherence to the loads on a wind turbine blade', no. June, 2019.

[31] E. Lehn, 'Sampling, filtrering og analyse'.

[32] 'IEC 61400-1:2019 | IEC Webstore | rural electrification, wind power'. [Online]. Available: https://webstore.iec.ch/publication/26423. [Accessed: 05-Jul-2019].

[33] J. C. Kaimal, J. C. Wyngaard, Y. Izumi, and O. R. Coté, 'Spectral characteristics of surface-layer turbulence', *Q. J. R. Meteorol. Soc.*, 1972.

[34] E. Smilden, A. Sørensen, and L. Eliassen, 'Wind Model for Simulation of Thrust Variations on a Wind Turbine', in *Energy Procedia*, 2016.

[35] J. Mann, 'Wind field simulation', *Probabilistic Eng. Mech.*, 1998.

[36] T. von Karman, 'Progress in the Statistical Theory of Turbulence', *Proc. Natl. Acad. Sci.*, 1948.

[37] N. K. Dimitrov and B. S. Lazarov, 'Reducing Wind Turbine Load Simulation Uncertainties by Means of a Constrained Gaussian Turbulence Field', 2019.

[38] FINO-1, 'FINO1 - research platform in the North Sea and the Baltic No. 1'. [Online]. Available: https://www.fino1.de/en/. [Accessed: 13-Apr-2019].

[39] 'THE LOW LEVEL JET'. [Online]. Available: http://www.theweatherprediction.com/severe/llj/. [Accessed: 13-Jun-2019].

[40] N. Svensson, 'Wind and atmospheric stability characteristics over the Baltic Sea', p. 37, 2016.

[41] H. J. Breedt, 'Atmospheric Boundary Layer Stability and its Application to Computational Fluid Dynamics', no. January, 2018.

[42] N. Kelley and B. Jonkman, 'TurbSim | NWTC Information Portal'. [Online]. Available: https://nwtc.nrel.gov/TurbSim. [Accessed: 01-Jul-2019].

[43] P. S. Veers, 'Three-Dimensional Wind Simulation', *J. Geophys. Res.*, 1987.

[44] R. Worsnop, J. K. Lundquist, and G. Bryan, 'Power spectrum and spatial coherence of turbulent structures inside an idealized major hurricane'.

[45] 'Welcome to HAWC2'. [Online]. Available: http://www.hawc2.dk/hawc2-info. [Accessed: 14-Jul-2019].

[46] E. Cheynet, J. B. Jakobsen, and J. Reuder, 'Velocity Spectra and Coherence Estimates in

the Marine Atmospheric Boundary Layer', *Boundary-Layer Meteorol.*, 2018.

[47] J. Jonkman, S. Butterfield, W. Musial, and G. Scott, 'Definition of a 5-MW Reference Wind Turbine for Offshore System Development', 2009.

[48] F. G. Nielsen, 'Support Structures for Offshore Wind Turbines', pp. 1–15, 2018.

[49] DNV (Det Norske Veritas), 'DNV-OS-J101 Design of Offshore Wind Turbine Structures', *May*, 2014.

[50] B. Skaare *et al.*, 'Integrated Dynamic Analysis of Floating Offshore Wind Turbines', no. January, pp. 671–679, 2007.

[51] T. T. Tran and D. H. Kim, 'The platform pitching motion of floating offshore wind turbine: A preliminary unsteady aerodynamic analysis', *J. Wind Eng. Ind. Aerodyn.*, 2015.

[52] W. Xue, 'Design, numerical modelling and analysis of a spar floater supporting the DTU 10MW wind turbine', no. June, 2016.

[53] B. Skaare, 'Development of the hywind concept', in *Proceedings of the International Conference on Offshore Mechanics and Arctic Engineering - OMAE*, 2017.

[54] Morten Hartvig Hansen ; Lars Christian Henriksen, *Basic DTU Wind Energy controller*. 2013.

[55] Q. Wang and E. Bachynski, 'A Note on the Modification of Controller before Putting the DTU 10MW RWT onto a Floating Platform'.

[56] V. Igwemezie, A. Mehmanparast, and A. Kolios, 'Materials selection for XL wind turbine support structures: A corrosion-fatigue perspective', *Mar. Struct.*, 2018.

[57] DNV-GL, 'Marine operations and mooring analysis software | Sima - DNV GL'. [Online]. Available: https://www.dnvgl.com/services/marine-operations-and-mooring-analysis-software-sima-2324. [Accessed: 22-Jul-2019].

[58] B. Skaare, T. D. Hanson, R. Yttervik, and F. G. Nielsen, 'Dynamic response and control of the hywind demo floating wind turbine', in *EWEA*, 2011, pp. 53–57.

[59] B. Skaare, T. D. Hanson, R. Yttervik, and F. G. Nielsen, 'Dynamic response and control of the hywind demo floating wind turbine', in *EWEA*, 2011.

[60] 'XL Monopiles'. [Online]. Available: http://www.esru.strath.ac.uk/EandE/Web_sites/14-15/XL_Monopiles/structural.html. [Accessed: 01-Aug-2019].

[61] S. Bhattacharya, 'Challenges in Design of Foundations for Offshore Wind Turbines',

Eng. Technol. Ref., 2014.

[62] P. J. Schubel and R. J. Crossley, 'Wind turbine blade design', in *Wind Turbine Technology: Principles and Design*, 2014.

[63] I. Abdallah, C. Lataniotis, and B. Sudret, 'Parametric hierarchical kriging for multi-fidelity aero-servo-elastic simulators — Application to extreme loads on wind turbines', *Probabilistic Eng. Mech.*, 2019.

[64] C. Sim, S. Basu, and L. Manuel, 'On space-time resolution of inflow representations for wind turbine loads analysis', *Energies*, 2012.

7 Appendix A

7.1 Selection process

7.1.1 Below rated (7.5 m/s)

The selected time series.

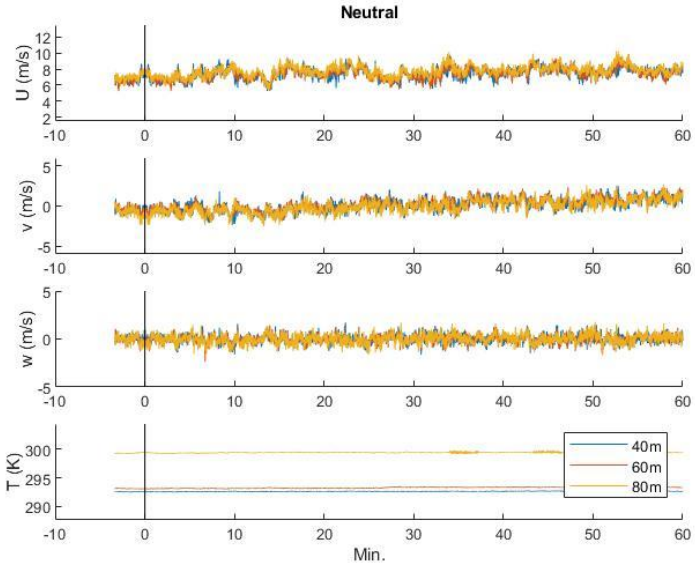

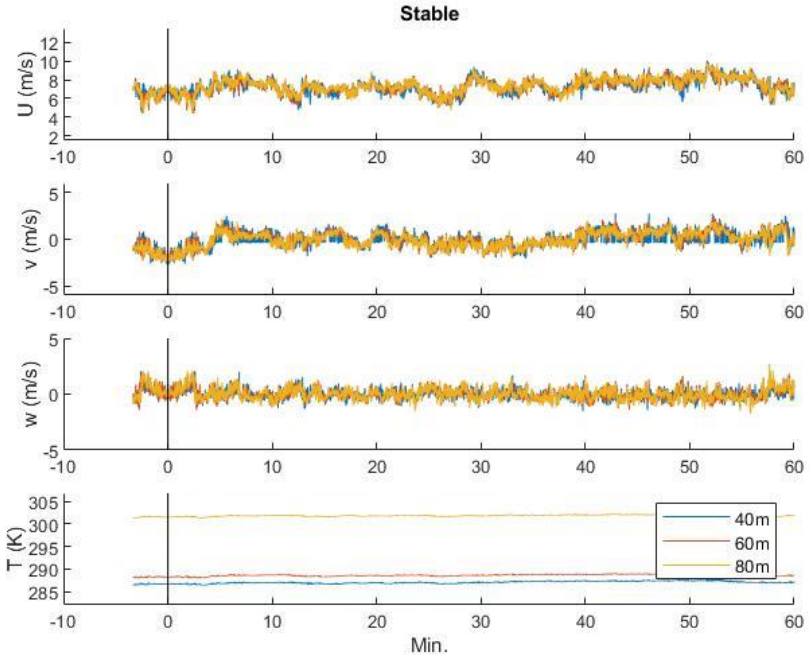

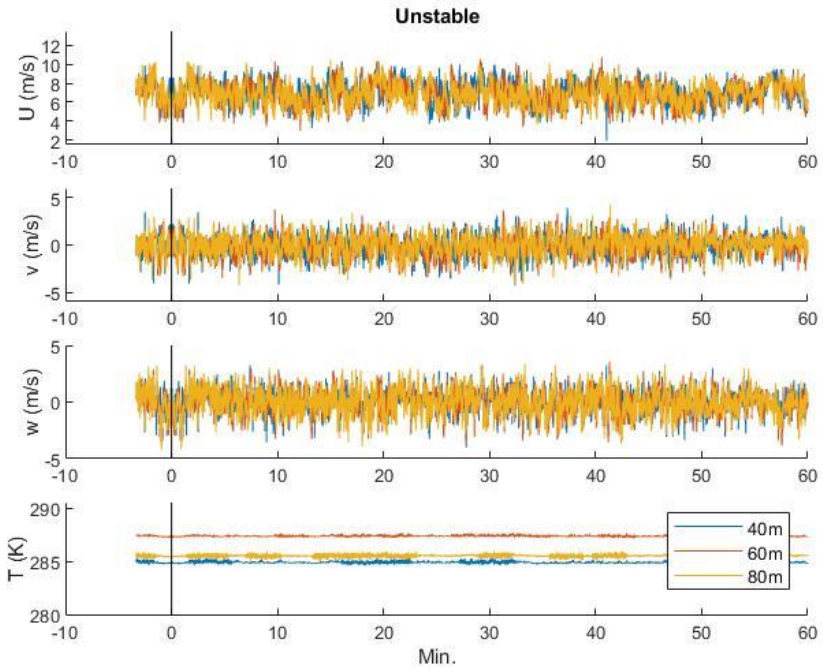

7.1.2 Close to rated (12.5 m/s)

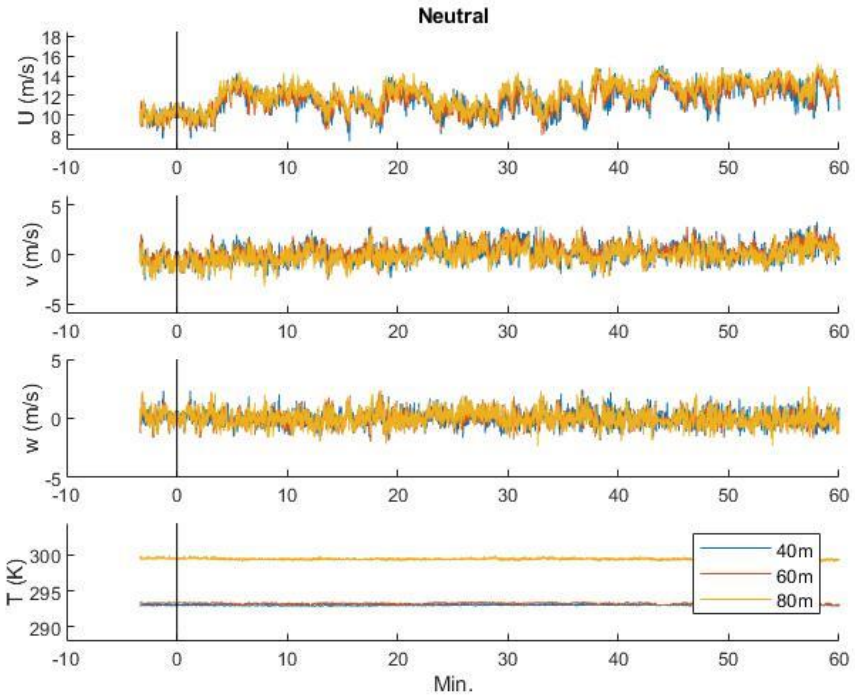

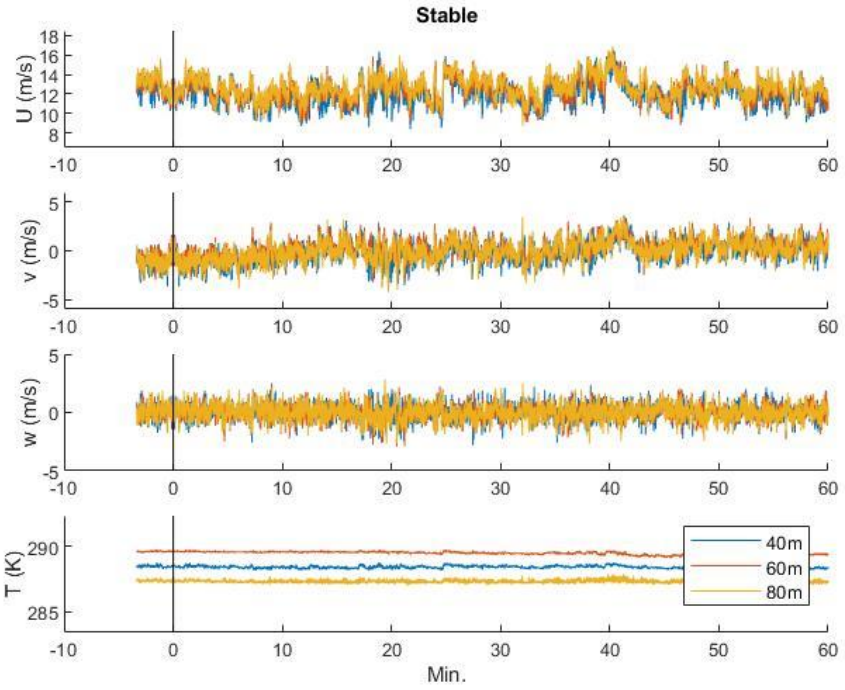
Stable
U (m/s)
v (m/s)
w (m/s)
T (K)
40m
60m
80m
Min.

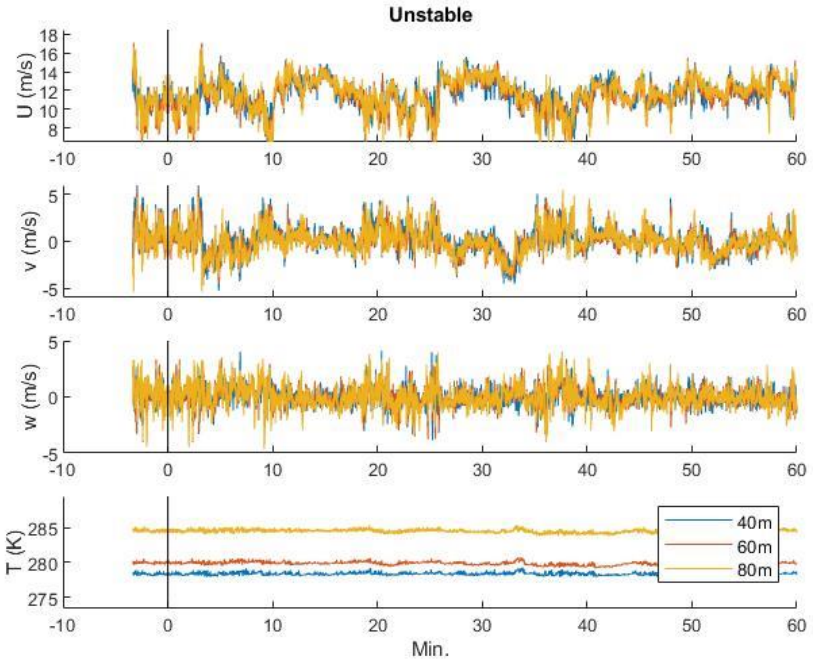
Unstable
U (m/s)
v (m/s)
w (m/s)
T (K)
40m
60m
80m
Min.

7.1.3 Above rated (17.5 m/s)

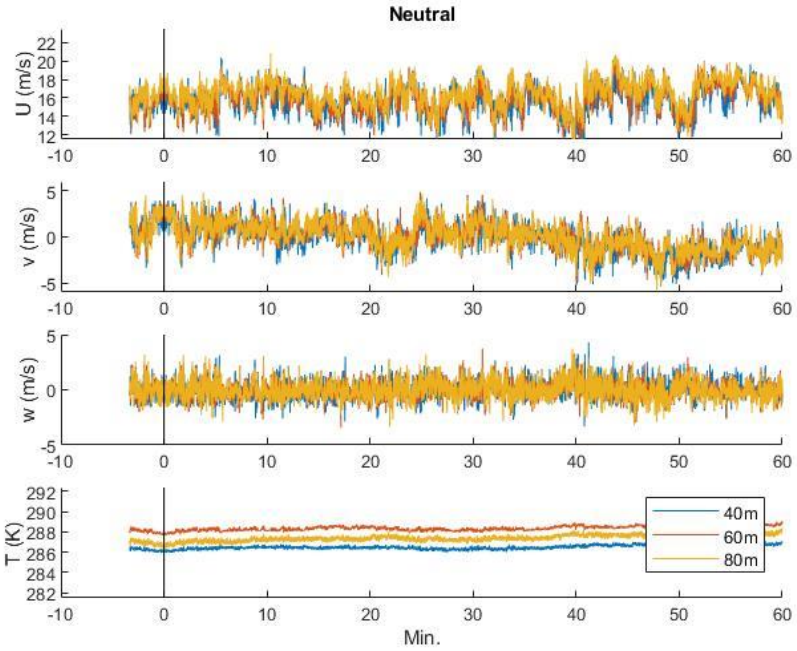

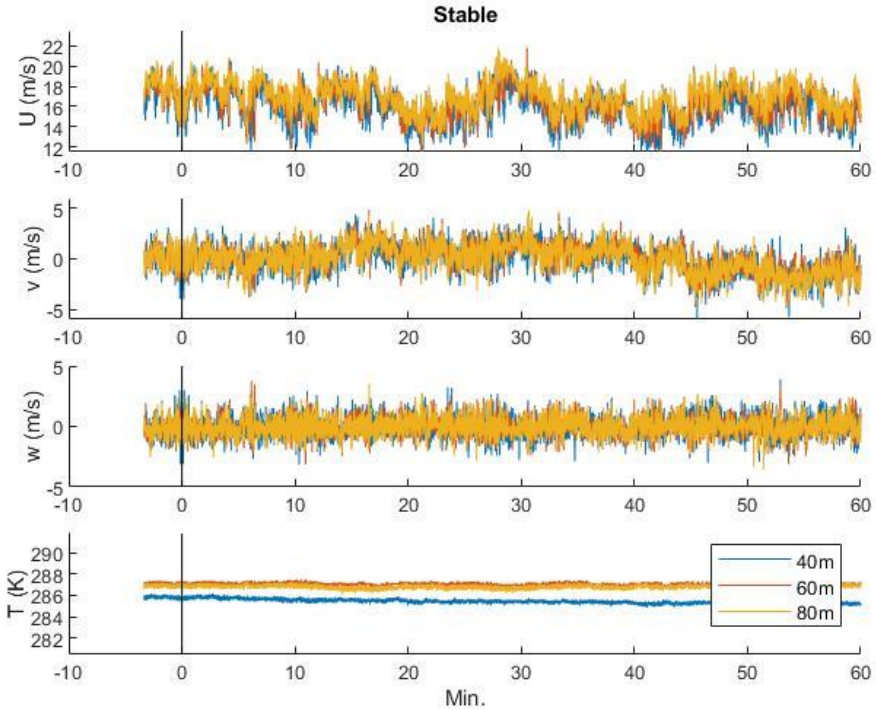

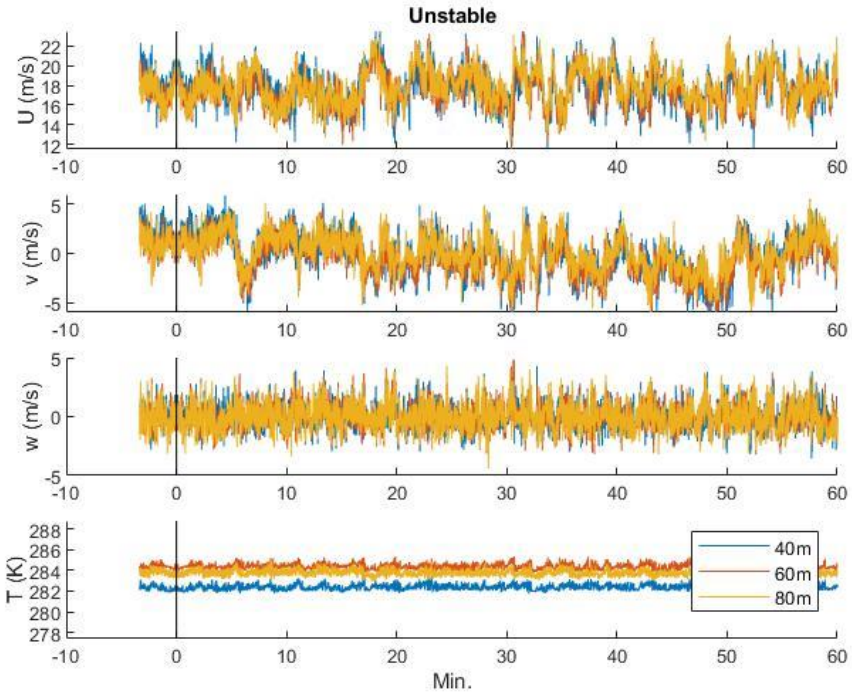
Unstable
U (m/s)
v (m/s)
w (m/s)
T (K)
40m
60m
80m
Min.

8 Appendix B

8.1 Input files and descriptions

Input file examples is close to rated wind speed in a stable atmosphere. The same has been done for all simulation cases, but we some different values of some of the parameters.

8.1.1 Description

Table 8-a Inputs TurbSim simulation [10]. *Yellow indicates values for TIMESR, green indicates values for Kaimal, black if they use the same value and black for the parameters that is not used.*

Inputs TIMESR / Kaimal	**Value**	**Comments**
Runtime options:		Tells TurbSim what output file to generate.
Echo	False	Used for debugging
Randseed1	43456	Used the default values which gives random phases. Same for all runs.
Randseed2	67894578	Give random phases. Same for all runs
WrBHHTP	False	Output file option
WrFHHTP	False	Output file option
WrADHH	False	Output file option
WrADFF	False	Output file option
WrBLFF	True	Output file which will give a full-field time series data as .wnd. This is required for further use in SIMA.
WrADTWR	False	Output file option
WrFMTFF	False	Output file option
WrACT	False	Output file option
Clockwise	True	Rotates the wind clockwise
ScaleIEC	0 / 1	How to scale the time domain velocity output. 0: No scaling: time series will remain as generated.

		1: Time series is scaled so that the hub point will have the exact specified TI.
Turbine/Model specifications:		Determines: 1. The size and shape of the wind field grid. 2. Time/frequency content is determined for the resulting time series 3. Sets the mean flow angles
NumGrid_Z	64	Grid points generated in vertical direction within the wind field. One grid point is always generated at the hub point.
NumGrid_Y	64	Horizontal grid points within the wind field.
TimeStep	0.1	Determines maximum frequency used when the simulation compute the inverse Fourier transform.
AnalysisTime	3800	Simulation length for analysing time series. One hour + transient time of 200 s.
UsableTime	Not used	
HubHt	119 m	The hub height is where the inflow is being generated. A reference height for the grid. Recommended to be > ½ *GridHeight
GridHeight	220.5 m	Sets the size of the grid from bottom to top. To be above ground level: 1/2 GridHeight < HubHt and at least 10 % higher than the rotor diameter.

GridWidth	220.5	Grid height and width: The value is chosen by using the grid points and the distance between the grid points as followed: 64*3.5-3.5 =220.5
VFlowAng	0	Vertical mean flow angle of the wind
HFlowAng	0	Horizontal mean flow angle of the wind
Meteorological Boundary conditions:		Simulation of velocity spectra by determine mean wnd speeds and setting boundary conditions for chosen spectral models, such as IEC Kaimal.
TurbModel	TIMESR / IECKAI	Tells TurbSim which spectral model to use.
UserFile	U_12.5.TimeSer (e.g.) / Unused	U_12.5.TimeSer: Time series input data from measurements
IECStandard	Unused / 3	Which IEC standard to use, 3 is for offshore wind turbines.
IECturbc	Not used / From measurements calculated for hub height	Turbulence characteristics. From measurements: Define TI from hub height to match the TI that is calculated in TIMESR.
IEC_WindType	Not used / NTM	Normal Turbulence model when IECturbc is specified as a percentage
ETMc	Default: not used when using NTM	Extreme Turbulence Model Parameter
WindProfileType	USR / PL	USR: Velocity profile is defined by values in a readable table (ProfileFile) and then the values are interpolated.

		PL: Power law wind profile
ProfileFile	Pro_12.5.Profiles (e.g.)	Pro_12.5.Profiles: defines the profile for wind speed and direction.
RefHt	80 / 119	80: To give correct wind speed at hub height from the measurements 119: Creates wind speed at hub height with power law
Uref	80 / From measurements at 119 m	Mean wind speed for 3800 s at reference height for the *u*-component. 80: Ignored when using USR wind profile type thus calculated from the profile data at reference height 119: Mean wind speed at 119 m calculated from measurements.
ZjetMax	Default	Not used
PLExp	Calculated value from measurements	Power law exponent matched to the measurements for each specific atmospheric stability
Z0	Default	Not used when using USR or Kaimal
Non_IEC Meteorological Boundary Conditions:		When Kaimal is defined this section is not used. Yet, some values for TIMESR must be defined here.
Latitude	Default	Latitude in degrees Not used
RICH_NO	From measurements	Gradient Richardson Number may be used to compute the velocity

		spectra and scale coherent structures. Test by Nybø, showed that this might not influence with user profile, but defined to be sure.
Ustar	Default	Friction or shear velocity is averaged over the rotor disk. Do not influence PL or LOG (Nybø tested).
ZI	Default	Depth of the mixing layer. Not used
PC_UW	Default	Hub mean u'v' Reynolds stress. TurbSim ignores input (Nybø tested)
PC_ UV	Default	Hub mean u'w' Reynolds stress. TurbSim ignores input (Nybø tested)
PC_VW	Default	Hub mean v'w' Reynolds stress. TurbSim ignores input (Nybø tested)
Spatial coherence parameters:		This input parameters tells TurbSim how to model spatial coherence.
SCMod1	General / Default	Defines what coherence model to use for u-component wind speed. General: In order to be inputs from the user. In this case to use Davenport coherence model. Default: IEC coherence model.
SCMd2	General / Default	Coherence model for v-component wind speed. General: in order to use Davenport.

		Default: Gives no coherence. Kaimal only provide coherence in u-component wind speed.
SCMod3	General / Default	Coherence model for w-component wind speed. General: in order to use Davenport Default: Gives no coherence. Kaimal only provide coherence in u-component wind speed.
IncDec1	a: values calculated from measurements by using Davenport model, b=0 / Default	Parameter to define spatial coherence, a, for u-component wind speed. b is an offset parameter. Davenport: Values defined here is used to find the degree of spatial coherence between the grid points. Default: uses default values according to IEC standard to calculate coherence between the points.
IncDec2	Values calculated from measurements by using Davenport model / Default	Davenport: same as IncDec1, yet for v-component wind speed. Default: is none. Due to no coherence model is defined for this wind speed component
IncDec3	Values calculated from measurements by using Davenport model	Davenport: As IncDec1 and IncDec2, yet for w-component wind speed. Default: same as IncDec2.

CohExp	0 / Default	Is the exponent in the general coherence model for all wind components Default: is zero
Coherent turbulence scaling Parameters:		**This section is not used**. It is for non-IEC spectral models with RICH_NO greater than -0.05 and when output file option WrACT is selected.

Table 8-b Inputs in DTU Mann generator

Inputs Mann	Value	Comments
Num. grid points in x-dir.	32768	Nx: Required to have a value corresponding to 2^n.
Num. grid points in y-dir.	64	Ny: Same as TurbSim. Also required to have a value corresponding to 2^n.
Num. grid points in z-dir.	64	Nz: Same as for y-direction.
Spacing of grid points in x-dir.	Calculated by using mean hub height wind speed from measurements	Dx = T*u/Nx. Should be between 0.9-2.08 m.
Spacing of grid points in y-dir.	3.5 m	
Spacing of grid points in z-dir.	3.5 m	
Filename u, v and w	Can be anything but must .bin	See example in Figure 8-i
Alphaepsilon	Varies for each case and is calculated with the equations (=	The calculation of this values includes TI and std from measurements.
L	33.6	The turbulence length scale

Seed	1209	Used same for all Mann cases.
High freq. compensation	Yes	Yes for representing point velocity from sonic anemometer measurements.

8.1.2 Simulation input files

One of the TurbSim inputs file for close to rated wind speed with stable atmospheric situation. Such input file is created for all simulation cases with varying parameters in each case.

TIMESR:

---------TurbSim v2.00.* Input File----------

for user-defined time series input

---------Runtime Options----------

False **Echo** - Echo input data to <RootName>.ech (flag)

43456 **RandSeed1** - First random seed (-2147483648 to 2147483647)

67894578 **RandSeed2** - Second random seed (-2147483648 to 2147483647) for intrinsic pRNG, or an alternative pRNG: "RanLux" or "RNSNLW"

False **WrBHHTP** - Output hub-height turbulence parameters in binary form? (Generates RootName.bin)

False **WrFHHTP** - Output hub-height turbulence parameters in formatted form? (Generates RootName.dat)

False WrADHH - Output hub-height time-series data in AeroDyn form? (Generates RootName.hh)

False **WrADFF** - Output full-field time-series data in TurbSim/AeroDyn form? (Generates RootName.bts)

True **WrBLFF** - Output full-field time-series data in BLADED/AeroDyn form? (Generates RootName.wnd)

False **WrADTWR** - Output tower time-series data? (Generates RootName.twr)

False **WrFMTFF** - Output full-field time-series data in formatted (readable) form? (Generates RootName.u, RootName.v, RootName.w)

False **WrACT** - Output coherent turbulence time steps in AeroDyn form? (Generates RootName.cts)

True **Clockwise** - Clockwise rotation looking downwind? (used only for full-field binary files - not necessary for AeroDyn)

0 **ScaleIEC** - Scale IEC turbulence models to exact target standard deviation? [0=no additional scaling; 1=use hub scale uniformly; 2=use individual scales]

--------Turbine/Model Specifications----------

64 **NumGrid_Z** - Vertical grid-point matrix dimension

64 **NumGrid_Y** - Horizontal grid-point matrix dimension

0.1 **TimeStep** - Time step [seconds]

3800 **AnalysisTime** - Length of analysis time series [seconds] (program will add time if necessary: AnalysisTime = MAX(AnalysisTime, UsableTime+GridWidth/MeanHHWS))

"ALL" **UsableTime** - Usable length of output time series [seconds] (program will add GridWidth/MeanHHWS seconds unless UsableTime is "ALL")

119 **HubHt** - Hub height [m] (should be > 0.5*GridHeight)

220.5 **GridHeight** - Grid height [m]

220.5 **GridWidth** - Grid width [m] (should be >= 2*(RotorRadius+ShaftLength))

0 **VFlowAng** - Vertical mean flow (uptilt) angle [degrees]

0 **HFlowAng** - Horizontal mean flow (skew) angle [degrees]

--------Meteorological Boundary Conditions----------

"TIMESR" **TurbModel** - Turbulence model ("IECKAI","IECVKM","GP_LLJ","NWTCUP","SMOOTH","WF_UPW","WF_07D","WF_14D","TIDAL","API","USRINP","TIMESR", or "NONE")

"U_12.5_stP62.TimeSer" **UserFile** - Name of the file that contains inputs for user-defined spectra or time series inputs (used only for "USRINP" and "TIMESR" models)

3 **IECstandard** - Number of IEC 61400-x standard (x=1,2, or 3 with optional 61400-1 edition number (i.e. "1-Ed2"))

"A" **IECturbc** - IEC turbulence characteristic ("A", "B", "C" or the turbulence intensity in percent) ("KHTEST" option with NWTCUP model, not used for other models)

"NTM" **IEC_WindType** - IEC turbulence type ("NTM"=normal, "xETM"=extreme turbulence, "xEWM1"=extreme 1-year wind, "xEWM50"=extreme 50-year wind, where x=wind turbine class 1, 2, or 3)

"default" **ETMc** - IEC Extreme Turbulence Model "c" parameter [m/s]

"USR" **WindProfileType** - Velocity profile type ("LOG";"PL"=power law;"JET";"H2L"=Log law for TIDAL model;"API";"USR";"TS";"IEC"=PL on rotor disk, LOG elsewhere; or "default")

"PRO_12.5_stP62.Profiles" **ProfileFile** - Name of the file that contains input profiles for WindProfileType="USR" and/or TurbModel="USRVKM" [-]

80 **RefHt** - Height of the reference velocity (URef) [m]

12.6371 **URef** - Mean (total) velocity at the reference height [m/s] (or "default" for JET velocity profile) [must be 1-hr mean for API model; otherwise is the mean over AnalysisTime seconds]

"default" **ZJetMax** - Jet height [m] (used only for JET velocity profile, valid 70-490 m)

"default" **PLExp** - Power law exponent [-] (or "default")

"default" **Z0** - Surface roughness length [m] (or "default")

--------Non-IEC Meteorological Boundary Conditions----------

"default" **Latitude** - Site latitude [degrees] (or "default")

0.1433 **RICH_NO** - Gradient Richardson number [-]

"default" **UStar** - Friction or shear velocity [m/s] (or "default")

"default" **ZI** - Mixing layer depth [m] (or "default")

"default" **PC_UW** - Hub mean u'w' Reynolds stress [m^2/s^2] (or "default" or "none")

"default" **PC_UV** - Hub mean u'v' Reynolds stress [m^2/s^2] (or "default" or "none")

"default" **PC_VW** - Hub mean v'w' Reynolds stress [m^2/s^2] (or "default" or "none")

--------Spatial Coherence Parameters----------

"GENERAL" **SCMod1** - u-component coherence model ("GENERAL","IEC","API","NONE", or "default")

"GENERAL" **SCMod2** - v-component coherence model ("GENERAL","IEC","NONE", or "default")

"GENERAL" **SCMod3** - w-component coherence model ("GENERAL","IEC","NONE", or "default")

"12.1145 0" **InCDec1** - u-component coherence parameters for general or IEC models [-, m^-1] (e.g. "10.0 0.3e-3" in quotes) (or "default")

"8.5416 0" **InCDec2** - v-component coherence parameters for general or IEC models [-, m^-1] (e.g. "10.0 0.3e-3" in quotes) (or "default")

"4.4337 0" **InCDec3** - w-component coherence parameters for general or IEC models [-, m^-1] (e.g. "10.0 0.3e-3" in quotes) (or "default")

0 **CohExp** - Coherence exponent for general model [-] (or "default")

--------Coherent Turbulence Scaling Parameters----------

".\EventData" **CTEventPath** - Name of the path where event data files are located

"les" **CTEventFile** - Type of event files ("LES", "DNS", or "RANDOM")

true **Randomize** - Randomize the disturbance scale and locations? (true/false)

1 **DistScl** - Disturbance scale [-] (ratio of event dataset height to rotor disk). (Ignored when Randomize = true.)

0.5 CTLy - Fractional location of tower centerline from right [-] (looking downwind) to left side of the dataset. (Ignored when Randomize = true.)

0.5 CTLz - Fractional location of hub height from the bottom of the dataset. [-] (Ignored when Randomize = true.)

10 CTStartTime - Minimum start time for coherent structures in RootName.cts [seconds]

==========

! NOTE: Do not add or remove any lines in this file!

==========

The time series input file for TIMESR: "U_12.5_stP62.TimeSer"

It is not represented in Appendix A due to the size of the file. It contains of wind speeds for u, v, w at 40, 60 and 80 m for all time steps in the simulation length, meaning 3800 wind speeds for each direction and height.

The profile input file for TIMESR: "PRO_12.5_stP62.Profiles"

The profile is derived by the logarithmic wind profile. It has the start height of 8.75 m, which is the height above sea level where the wind field grid bottom is located.

---------TurbSim v2.00.* Profile Input File----------

Made up profiles

-------- User-Defined Profiles (Used only with USR wind profile or USRVKM spectral model) ----------

64 NumUSRz - Number of Heights

1 StdScale1 - u-component scaling factor for the input standard deviation (USRVKM only)

1 StdScale2 - v-component scaling factor for the input standard deviation (USRVKM only)

1 StdScale3 - w-component scaling factor for the input standard deviation (USRVKM only)

.....

Height	Wind Speed	Wind --Direction--
(m)	(m/s)	(deg, cntr-clockwise)
8.7500	11.0732	0.0000
12.2500	11.2456	0.0000
15.7500	11.3823	0.0000
19.2500	11.4977	0.0000
22.7500	11.5990	0.0000
26.2500	11.6903	0.0000
29.7500	11.7740	0.0000
33.2500	11.8519	0.0000
36.7500	11.9251	0.0000
40.2500	11.9945	0.0000
43.7500	12.0607	0.0000
47.2500	12.1242	0.0000
50.7500	12.1854	0.0000
54.2500	12.2446	0.0000
57.7500	12.3020	0.0000
61.2500	12.3579	0.0000
64.7500	12.4124	0.0000
68.2500	12.4657	0.0000
71.7500	12.5179	0.0000
75.2500	12.5691	0.0000
78.7500	12.6194	0.0000

82.2500	12.6688	0.0000
85.7500	12.7175	0.0000
89.2500	12.7655	0.0000
92.7500	12.8129	0.0000
96.2500	12.8596	0.0000
99.7500	12.9058	0.0000
103.2500	12.9515	0.0000
106.7500	12.9966	0.0000
110.2500	13.0414	0.0000
113.7500	13.0857	0.0000
117.2500	13.1296	0.0000
120.7500	13.1732	0.0000
124.2500	13.2163	0.0000
127.7500	13.2592	0.0000
131.2500	13.3017	0.0000
134.7500	13.3440	0.0000
138.2500	13.3859	0.0000
141.7500	13.4276	0.0000
145.2500	13.4691	0.0000
148.7500	13.5103	0.0000
152.2500	13.5512	0.0000
155.7500	13.5920	0.0000
159.2500	13.6325	0.0000
162.7500	13.6728	0.0000

166.2500	13.7129	0.0000
169.7500	13.7529	0.0000
173.2500	13.7926	0.0000
176.7500	13.8322	0.0000
180.2500	13.8716	0.0000
183.7500	13.9109	0.0000
187.2500	13.9500	0.0000
190.7500	13.9890	0.0000
194.2500	14.0278	0.0000
197.7500	14.0665	0.0000
201.2500	14.1051	0.0000
204.7500	14.1435	0.0000
208.2500	14.1818	0.0000
211.7500	14.2200	0.0000
215.2500	14.2581	0.0000
218.7500	14.2961	0.0000
222.2500	14.3339	0.0000
225.7500	14.3717	0.0000
229.2500	14.4093	0.0000

Kaimal:

```
---------TurbSim v2.00.* Input File------------------------

for user-defined time series input
```

---------Runtime Options----------

False Echo - Echo input data to <RootName>.ech (flag)

43456 RandSeed1 - First random seed (-2147483648 to 2147483647)

67894578 RandSeed2 - Second random seed (-2147483648 to 2147483647) for intrinsic pRNG, or an alternative pRNG: "RanLux" or "RNSNLW"

False WrBHHTP - Output hub-height turbulence parameters in binary form? (Generates RootName.bin)

False WrFHHTP - Output hub-height turbulence parameters in formatted form? (Generates RootName.dat)

False WrADHH - Output hub-height time-series data in AeroDyn form? (Generates RootName.hh)

False WrADFF - Output full-field time-series data in TurbSim/AeroDyn form? (Generates RootName.bts)

True WrBLFF - Output full-field time-series data in BLADED/AeroDyn form? (Generates RootName.wnd)

False WrADTWR - Output tower time-series data? (Generates RootName.twr)

False WrFMTFF - Output full-field time-series data in formatted (readable) form? (Generates RootName.u, RootName.v, RootName.w)

False WrACT - Output coherent turbulence time steps in AeroDyn form? (Generates RootName.cts)

True Clockwise - Clockwise rotation looking downwind? (used only for full-field binary files - not necessary for AeroDyn)

1 ScaleIEC - Scale IEC turbulence models to exact target standard deviation? [0=no additional scaling; 1=use hub scale uniformly; 2=use individual scales]

--------Turbine/Model Specifications----------

64 NumGrid_Z - Vertical grid-point matrix dimension

64 NumGrid_Y - Horizontal grid-point matrix dimension

```
      0.1   TimeStep       - Time step [seconds]

     3800   AnalysisTime    - Length of analysis time series [seconds] (program will add time if necessary: AnalysisTime = MAX(AnalysisTime, UsableTime+GridWidth/MeanHHWS) )

"ALL"        UsableTime      - Usable length of output time series [seconds] (program will add GridWidth/MeanHHWS seconds unless UsableTime is "ALL")

      119   HubHt          - Hub height [m] (should be > 0.5*GridHeight)

    220.5   GridHeight      - Grid height [m]

    220.5   GridWidth       - Grid width [m] (should be >= 2*(RotorRadius+ShaftLength))

        0   VFlowAng        - Vertical mean flow (uptilt) angle [degrees]

        0   HFlowAng        - Horizontal mean flow (skew) angle [degrees]



--------Meteorological Boundary Conditions-------------------

"IECKAI"     TurbModel       - Turbulence model ("IECKAI","IECVKM","GP_LLJ","NWTCUP","SMOOTH","WF_UPW","WF_07D","WF_14D","TIDAL","API","USRINP","TIMESR", or "NONE")

"unused"     UserFile        - Name of the file that contains inputs for user-defined spectra or time series inputs (used only for "USRINP" and "TIMESR" models)

        3   IECstandard     - Number of IEC 61400-x standard (x=1,2, or 3 with optional 61400-1 edition number (i.e. "1-Ed2") )

   7.7338   IECturbc        - IEC turbulence characteristic ("A", "B", "C" or the turbulence intensity in percent) ("KHTEST" option with NWTCUP model, not used for other models)

"NTM"        IEC_WindType    - IEC turbulence type ("NTM"=normal, "xETM"=extreme turbulence, "xEWM1"=extreme 1-year wind, "xEWM50"=extreme 50-year wind, where x=wind turbine class 1, 2, or 3)

"default"    ETMc            - IEC Extreme Turbulence Model "c" parameter [m/s]

"PL"         WindProfileType - Velocity profile type ("LOG";"PL"=power law;"JET";"H2L"=Log law for TIDAL model;"API";"USR";"TS";"IEC"=PL on rotor disk, LOG elsewhere; or "default")

"unused"     ProfileFile     - Name of the file that contains input profiles for WindProfileType="USR" and/or TurbModel="USRVKM" [-]
```

```
      119   RefHt         - Height of the reference velocity (URef) [m]

   13.1514   URef          - Mean (total) velocity at the reference height [m/s] (or "default" for JET
velocity profile) [must be 1-hr mean for API model; otherwise is the mean over AnalysisTime
seconds]

"default"    ZJetMax       - Jet height [m] (used only for JET velocity profile, valid 70-490 m)

    0.0759   PLExp         - Power law exponent [-] (or "default")

"default"    Z0            - Surface roughness length [m] (or "default")



--------Non-IEC Meteorological Boundary Conditions------------

"default"    Latitude      - Site latitude [degrees] (or "default")

     0.5     RICH_NO       - Gradient Richardson number [-]

"default"    UStar         - Friction or shear velocity [m/s] (or "default")

"default"    ZI            - Mixing layer depth [m] (or "default")

"default"    PC_UW         - Hub mean u'w' Reynolds stress [m^2/s^2] (or "default" or "none")

"default"    PC_UV         - Hub mean u'v' Reynolds stress [m^2/s^2] (or "default" or "none")

"default"    PC_VW         - Hub mean v'w' Reynolds stress [m^2/s^2] (or "default" or "none")



--------Spatial Coherence Parameters----------------------------

"default"    SCMod1        - u-component coherence model ("GENERAL","IEC","API","NONE", or
"default")

"default"    SCMod2        - v-component coherence model ("GENERAL","IEC","NONE", or "default")

"default"    SCMod3        - w-component coherence model ("GENERAL","IEC","NONE", or "default")

"default"    InCDec1       - u-component coherence parameters for general or IEC models [-, m^-1]
(e.g. "10.0  0.3e-3" in quotes) (or "default")

"default"    InCDec2       - v-component coherence parameters for general or IEC models [-, m^-1]
(e.g. "10.0  0.3e-3" in quotes) (or "default")
```

"default" InCDec3 - w-component coherence parameters for general or IEC models [-, m^-1] (e.g. "10.0 0.3e-3" in quotes) (or "default")

"default" CohExp - Coherence exponent for general model [-] (or "default")

--------Coherent Turbulence Scaling Parameters----------

".\EventData" CTEventPath - Name of the path where event data files are located

"les" CTEventFile - Type of event files ("LES", "DNS", or "RANDOM")

true Randomize - Randomize the disturbance scale and locations? (true/false)

1 DistScl - Disturbance scale [-] (ratio of event dataset height to rotor disk). (Ignored when Randomize = true.)

0.5 CTLy - Fractional location of tower centerline from right [-] (looking downwind) to left side of the dataset. (Ignored when Randomize = true.)

0.5 CTLz - Fractional location of hub height from the bottom of the dataset. [-] (Ignored when Randomize = true.)

10 CTStartTime - Minimum start time for coherent structures in RootName.cts [seconds]

==

! NOTE: Do not add or remove any lines in this file!

==

Inputs for simulation of Mann turbulence wind fields.

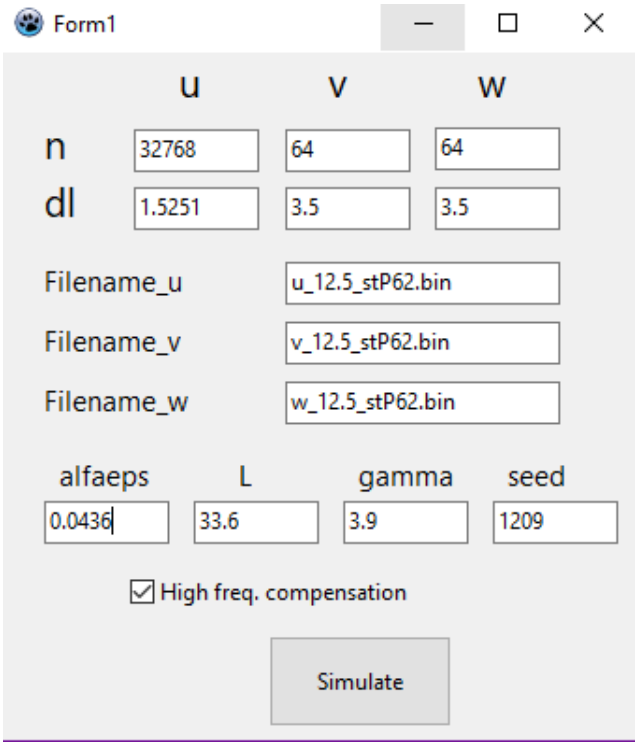

Figure 8-i Simulation by DTU Mann generator

8.1.3 Environmental input in SIMA

Environment	Mann	TurbSim: Kaimal/TIMESR	
Wave	Approximately equal to zero	Approximately equal to zero	
Swell	No swell wave	No swell wave	
Wind direction	0	0	
Mean speed	U at 119m		
Shear profile levels	From Mann scaling procedure in MATLAB		
Longitudinal file name	Mann generator output file (.bin)	TurbSim output file (.wnd and .sum)	Only one wind file and sum file

			needed for TurbSim
Lateral file name	Mann generator output file (.bin)		
Vertical file name	Mann generator output file (.bin)		
Wind field domain position			
Lower left X	-7.073		At the tip of the hub point
Lower left Y	-110.25		To surround the wind turbine
Lower left Z	8.75		To surround the wind turbine
Wind field domain size			
Num. Points X	32768		
Num. Points Y	64		
Num. Points Z	64		
Wind field size			
Size X			
Size Y	224		64*3.5 m
Size Z	224		64*3.5 m
Current	No current	No current	
Dynamic calculations			
Time increment	0.115966796875	0.1	
Time step	0.0115966796875	0.01	Time increment/10

9 Appendix C

9.1 Wind turbine tests

9.1.1 Controller modification test

The change of blade-pitch natural frequency from 0.02 Hz (to the left) to 0.01 Hz (to right). The test performed is with uniform wind.

Power output

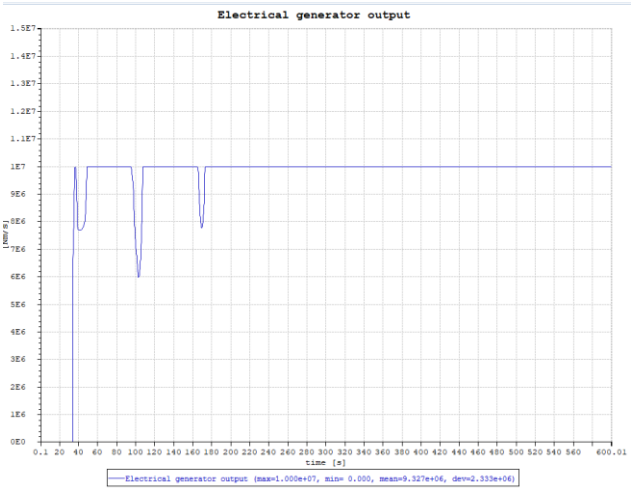

Tip in-plane deflection

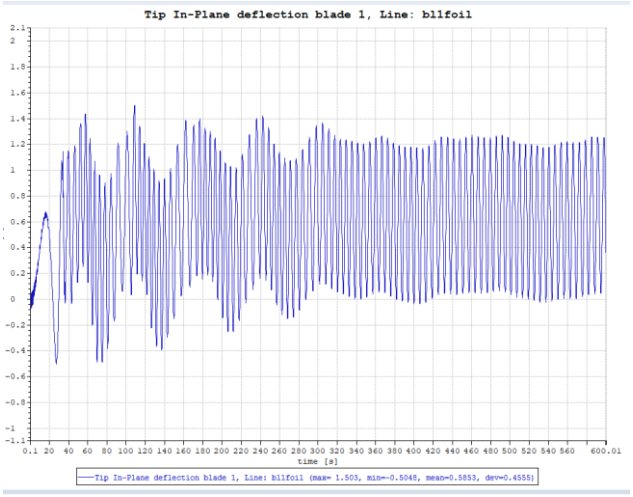

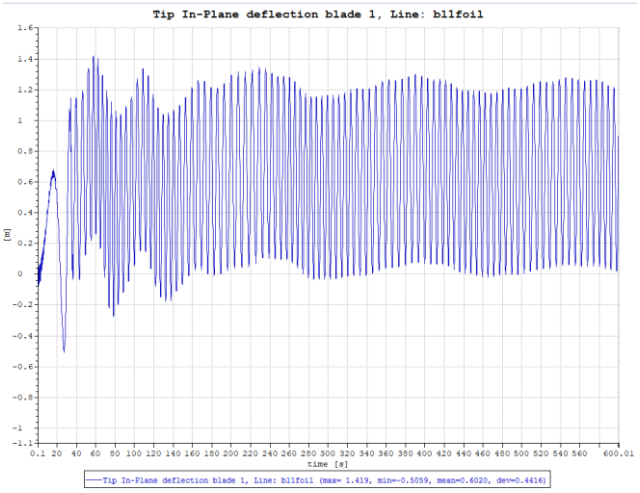

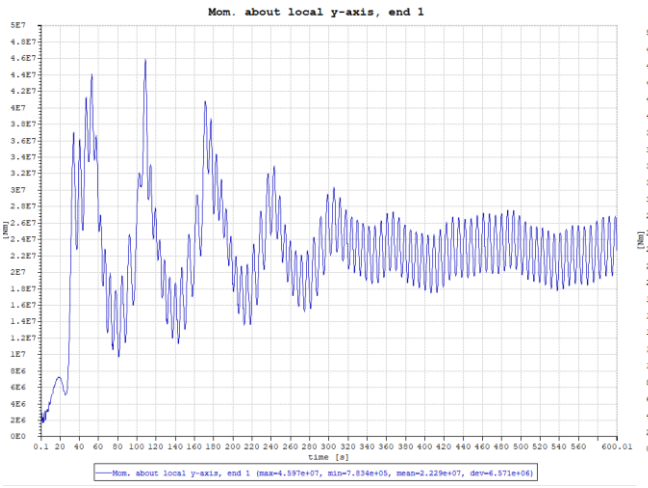
Mom. about local y-axis, end 1
[Nm]
time [s]
Mom. about local y-axis, end 1 (max=4.597e+07, min=7.834e+05, mean=2.229e+07, dev=6.571e+06)

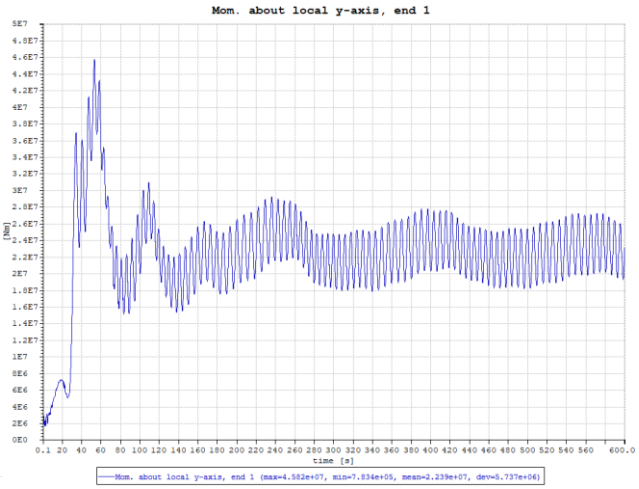
Mom. about local y-axis, end 1
[Nm]
time [s]
Mom. about local y-axis, end 1 (max=4.582e+07, min=7.834e+05, mean=2.239e+07, dev=5.737e+06)

Pitch

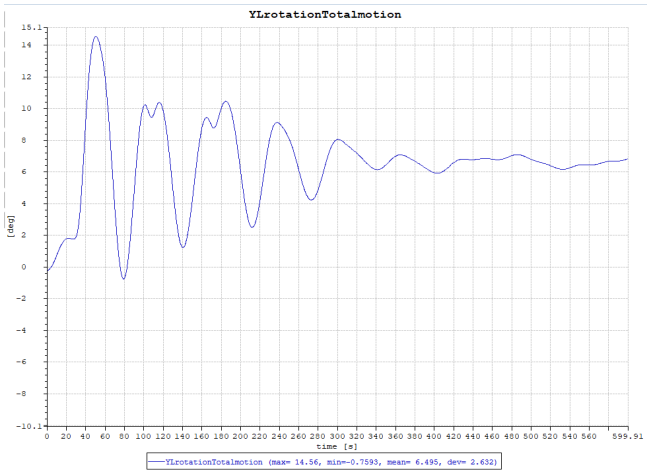
YLrotationTotalmotion
[deg]
time [s]
YLrotationTotalmotion (max= 14.56, min=-0.7593, mean= 6.495, dev= 2.632)

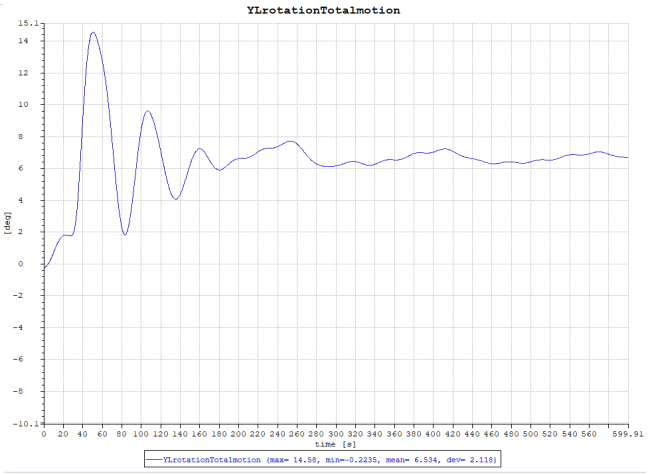
YLrotationTotalmotion
[deg]
time [s]
YLrotationTotalmotion (max= 14.58, min=-0.2235, mean= 6.534, dev= 2.118)

Yaw

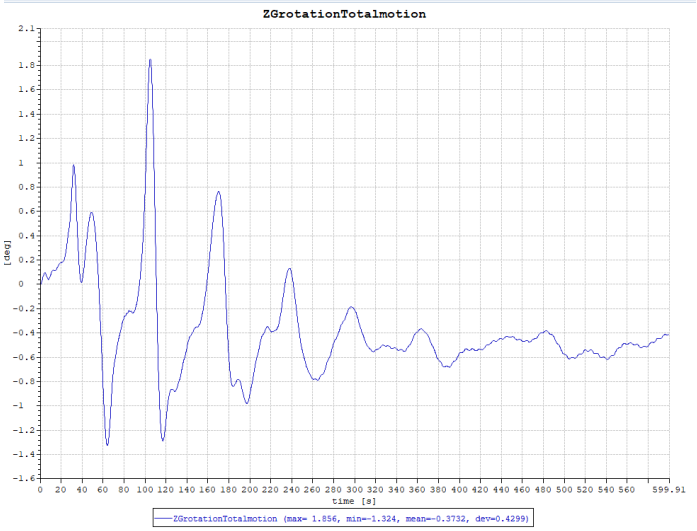
ZGrotationTotalmotion
[deg]
time [s]
ZGrotationTotalmotion (max= 1.856, min=-1.324, mean=-0.3732, dev=0.4299)

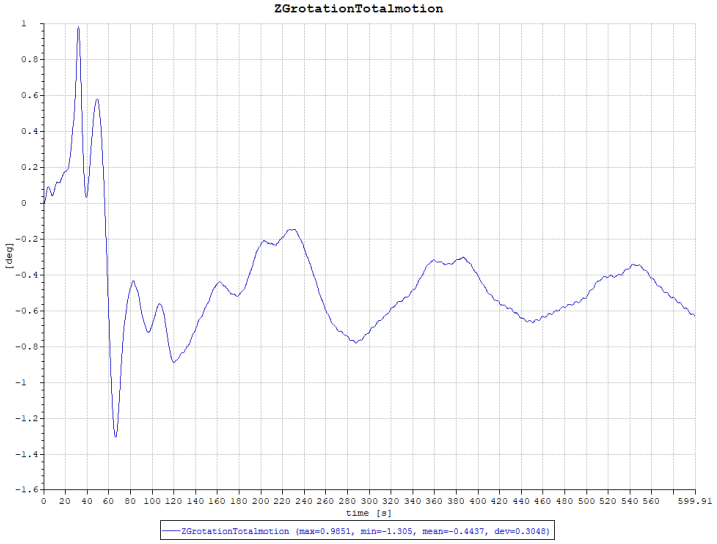
ZGrotationTotalmotion
[deg]
time [s]
ZGrotationTotalmotion (max=0.9851, min=-1.305, mean=-0.4437, dev=0.3048)

9.1.2 The floating turbine becomes unstable

The turbine fails after becoming dynamical unstable for above rated wind speeds and the simulation crash after 2000 seconds.

Simulation test:

Wind speed: over rated (uniform 18m/s)
Time step: 0.005 s

Translation modes:

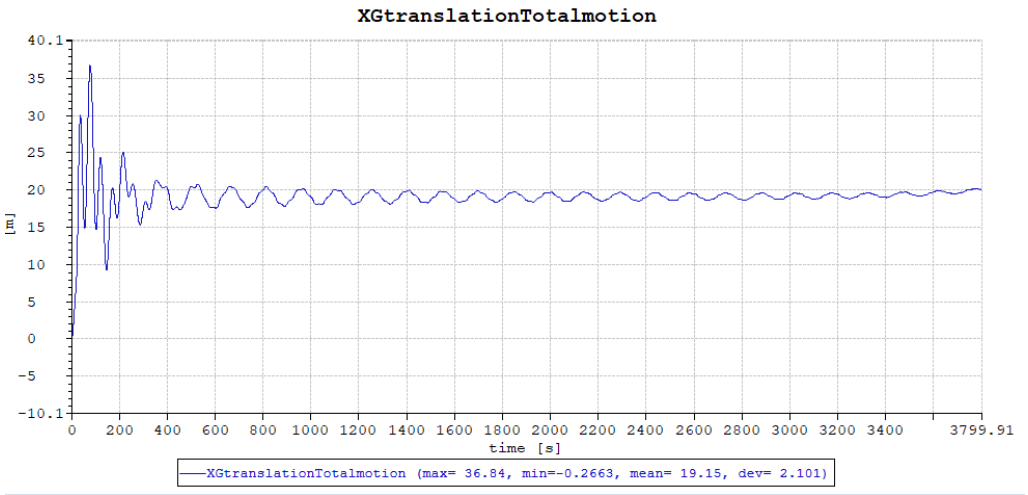

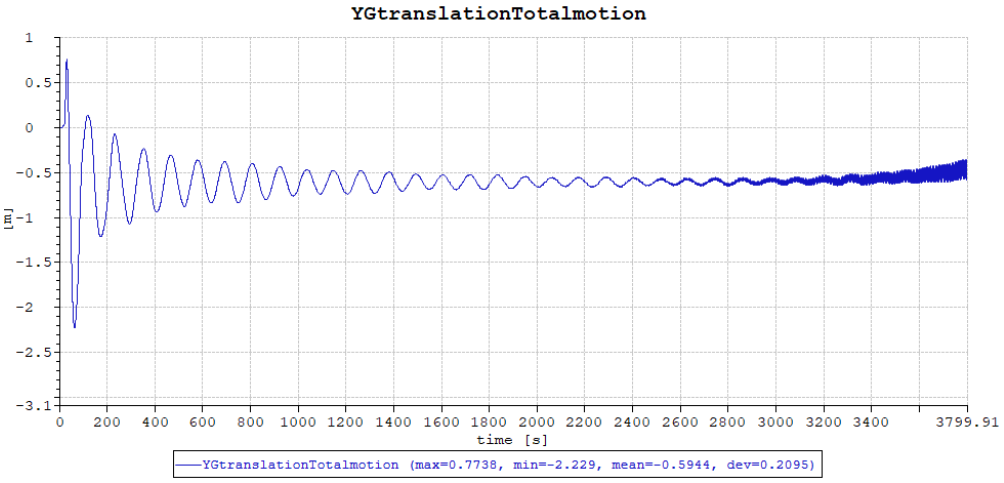

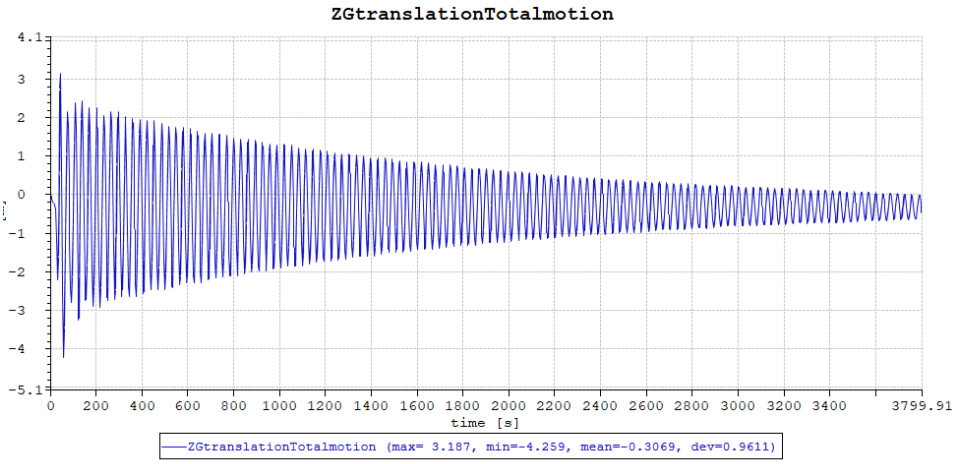

Rotation modes

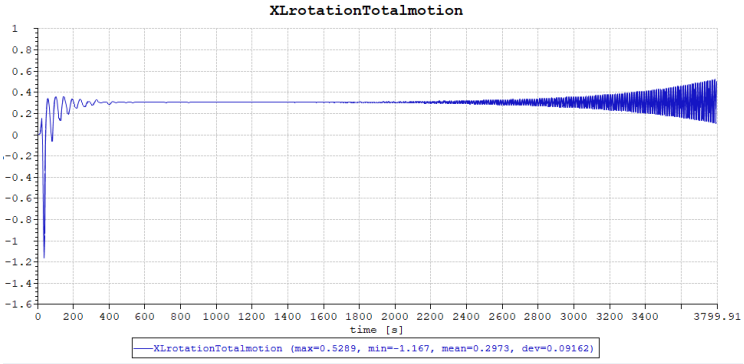

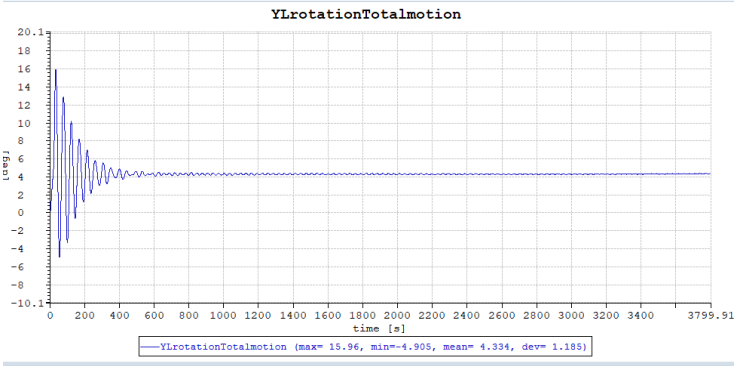

Output

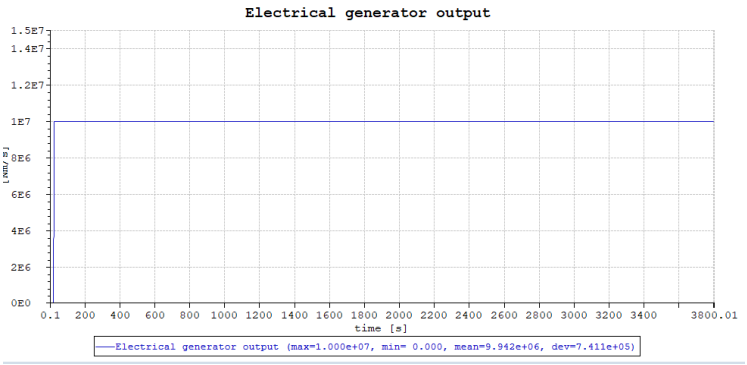

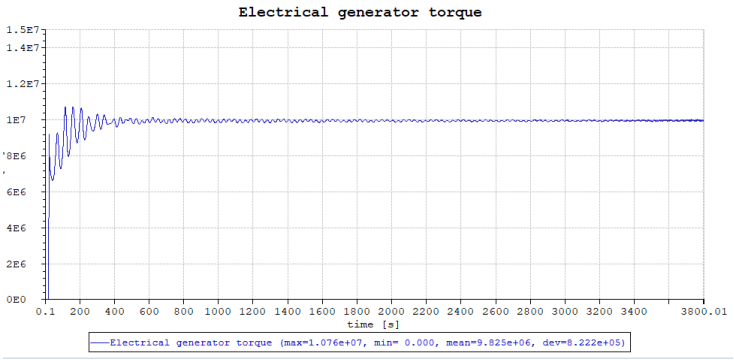

Turbulent test

Wind speed: 18 m/s

Time step: 0.005 s

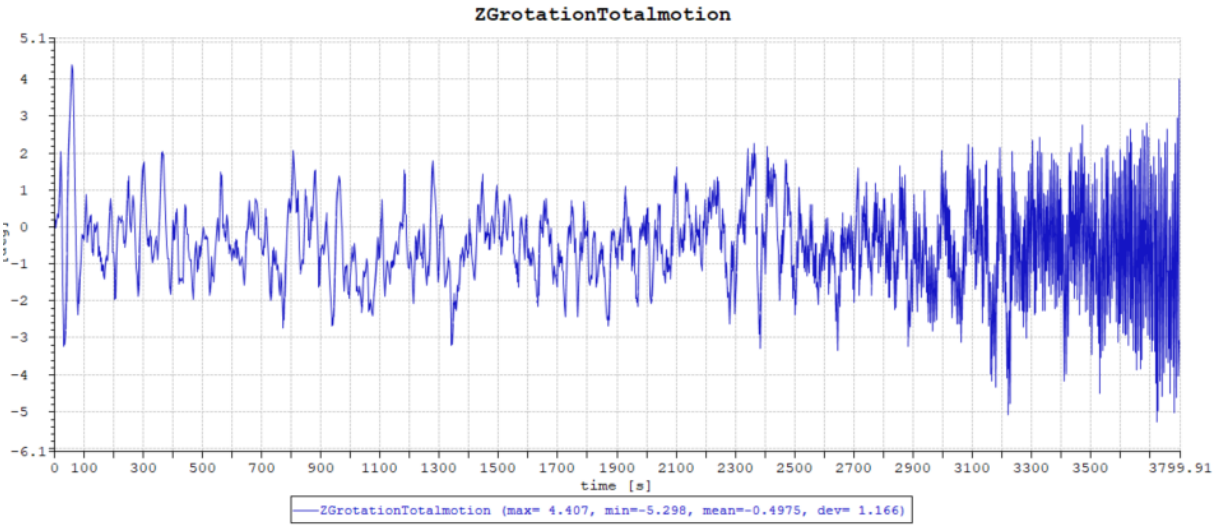
ZGrotationTotalmotion
time [s]
ZGrotationTotalmotion (max= 4.407, min=-5.298, mean=-0.4975, dev= 1.166)

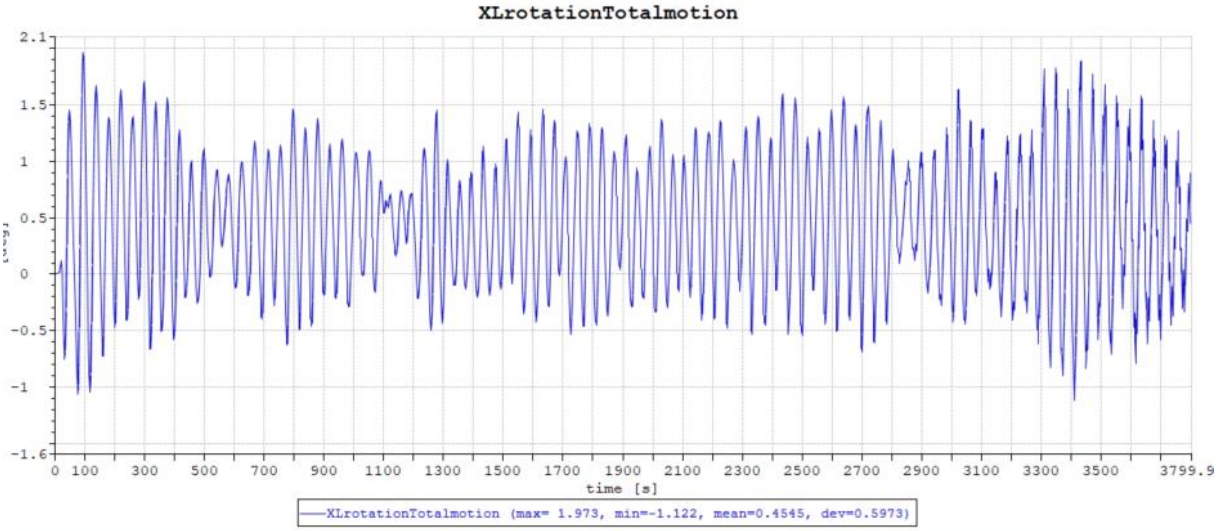
XLrotationTotalmotion
time [s]
XLrotationTotalmotion (max= 1.973, min=-1.122, mean=0.4545, dev=0.5973)

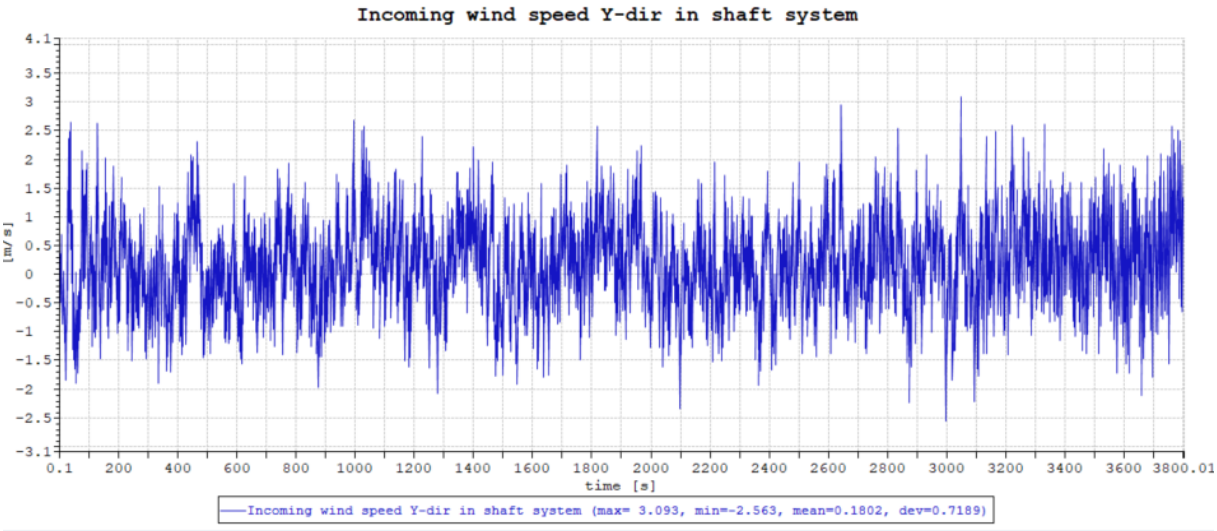
Incoming wind speed Y-dir in shaft system
[m/s]
time [s]
Incoming wind speed Y-dir in shaft system (max= 3.093, min=-2.563, mean=0.1802, dev=0.7189)

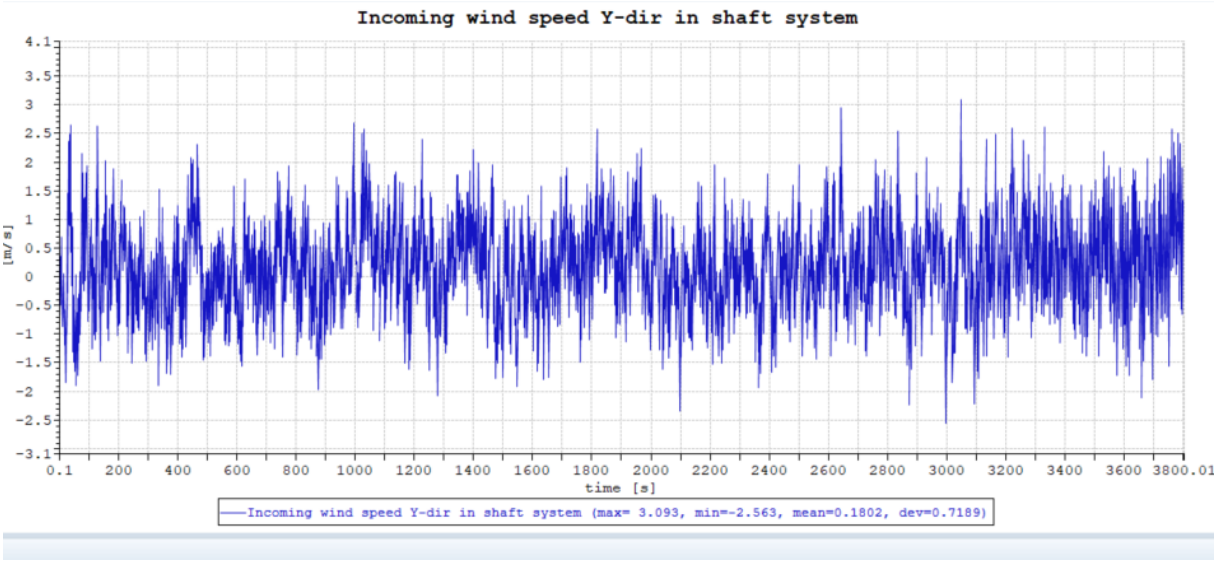

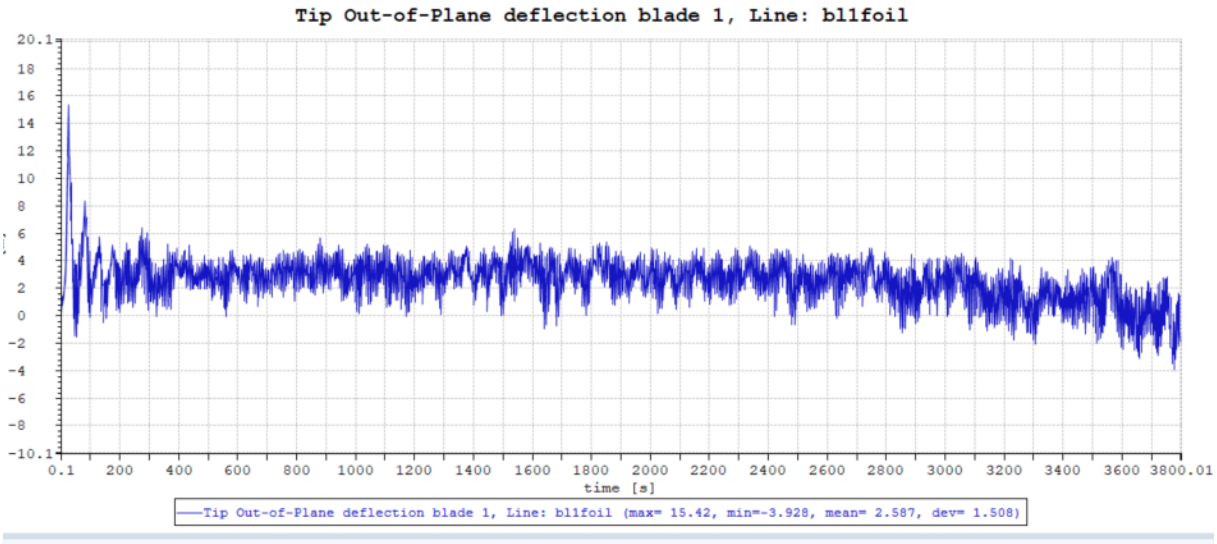

9.1.3 The approach to find the damping values to the spar

The rounds to achieve correct damping level. Performed in SIMA.

Wanted to achieve 5% damping for surge and sway and 8% for pitch and roll.

The damping level for the received turbine:

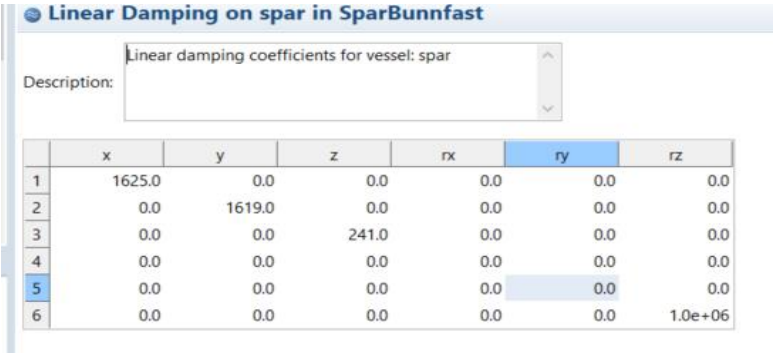

	x	y	z	rx	ry	rz
1	1625.0	0.0	0.0	0.0	0.0	0.0
2	0.0	1619.0	0.0	0.0	0.0	0.0
3	0.0	0.0	241.0	0.0	0.0	0.0
4	0.0	0.0	0.0	0.0	0.0	0.0
5	0.0	0.0	0.0	0.0	0.0	0.0
6	0.0	0.0	0.0	0.0	0.0	1.0e+06

Changed the values to zero to concentrate on finding the damping via linear drag.

	x	y	z	rx	ry	rz
1	0.0	0.0	0.0	0.0	0.0	0.0
2	0.0	0.0	0.0	0.0	0.0	0.0
3	0.0	0.0	241.0	0.0	0.0	0.0
4	0.0	0.0	0.0	0.0	0.0	0.0
5	0.0	0.0	0.0	0.0	0.0	0.0
6	0.0	0.0	0.0	0.0	0.0	1.0e+06

Linear drag must be defined under the spar body (Hydrodynamical properties).

The linear drag was first performed by the eigen period of sway/surge 140 s and mass (including added mass). This gave the linear damping to be:

T= 140 s:

$$B_{11} = 2\,\zeta M\omega_0 \;\approx\; 2\zeta\,(1.3+1.4)10^7\frac{2\pi}{140} = \zeta 2.424e06$$

With $\zeta = 0.05$:

$B_{11} = 121200$ and with the length of the spar unit, L, z=-12-(-120) m = 108 m. $\frac{B_{11}}{L} = 1122.2\frac{kg}{sm}$. These values were tested in the x- and y-direction.

Linear drag:

C1x	C1y	C1z
1122.2	1122.2	140.0

Result: Not good enough damping occurred.

T= 40 s:

$$B_{11} = 2\,\zeta M\omega_0 \;\approx\; 2\zeta\,(1.3+1.4)10^7\frac{2\pi}{40} = \zeta 8.48e10^6$$

With $\zeta = 0.05$:

$B_{11} = 4.241e05$ gives $\frac{B_{11}}{L} = 3926.9\ \frac{kg}{sm}$. These values were tested in the x- and y-direction (C1x and C1y).

Result: Did not achieve the correct wanted damping of the behaviour of the spar floater.

Several calculations of linear drag were performed to achieve correct damping level, but without good results as the examples below illustrates.

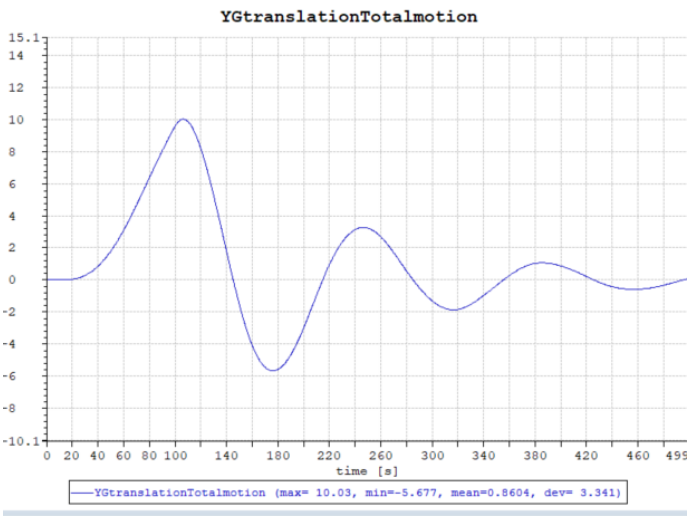

Sway

$$\delta = \ln\left(\frac{10.03}{3.26}\right) = 1.12$$

$$\zeta = \frac{1.12}{2\pi} = 0.178 = 17.8\%$$

ROLL

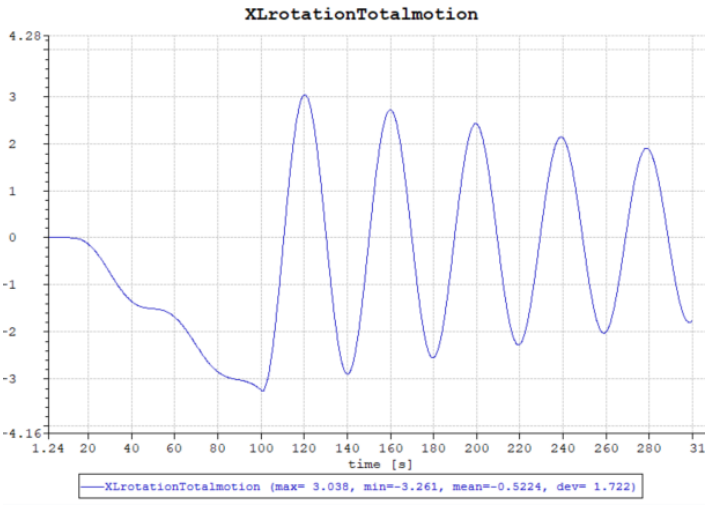

$$\delta = \ln\left(\frac{3.08}{2.72}\right) = 0.12$$

$$\zeta = \frac{0.12}{2\pi} = 0.019 = 1.9\%$$

Then tried started all over again by finding the correct eigen periods.

1. Defined all damping values to be zero (drag and damping matrix) and then tested with a force in the y-direction:

Ramp force at the tower top

Time	on:	after	10	s
Time	off:	after	100	s

Force: 6000 N/s

- Roll:

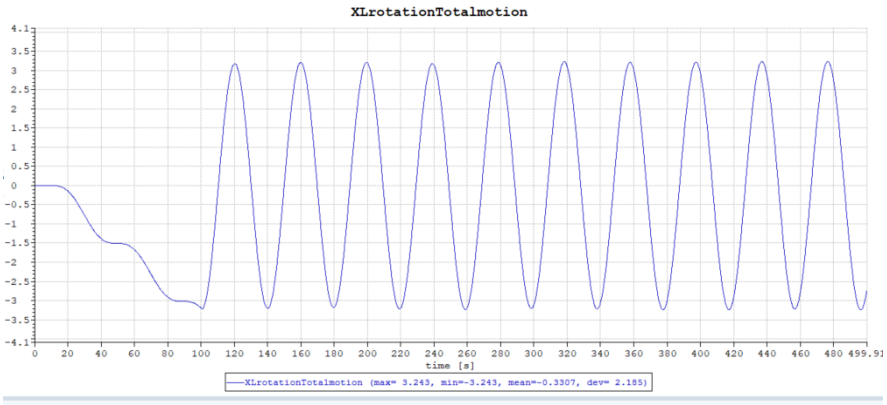

T = 160 – 120 = 40 s

- Sway:

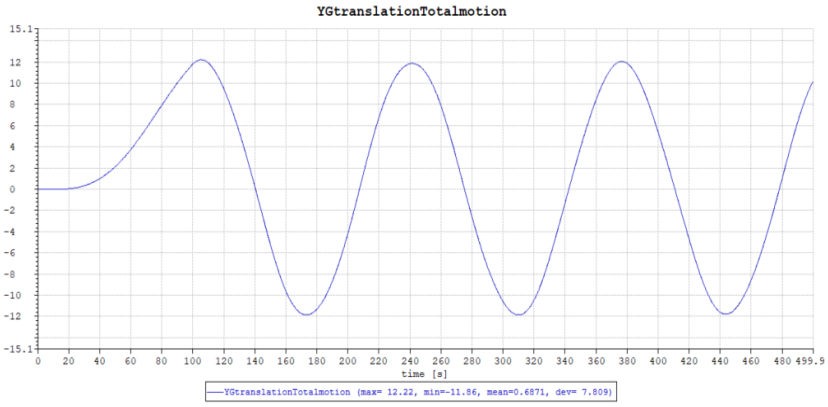

T= 376.5 - 241.5= 135s

2. Do the same as in 1 to find eigen period of surge and pitch

The ramp force is applied in the x-direction at the tower top

- Pitch:

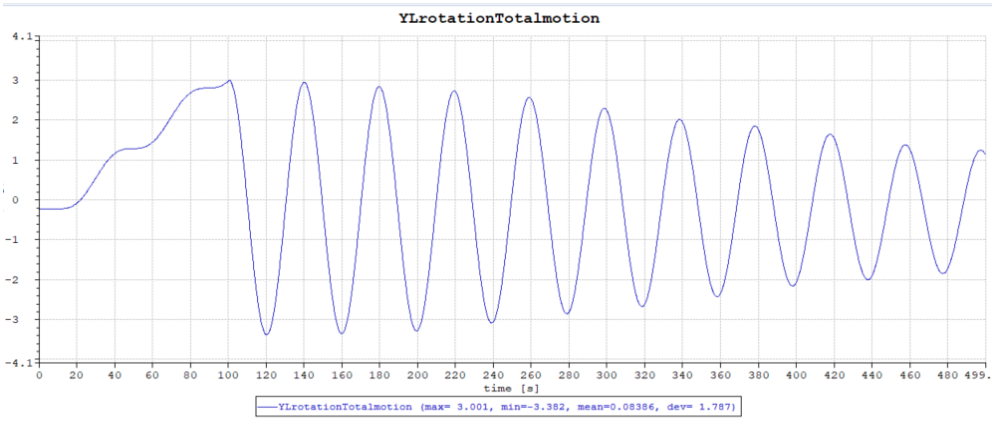

T=180-140 = 40s

Stamp showed some damping after the test. Tried to take away the damping in the tower cross sections (Figure below), but the test results did not change. The differences might be linked to drag on the turbine blades and the differences between pitch and roll are assumed to be small. Therefore, nothing has been done about this.

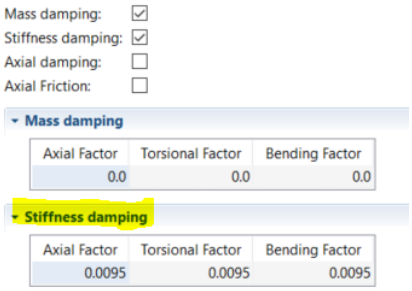

- Surge

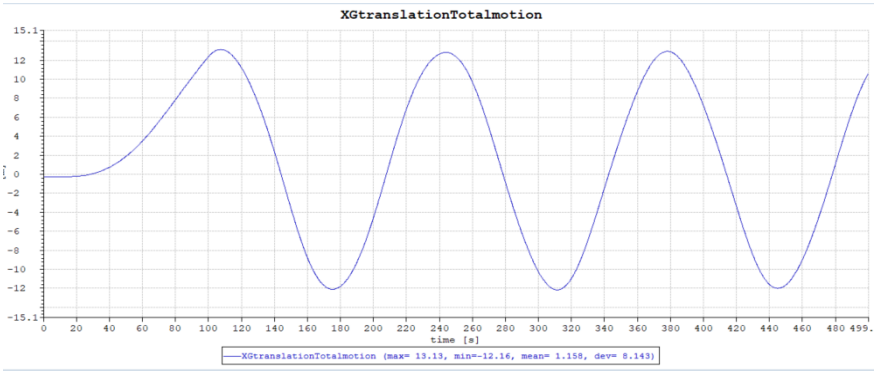

T= 378.2 - 243.8 = 134.4 s

3. Used the eigen periods to calculate the linear drag values:

T (sway) =140s

T (surge) =134.4s

$\zeta = 0.05$

$$B_{11} = 2\,\zeta M\omega_0 \;\approx\; 2 * 0.05(1.3 + 1.4)10^7 \frac{2\pi}{140} = \; 121175.72$$

$$\frac{B_{11}}{L} = \frac{121175.72}{108} = 1121.99$$

$$B_{11} = 2\,\zeta M\omega_0 \;\approx\; 2 * 0.05(1.3 + 1.4)10^7 \frac{2\pi}{134.4} = \; 126224.7$$

$$\frac{B_{11}}{L} = \frac{126224.7}{108} = 1168.7$$

Use a value in between for $B_{11} = 1145.35$

Linear drag:

C1x	C1y	C1z
1145.4	1145.4	0.0

This gave satisfying results in the translation damping tests. The rotation on the other hand was not as wanted. This was a pervasive problem and the first problem to be fixed.

Problem 1: The surge and pitch were observed to have no reaction for the values defined in C1x.

Found out that the movements had a reaction to the linear drag when it was defined in the C1z, which are probably because the spar body has a local coordinate system. With x along the element axis, while it is the y and z that we needed to find the correct damping level. Test showed that the values used in the previous test, only damped the pitch rotation by 1.74%. This was the second problem arisen under the study of damping the system.

Problem 2: We achieved desired damping in the roll rotation, but then sway was to much damped and vice versa. Found therefore out that the translational and rotational behaviour are coupled. Meaning that surge happens when the turbine pitches. To solve this, we tried to define the damping in the linear damping matrix as followed.

If $b_{11} = 1121.9$ then $B_{11}L = 1121.9 \cdot \big(-12 - (-120)\big) = 1.2e05$

$$B_{15} = b11 \int_{z_b}^{z_t} z dz = \int_{-120}^{12} z dz = \frac{1}{2}\, b_{11} \cdot 12^2 - 120^2 = \; -8.00e06$$

$$B_{24} = -B_{15}$$

$$B_{ij} = B_{ji}$$

$$B_{55} = b11 \int_{-120}^{12} z^2 dz = \frac{1}{3} b_{11} \cdot -12^3 - -120^3 = 6.47e08 = \mathrm{B}_{44}$$

The linear damping matrix:

	x	y	z	rx	ry	rz
1	1.211e+05	0.0	0.0	0.0	-8.0e+06	0.0
2	0.0	1.211e+05	0.0	8.0e+06	0.0	0.0
3	0.0	0.0	241.0	0.0	0.0	0.0
4	0.0	8.0e+06	0.0	6.48e+08	0.0	0.0
5	-8.0e+06	0.0	0.0	0.0	6.48e+08	0.0
6	0.0	0.0	0.0	0.0	0.0	1.0e+06

Result: Almost non damping in the pitch motion, but surge are as we want it.

Therefore, uses the b11 from rotation to get larger values to fill into the matrix.

$$B_{11} = 2\,\zeta M \omega_0 \;\approx\; 2 * 0.08(1.3 + 1.4)10^7 \frac{2\pi}{40} = \; 6.7858E05$$

$$b1 = \frac{6.7858E05}{108} = 6283$$

$$B_{15} = \int_{-120}^{-12} 6283\; z\; dz = -\; 4.5E07$$

$$B_{55} = \int_{-120}^{-12} 6283 * z^2 dz = 3.62E09$$

Result: Get a divergence in the results.

It is not possible to linearize drag damping in surge and pitch in a consistent way, which in certain circumstances, can get a divergence in the results, as it happened here. Also found out that B15 should be different from B51, but both negative. Neither this gave any satisfying results.

4. Focus on quadratic drag and a smaller linear drag

Previously tests we put on max thrust force and got up to 9 degrees in pitch /roll. This is a lot and thus we want to approach 6 degrees to be inside the max pitch movement, which is more realistic when the force is the wind. This is done by rise the quadratic coefficient (CD) and lowering the power.

Initial:

$$\frac{Thrust\ kraft}{ramp\ tid} = \frac{1500e03N}{90s} = 16667\frac{N}{s}$$

Quadratic drag:

$$F_{drag} = \frac{1}{2}\rho C_D D U^2$$

$$\rho: 1025, C_D: 1.5, D: 12, U^2$$

$$F_{drag} = \frac{1}{2} * 1025 * 1.5 * 12 = 9225$$

Quadratic drag:

C2x	C2y	C2z
0.0	9225.0	9225.0

Linear drag:

C1x	C1y	C1z
0.0	140.0	140.0

Greatest power in the quadratic drag because this achieve a greater effect in the roll/pitch than the surge/sway and the linear drag will pick up the smaller vibrations.

Appendix E

9.2 Overview of dynamical load response

9.2.1 Below rated

9.2.2 Rated

9.2.3 Above rated

10 Appendix F

10.1 MATLAB codes

The MATLAB codes used in this study are only listed here since it would take a lot of space. The codes are divided into two sections.

1. Codes generated by Maylinn H. Myrtvedt

Bars: Tower bottom and flapwise bending moments illustrated by bars for the simulation runs of Kaimal, Mann and TIMESR. For both turbines.

PSD: Power spectral density of the load results for all wind speeds and stabilities.

2. Codes generated by Astrid Nybø with adjustments for this study.

Statistics: From measurements to time series ready for use in TurbSim

Mann scaling: longitudinal velocity (used for input in SIMA)

Wind field results: Gives different outputs of the generated wind field

SIMA: The result after simulation runs in SIMA (mean and std)